THERMOPHYSICAL AND ADSORPTION CHARACTERIZATION OF FUNCTIONAL AND PORE MODIFIED ADSORBENTS

ムハッマド, アミルル, イスラム

KYUSHU UNIVERSITY

Thermophysical and Adsorption Characterization of Functional and Pore Modified Adsorbents

Dissertation

Doctor of Philosophy

by

MD. AMIRUL ISLAM

M. Eng. (KU, Japan), M. Sc. (DU, Bangladesh)

Department of Energy and Environmental Engineering

Interdisciplinary Graduate School of Engineering Sciences

Kyushu University

Japan

May 2019

THERMOPHYSICAL AND ADSORPTION CHARACTERIZATION OF FUNCTIONAL AND PORE MODIFIED ADSORBENTS

A dissertation submitted in partial fulfilment of the requirements for the award of the degree of

𝔇𝔬𝔠𝔱𝔬𝔯 𝔬𝔣 𝔓𝔥𝔦𝔩𝔬𝔰𝔬𝔭𝔥𝔶

by

MD. AMIRUL ISLAM

M. Eng. (KU, Japan), M. Sc. (DU, Bangladesh)

Supervisor: **Professor Bidyut Baran Saha**

Department of Energy and Environmental Engineering
Interdisciplinary Graduate School of Engineering Sciences
Kyushu University
Japan

May 2019

Dedicated to

My Parents

&

Family

ABSTRACT

Cooling and refrigeration systems are inevitable in chemical productions, pharmaceutical industries, data center cooling, factories and manufacturing plants, preservation of food/beverage/agricultural products, and to attain thermal comfort in residential/commercial buildings. Most of the conventional cooling/refrigeration systems are vapor compression based and consume a huge amount of electricity. This electricity is generated from centralized power plants which are predominantly fossil fuel based and ultimately releases greenhouse gases during power generation. Hence, conventional cooling/refrigeration systems are indirectly accountable for global warming by consuming electricity. Moreover, the working fluid of those systems are basically high GWP (global warming potential) refrigerants. A significant percentage of working fluid is leaked from the high-pressure side of the system and thus directly contribute to global warming. The summation of indirect and direct warming impact namely, total equivalent warming impact (TEWI) of these systems are alarmingly high. A high performance thermally-powered adsorption cooling system (ACS) can resolve this critical environmental concern.

From the above mentioned perceptions, this research work rigorously focuses on – (i) quantitative assessment of global warming: conventional vs. adsorption cooling systems, (ii) adsorbent characterization (surface area, pore volume, pore size distribution, specific heat capacity) for next generation cooling systems, (iii) modification of pore structure to enhance the quality of carbon based adsorbent, (iv) investigation of adsorption characteristics of novel adsorbent/adsorbate pairs.

A quantitative assessment of global warming has been performed by evaluating the TEWI for conventional and adsorption cooling systems considering similar operating conditions. The results reveal that, the environmental adversity of existing conventional cooling systems is significantly higher with compared to adsorption cooling systems. Employment of an adsorption cooling system instead of a conventional one in residential applications can cut the environmental impact to half or even more than that. Approximately, 70% to 85% global warming impact reduction is conceivable for medium and low temperature applications. However, COP values of the current adsorption cooling systems are very poor. There are huge prospects to enhance the performance by deploying superior adsorbent/adsorbate pair. Therefore, next objective of this research is to determine

various porous and thermophysical properties of adsorbent materials to identify the best adsorbent.

High surface area and pore volume of adsorbent leads to higher adsorption capacity. Whereas, low specific heat capacity is expected for faster desorption. Hence, porous properties (surface area, pore volume, pore size distribution) and specific heat capacity of six different types of silica gel (total thirteen samples including subcategories) have been experimentally investigated with temperature ranging from 30 to 100 °C. Specific heat capacity of four types activated carbon (Maxsorb III, H_2 treated Maxsorb III, KOH–H_2 treated Maxsorb III, KOH treated spherical phenol resin) and two thermal conductivity enhancer (EC–1000 and EC–1500) have been measured. The specific heat capacity data are successfully fitted with Green and Perry equation. These porous properties and specific heat capacity data are essential to design and simulate adsorption cooling systems.

As of the adsorbents for adsorption heat pump (AHP) application, activated carbon sample possesses very high surface area and high adsorption affinity for refrigerant vapor. However, they contain a significant percentage of ultramicropores (< 0.7 nm). Commonly used refrigerant molecule clusters are unable to enter into such tiny pores and no adsorption occurs there. Hence, these ultramicropores decrease thermal conductivity and increase specific heat capacity of the material which ultimately degrade the performance of an adsorption cooling system. Chemical vapor deposition (CVD) of various carbonaceous materials has been performed at elevated temperature to block those unusable pores. Porosity analysis of these modified activated carbon samples has been carried out to compare the adsorbent quality improvement than parent sample. Pyrolization of methane (T_{pyr} = 1000 °C, $\dot{m}$ = 50 mL/min, t = 30 min) and benzene (T_{pyr} = 800 °C, $\dot{m}$ = 25 mL/min, t = 10 min) removes the ultramicropores and most of the mesopores in activated carbon and improves its suitability in AHP applications.

Finally, adsorption isotherm and isosteric heat of adsorption of two novel adsorbent/adsorbate pairs have been investigated. The selected working fluid is HFC32 having low GWP and two adsorbents are activated carbon synthesized from biomass (mangrove wood and waste palm trunk). The experimental data shows remarkably high uptake for both the pairs. The Dubinin Astakhov (D–A) and Tóth models are efficaciously employed to correlate the adsorption isotherms of the assorted pairs. A modified Clausius–Clapeyron model is adopted to determine the isosteric heat of adsorption (Q_{st}) data. Change of Q_{st} with respect to surface coverage is also reported.

ACKNOWLEDGEMENTS

First of all, I show my heartiest gratitude to the most merciful ALLAH who has given me the strength and ability to write this thesis; without His help it would have been impossible to perform my research and write this doctoral thesis.

Then, I would like to express my deepest sense of gratitude and indebtedness to my supervisor, **Professor Bidyut Baran Saha**, for giving me the opportunity to work in his laboratory under his guidance. In particular, suggestions and recommendations of my supervisor during the course of this research work have been invaluable.

I would like to express my gratefulness to **Late Professor Shigeru Koyama** and **Professor Takahiko Miyazaki** for their invaluable suggestion and encouragement throughout my entire study life in Japan. **Professor Shigeru Koyama** was a great researcher and a nice friend. May his soul rest in peace.

I am indebted to my mentor **Associate Professor Kyaw Thu** for his guidance and advice at various stages of my doctoral work. An expert in the field of adsorption, his proficient inputs on research work and writing manuscript helped me a lot.

I would like to remember with great respect **Professor Kandadai Srinivasan** for teaching me about vapor compression refrigeration system in depth. He is a prominent researcher and a great motivator of my life.

I am also grateful to **Professor Yukihiro Higashi**, **Dr. Sourav Mitra**, **Dr. Animesh Pal**, **Dr. Sivasankaran Harish** for their valuable assistance and providing me the opportunity to discuss technical results of this work at any time. I express my gratitude to **Dr. Skander Jribi** for his valuable assistance at the beginning of my journey.

I acknowledge my thanks to **Associate Professor Enoki Koji** for hosting the domestic internship in University of Electro-Communications, Tokyo. I am very grateful to **Assistant Professor Nenad Miljkovic** to give me the opportunity to work with him in University of Illinois at Urbana-Champaign, USA.

I am thankful to **Professor Seong-Ho Yoon** and **Associate Professor Jin Miyawaki** for providing me a great chance to discuss and do experiments in his laboratory. Their wise guidance and support helped me a lot during my doctoral study. I express my gratitude to master student **Mr. Kouhei Kuroda** and **Mr. Tatsuya Tomoda** for helping me in the experiment and data analysis.

LIST OF PUBLICATIONS

Journal Publications

1. **M.A. Islam**, A. Pal, K. Thu, B.B. Saha, "Study on performance and environmental impact of supermarket refrigeration system in Japan", *Evergreen Joint Journal of Novel Carbon Resource Sciences & Green Asia Strategy*. Vol. 6, No. 2, pp. 168–176, **2019**.
   DOI: 10.5109/2321014.

2. Y. Higashi, N. Sakoda, **M.A. Islam**, Y. Takata, S. Koyama, and R. Akasaka, "Measurements of Saturation Pressures for Trifluoroethene (R1123) and 3,3,3-Trifluoropropene (R1243zf)", *Journal of Chemical and Engineering Data*. Vol. 63, No. 2, pp. 417–421, **2018**.
   DOI: 10.1021/acs.jced.7b00818.

3. K. Uddin, **M.A. Islam**, S. Mitra, J.B. Lee, K. Thu, B.B. Saha, S. Koyama, "Specific heat capacities of carbon-based adsorbents for adsorption heat pump application", *Applied Thermal Engineering*. Vol. 129, pp. 117–126, **2018**.
   DOI: 10.1016/j.applthermaleng.2017.09.057.

4. **M.A. Islam**, K. Srinivasan, K. Thu, B.B. Saha, "Assessment of total equivalent warming impact (TEWI) of supermarket refrigeration systems", *International Journal of Hydrogen Energy*. Vol. 42, No. 43, pp. 26973–26983, **2017**.
   DOI: 10.1016/j.ijhydene.2017.07.035.

5. M.S. Rahman, **M.A. Islam**, B.B. Saha, T. Nakagawa, S. Mizuno, "Structure determination of the ordered (2×1) phase of NiSi surface alloy on Ni(111) using low-energy electron diffraction", *Japanese Journal of Applied Physics*. Vol. 54, No. 12, pp. 125701, **2015**.
   DOI: 10.7567/JJAP.54.125701.

Book Chapter

1. **M.A. Islam**, B.B. Saha, "TEWI Assessment of Conventional and Solar Powered Cooling Systems", *Solar Energy: Systems, Challenges, and Opportunities,* Springer, **2019**.

Awards

1. **"President's Award"** from the President of Kyushu University for producing most excellent results as a team in the Kyushu University Challenge and Creation Project **2018** (Awarded on March 29, 2019).

2. **"HULT Prize Japan National Winner"** for the most innovative idea entitled "Distributed Cold Storage for Vegetables and Life Saving Drugs Without Electricity", Osaka, Japan, 20th May **2018**.

3. **"Best Oral Presentation Award"** for conference paper entitled "A Quantitative Approach to Analyze Total Equivalent Warming Impact (TEWI) for Supermarket Refrigeration System in Japan" presented at the 3rd International Exchange and Innovation Conference on Engineering and Sciences (IEICES), Kyushu University, Japan, 19–20th October **2017**.

Presentation at an International Conference

1. **M.A. Islam***, K. Uddin, A. Pal, K. Thu, Nasruddin, M.I. Alhamid, B.B. Saha, "Measurement and Evaluation of the Specific Heat Capacity of Silica Gels for Adsorption Heat Pump Applications", International Conference on Polygeneration (ICP), Kyushu University, Japan, pp. 53–54, 15–17th May **2019**. [Poster]

2. **M.A. Islam***, A. Pal, K. Thu, B.B. Saha, "Specific heat capacity of mangrove and waste palm trunk in raw, carbonized and activated form", 4th International Exchange and Innovation Conference on Engineering & Sciences (IEICES 2018), Kyushu University, Japan, pp. 151–152, 18th October **2018**. [Poster]

3. **M.A. Islam***, S. Mitra, K. Thu, B.B. Saha, "A Quantitative Approach to Analyze Total Equivalent Warming Impact (TEWI) for Supermarket Refrigeration System in Japan", 3rd International Exchange and Innovation Conference on Engineering and Sciences (IEICES), Fukuoka, Japan, pp. 97–100, 19–20th October **2017**. [Oral]

4. Y. Higashi*, N. Sakoda, **M.A. Islam**, Y. Takata, "Saturation Pressure Measurements for New Low-GWP Refrigerants", 38th Japan Symposium on Thermophysical Properties (JSTP), Tsukuba, Japan, 7–9th November **2017**. [Oral]

5. **M.A. Islam***, K. Srinivasan, B.B. Saha, K. Thu, "Assessment of Total Equivalent Warming Impact (TEWI) of Supermarket Refrigeration in Japan", Innovative Materials for Process in Energy Systems (IMPRES), Taormina, Sicily, Italy, pp. 169–170, 23–26th October **2016**. [Oral]

6. M. Ono*, T. Nakamura, **M.A. Islam**, K. Enoki, T. Okawa, M. Ozawa, "Boiling Heat Transfer and Flow regime of Water Flowing Vertically Upward in a Mini-channel", 4th International Forum on Heat Transfer (IFHT), Sendai, Japan, pp. 4–9, 2–4th November **2016**,. [Oral]

7. **M.A. Islam***, B.B. Saha, S. Jribi, K. Thu, T. Miyazaki, S. Koyama. "Adsorption isotherms and kinetics of ethanol onto powder and consolidated activated carbon", 2nd International Exchange and Innovation Conference on Engineering and Sciences (IEICES), Fukuoka, Japan, pp. 2–5, 19–20th October **2016**. [Oral]

* Presenting Author.

Presentation at a Domestic Conference and Symposium

1. **M.A. Islam***, B.B. Saha, J. Miyawaki, S.–H. Yoon, "Pore Modification to Enhance the Quality of Adsorbent for Heat Pump Applications". I^{2}CNER, Kyushu University, Ito Campus, Japan, July 10th **2019**. [Poster]

2. T. H. Rupam*, **M.A. Islam**, A. Pal, K. Uddin, K. Thu, B.B. Saha, "Thermodynamic Property Fields for Various Adsorbent/Adsorbate Pairs", Cross Straits Symposium (CSS), Energy and Environmental Science and Technology (EEST), Pusan National University, Korea, 26–28th November **2018**. [Oral]

3. **M.A. Islam***, S. Mitra, K. Thu, B.B. Saha, "Environmental Impact of Supermarket Refrigeration System", Kyushu University Educational Reform Symposium 2017, Japan, 8th July **2017**, Ito Campus, Kyushu University. [Poster]

4. **M.A. Islam***, K. Uddin, K. Thu, B.B. Saha, S. Koyama, "Specific Heat Capacity Measurements of Functional Activated Carbons", I^{2}CNER, Kyushu University, Ito Campus, Japan, 28–29th June **2017**. [Poster]

5. **M.A. Islam***, B.B. Saha, "Total Equivalent Warming Impact (TEWI) Evaluation of a Typical Supermarket Refrigeration System in Japan". Q-pit Energy week, I^{2}CNER, Kyushu University, Ito Campus, Japan, 31st January **2017**. [Poster]

6. **M.A. Islam***, N.A. Lestari, F. Hazwani, W. Shun, K. Oyama, S. Dwiki, S. Matsumoto, T. Fujisaki, "e-Waste Management", International Forum for Green Asia 2016, Kyushu University, Japan, 1st December **2016**. [Oral]

7. **M.A. Islam***, B.B. Saha, K. Thu, "Adsorption Isotherms and Kinetics of Ethanol onto Powder and Consolidated Activated Carbon", International Forum for Green Asia 2016, Kyushu University, Japan, 31st November **2016**. [Poster]

8. **M.A. Islam***, M.S. Rahman, B.B. Saha, T. Nakagawa, S. Mizuno, "Structure Determination of the Ordered (2×1) Phase of NiSi Surface Alloy on Ni(111) using LEED", The 2nd Joint Symposium of Kyushu University and Yonsei University, Yonsei University, Seoul, Korea, 3–6th February **2016**. [Oral]

9. **M.A. Islam***, A.B.M. Berhanu, D. Felix, N.T.P. Hao. "Feasibility of Vehicle to Grid Technology", Summer Course 2015 in Oki Island, Okinoshima, Shimane, Japan, 17–21st August **2015**. [Oral]

* Presenting Author.

Contents

List of Figures

List of Tables

Nomenclature

b	adsorption affinity	[kPa^{-1}]
b_0	adsorption affinity at infinite temperature	[kPa^{-1}]
C	adsorption uptake	[kg kg^{-1}]
C_0	saturated amount adsorbed	[kg kg^{-1}]
D	particle diameter	[mm]
E	characteristic energy	[J mol^{-1}]
E_p	electricity consumption	[kWh]
h	enthalpy	[kJ kg^{-1}]
h_{fg}	latent heat of vaporization	[kJ kg^{-1}]
k	constant for pseudo saturated vapor pressure equation	[−]
m	mass	[kg]
M	molar mass	[g mol^{-1}]
n	heterogeneity parameter	[−]
P	pressure	[kPa]
P_c	critical pressure	[kPa]
P_s	saturated vapor pressure	[kPa]
Q	cooling/condensing capacity	[kW]
Q_{st}	isosteric heat of adsorption	[kJ mol^{-1}]
R	universal gas constant	[J mol^{-1} K^{-1}]
S	entropy	[kJ kg^{-1} K^{-1}]
t	heterogeneity parameter	[−]
T	temperature	[°C]
T_c	critical temperature	[°C]
T_t	triple point temperature	[°C]
υ_a	adsorbent pore volume	[cm^3 g^{-1}]
V_m	molar volume	[cm^3 g^{-1}]

V_t	triple point molar volume	[cm^3 g^{-1}]
W	instantaneous volumetric adsorption uptake	[cm^3 g^{-1}]
W_0	maximum volumetric adsorption capacity	[cm^3 g^{-1}]
y	number of years	[–]

Greek Symbols

α	thermal expansion coefficient of the adsorbed gas	[K^{-1}]
ε	CO_2 emission factor for per unit electricity generation	[kg-CO_2 eq./kWh]
η	efficiency	[%]
ϕ	uptake	[kg kg^{-1}]
Θ	surface coverage	[–]
$\dot{m}$	mass flow rate	[kg h^{-1}]
ρ	density	[kg L^{-1}]

Subscripts

$a-d, a'-d'$	state points of refrigeration cycle
ads	adsorption
c	cooling load
com	compressor
con	condenser
dis	discharge gas
eva	evaporator
liq	liquid
m	material
in	input
$isen$	isentropic
r	refrigerant
sub	subcooling
suc	suction gas
sup	superheating
vap	vapor

Superscripts

I	stage–1
II	stage–2

Acronyms

AC	activated carbon	
ACS	adsorption cooling system	
AHP	adsorption heat pump	
ASHRAE	American society of heating, refrigerating and air-conditioning engineers	
BET	Brunauer–Emmett–Teller	
CCHP	combined cooling, heating, and power systems	
CFC	chlorofluorocarbons	
COP	coefficient of performance	[–]
CVD	chemical vapor deposition	
DSC	differential scanning calorimetry	
GHG	greenhouse gas	
GWP_{100}	global warming potential (100 years integration)	[kg–CO_2 eq.]
HFC	hydrofluorocarbon	
HCFC	hydrochlorofluorocarbons	
HT	high temperature	
kWh	kilowatt–hour	
LT	low temperature	
M	mangrove	
MOF	metal–organic framework	
MT	medium temperature	
MVCR	mechanical vapor compression refrigeration	
sccm	standard cubic centimeters per minute	
t	tonne	
TEWI	total equivalent warming impact	[t–CO_2 eq.]
TGA	thermogravimetric analysis	
VCR	vapor compression refrigeration	
WPT	waste palm trunk	

Chapter 1

Introduction

Temperature is the most significant environmental variable that needs to be controlled for both living and non-living beings to live a healthy and comfortable life. Outdoor temperature variation depends on the location and season changing pattern of that region. However, indoor heat can be regulated by installing refrigeration/air-conditioning systems. Development of modern mechanical vapor compression refrigeration (MVCR) system started few hundred years ago. At that era, achieving cooling was more important than worrying about saving the environment. Nowadays, usage of cooling/refrigeration systems in the whole world have enormously increased. Hence, these cooling systems are greatly responsible for environmental degradation such as global warming. A huge natural catastrophe is obvious if the concept of current cooling system is not changed. Adsorption cooling technique is the most prospective candidate resolve this critical issue. A quantitative assessment of global warming has been performed for both conventional system (MVCR) and adsorption cooling system (ACS). The results of the analysis of confirms the fact that current MVRC releases 60 to 85% more global warming gases than ACS. Hence, adsorption cooling systems are becoming more popular gradually. However, these systems have poor performance and huge size. Therefore, this chapter discusses about the motivation of this thesis and the approach to improve the existing adsorption cooling systems by material characterization, material modification and finding novel functional pairs. The ultimate goal and outline of this thesis are presented in the later part of the chapter.

1.1 Background

Ozone layer depletion and global warming are the most alarming environmental issues nowadays. Conventional mechanical vapor compression refrigeration (MVCR) systems are the major contributor of these global issues [1]. An MVCR can release global warming gases directly (refrigerant leakage having high GWP) and indirectly (electricity generation process that is used to drive the MVCR system and materials extraction process that is used to build the system). Rules and regulations defined in Montreal (1987) and

Kyoto (1997) protocols have already phased out the ozone depleting refrigerants such as CFCs and HCFCs. Currently used refrigerants still have high global warming potential and needs to be replaced with low GWP refrigerants to diminish the direct warming impact [2]. Moreover, indirect global warming impact can be reduced by decreasing the electricity consumption and increasing the lifetime of the system. All these requirements are satisfied in adsorption cooling systems. Natural refrigerants (e.g. water, ethanol, ammonia) are used in adsorption cooling system hence there is no direct emission. Electricity consumption is 80 to 90 % lower than conventional cooling systems and life time is almost double [3]. Hence, indirect emission can also be significantly reduced. However, the adsorption cooling technique started developing few decades ago and still have a lot of scopes for improvement.

1.2 Refrigeration technique

1.2.1 Mechanical vapor compression refrigeration (MVCR) system

A simple MVCR system with basic components is depicted in Fig. 1.1. A working fluid flows through the various sections of this system, changes its phase due to pressure variation and provides the desired cooling.
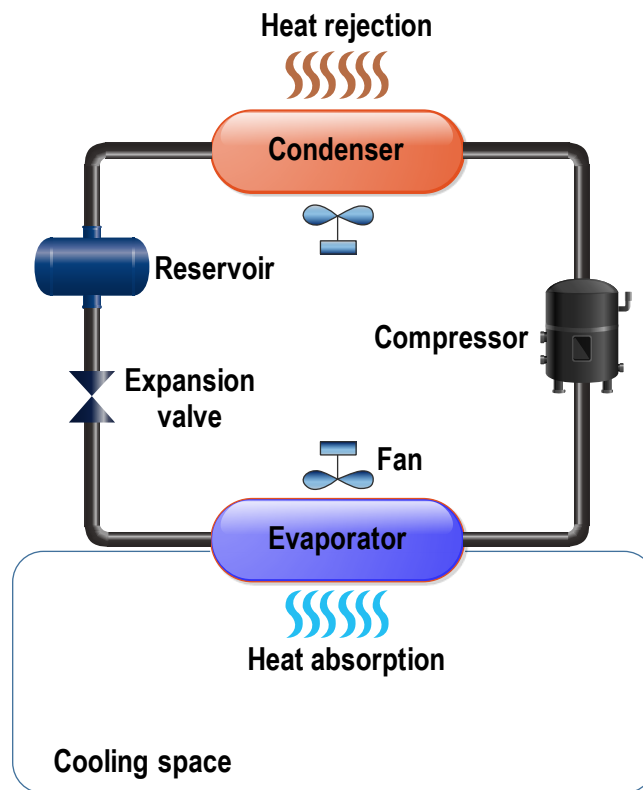
Fig. 1.1.   Mechanical vapor compression refrigeration (MVCR) system.

Liquid refrigerant is accumulated into the reservoir and a certain amount is pumped to the evaporator through the expansion valve. The capillary end of expansion device sprinkles the liquid refrigerant to evaporator section and vaporizes due to low pressure. During evaporation, latent heat of vaporization is collected from the surroundings which cools down the space at some degree. This vapor refrigerant is then pumped to the compressor section and get compressed at very high pressure. Temperature of the vapor refrigerant increases a lot due to the high pressure. This superheated vapor is passed through the condenser coil and cooled down naturally. Heat is rejected to the environment and the refrigerant changes its phase to liquid due to temperature drop. This liquid refrigerant is collected again into the reservoir and pumped to evaporator. In this way, the cycle continues until the desired temperature is reached.

1.2.2 Adsorption cooling system (ACS)

A two bed adsorption cooling system is illustrated in Fig. 1.2. The major difference with conventional MVCR is the replacement of mechanical compressor with thermal compressor namely, adsorption/desorption bed. Additionally, commonly used refrigerants in MVCR system are HFC based and possess very high GWP. However, natural refrigerants (e.g. water, ammonia, CO_2, ethanol) with negligible GWP is used in the ACS.

The adsorption/desorption bed contains the adsorbent material. This material are porous and can adsorb the refrigerant molecule. The adsorption stage is analogous to the suction of refrigerant by the compressor for a MVCR. When one bed is adsorbing the refrigerant, the other bed is desorbing the refrigerant by flowing hot water through the heat exchanger of the bed. The desorption process is analogous to the release of refrigerant from the discharge line of the compressor. The adsorption and desorption bed switches their operation after a certain duration. This switching can be controlled by the valves $V_1 - V_4$.
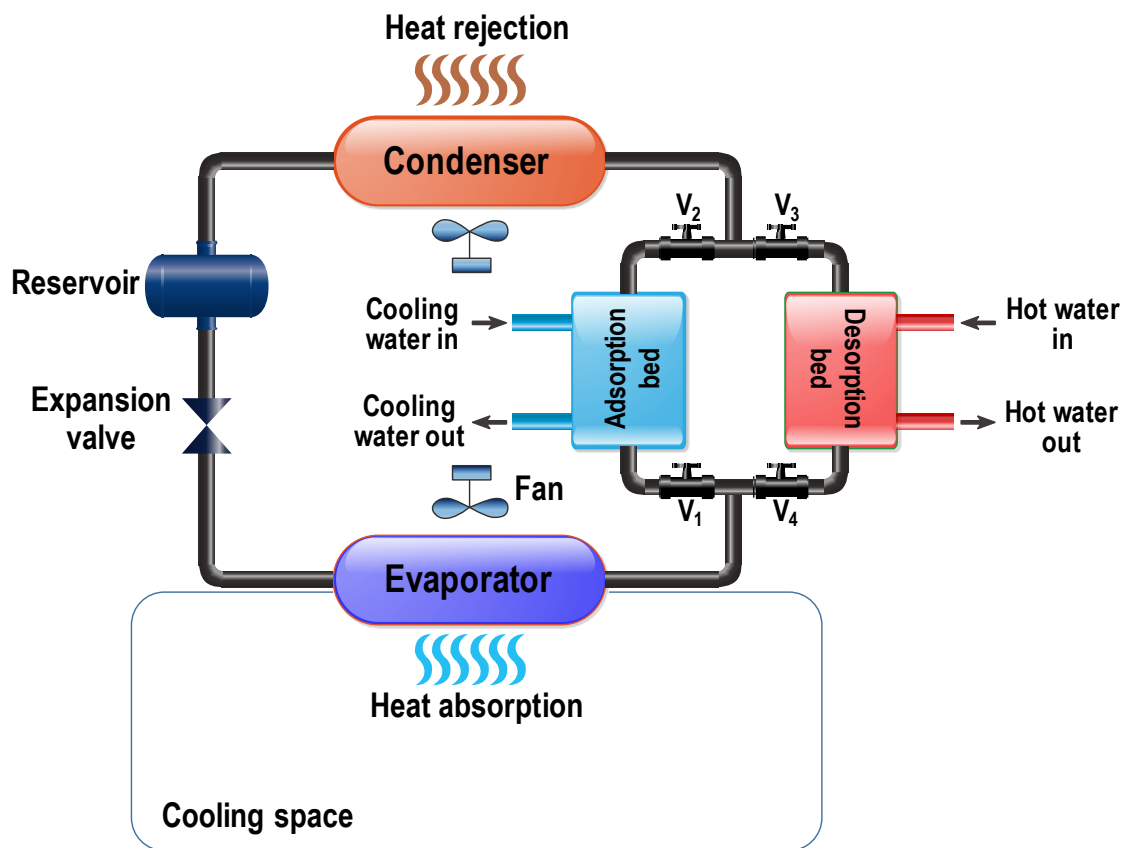
Fig. 1.2.   Adsorption cooling system (ACS).

1.3   Advantages and shortcomings

The following Table 1.1 illustrates the major benefits and drawbacks of both mechanical vapor compression and adsorption cooling systems. Adsorption cooling systems is undoubtedly more environment friendly than the conventional systems. However, the drawbacks are of major concern and needs to be resolved to design an efficient system.

Table 1.1. Comparison of mechanical vapor compression and adsorption cooling system.

	MVCR	**ACS**
Advantages	• Compact size	• Low electricity consumption
	• High COP	• Natural refrigerant
	• Low cost	• Waste heat utilization
	• Wide operating temperature range	• Low temperature heat source required
	• Commercially available and lots of choices	• Low noise and less vibration
		• Less moving parts
		• Long lifetime ($\approx$ 25 years)
		• Lower maintenance required
Shortcomings	• High electricity consumption	• Large size
	• High GWP refrigerant	• Initial cost very high
	• High pressure, more leakage	• Low thermal COP
	• Noisy and more vibration	• Insufficient data about functional pairs
	• High voltage required	• Limited operating temperature range
	• A lot of moving parts	• Few manufacturers
	• Short lifetime ($\approx$ 15 years)	

1.4   Motivation and objectives

The motivation of this research is originated from the drawbacks of adsorption cooling systems. Adsorption cooling technology is still tender and there are insufficient data about the adsorbents, refrigerants and other parameters that affects the system performance. Hence, the research mainly stresses, firstly, on the characterization of commonly used adsorbents. Porous properties such as surface area, pore size, pore volume, pore size distribution of six types silica gel samples have been reported. Specific heat capacity of those silica gel samples, four types of activated carbons and two types of thermal conductivity enhancer is also investigated. Secondly, selective removal of unusable ultramicropores from activated carbon have been studied. Two organic compounds (methane and benzene) are used for the pore blocking process. Thirdly, adsorption characteristics of two biomass derived activated carbon with low GWP

refrigerant R32 is experimentally investigated. The carbon samples have benchmark uptake which indicates the development of a promising adsorption cooling system to cope with the next generation cooling applications. To achieve the above mentioned objectives, following initiatives have been taken and the results are reported in this thesis:

I. A quantitative assessment of annual total equivalent warming impact generated from conventional vapor compression system and adsorption cooling system have been performed. The results of this assessment suggests the superiority of adsorption cooling system from the environmental safety perspective.

II. Porous and thermophysical properties of the adsorbents are most important to simulate and predict the performance of existing cooling systems. Hence, porous properties such as surface area, pore volume, pore size distribution of RD, type A, type B, indicator type A, chromatorex and home silica gel samples have been experimentally investigated. N_2 adsorption technique is adopted for the experiment and DFT analysis is performed to obtain pore size distribution.

III. Specific heat capacity of adsorbents greatly affect the desorption process. Researchers typically use a constant value of specific heat capacity to determine the adsorption bed characteristics. However, the specific heat capacity changes with temperature. Hence, the specific heat capacity of the above mentioned silica gels have been measured using differential scanning calorimetry. The measurement temperature range is chosen from 30 to 100 °C which is the typical operating temperature range of an adsorption cooling system.

IV. Specific heat capacity of four types activated carbon (Maxsorb III, H_2 treated Maxsorb III, KOH-H_2 treated Maxsorb III, and spherical phenol resin derived activated carbon) and two types of thermal conductivity enhancer (EC-1000 and EC-1500) have been measured.

V. Specific heat capacity data of silica gel, activated carbon and expanded graphite is fitted with a temperature depended Green–Perry equation and the adjustable parameters have been optimized to fit with the equation.

VI. Unusable ultramicropores of activated carbon degrades the performance of a system. Removal of those pores can improve the quality of the adsorbent and hence enhance the performance of the cooling system. Chemical vapor deposition at elevated temperature is performed to block those ultramicropores. Methane and benzene is used as the carbon source to deposit into the pores.

VII. Adsorption isotherm of two novel pairs M–AC/R32 (R32 onto mangrove derived activated carbon) and WPT–AC/R32 (R32 onto waste palm trunk derived activated carbon) have been experimentally investigated. Highly accurate thermogravimetric analysis (TGA) data shows remarkably high uptake.

VIII. Experimental data is theoretically analysed and successfully correlated with well-known D–A and Tóth models. The adjustable parameters are optimized to minimize the fitting error at an acceptable range.

IX. Variation of isosteric heat of adsorption with surface coverage have been theoretically determined with a temperature dependent modified Clausius-Clapeyron equation.

1.5 Organization of the thesis

The thesis includes seven chapters explaining the various theoretical and experimental findings. Adsorption characterization, pore structure modification and adsorption characteristics have been studied for novel pairs. The arrangement of the thesis is as follows:

Chapter 1: Introduction

Chapter 2: Literature review: Scientific advancement of cooling systems

Chapter 3: TEWI comparison of cooling systems

Chapter 4: Specific heat capacity measurement of potential adsorbents

Chapter 5: Pore shaping to enhance the quality of adsorbents

Chapter 6: Adsorption characteristics and isosteric heat of adsorption determination for biomass derived activated carbon/R32 pair

Chapter 7: Overall conclusions and recommendations

The key points of each chapter are given as follows:

Chapter 1 gives an overview of the working principle of conventional vapor compression system. Their advantages and limitations are compared to make a decision which system is better and where are the scopes of improvement. Finally, this chapter clarifies the motivation and objectives of the thesis.

Chapter 2 provides a comprehensive literature review of the historical progress of cooling systems. The conventional vapor compression system became very popular after the invention of Freon in 1930. However, adsorption cooling system attracted the attention of people in 1970 when energy crisis and heavy environmental pollution started to occur. The development of adsorption cooling system and the scope of improvement related to this research work is also discussed in this chapter.

Chapter 3 explains the procedure to assess environmental impact of a cooling system. Same operating conditions are set and some necessary assumptions are considered to evaluate total equivalent warming impact (TEWI) from both mechanical vapor compression refrigeration (VCR) system and adsorption cooling system (ACS). Three types of applications have been considered for this assessment: residential cooling, medium temperature applications and low temperature applications. Results of assessment are compared to know which system causes more environmental damage and how severe that is.

Chapter 4 explains the N_2 adsorption technique to evaluate the porous properties of any adsorbent material. Differential scanning calorimetric (DSC) method is also described to measure the specific heat capacity of the adsorbent material for a particular temperature range. Since this properties greatly affect the performance of an adsorption cooling system, it is necessary to evaluate this parameters before designing an actual system. Most commonly used adsorbents such as silica gel and activated carbons are experimentally investigated. Pore size distribution and specific heat capacity variation of the same sample with different particle sizes is also observed. The comparison of their porous properties and specific heat capacity gives an insight of which adsorbent could be better for cooling system.

Chapter 5 illustrates the method to modify the pore structure of activated carbon to enhance its quality as an adsorbent. Pyrolysis of organic materials onto activated carbon has been performed in an inert environment at elevated temperature. Carbon atoms are deposited and block undesired micropores/mesopores. Pyrolization material (methane and benzene), time, flow rate and temperature is varied to find the optimum value that blocks

only the unusable pores. Porous properties of modified activated carbon is also determined with N_2 adsorption experiment to understand the effect of pyrolization.

Chapter 6 presents the adsorption isotherms of two novel adsorbent/adsorbate pairs at adsorption temperature 30, 50, 70 and 90 °C. The adsorbents are mangrove and waste palm derived activated carbon. The selected adsorbate is current generation working fluid HFC32 having low GWP. Experimental data is fitted with two well-known adsorption isotherm model known as D–A and Tóth. Isosteric heat of absorption is also quantified for both the pairs as a function of adsorption temperature and surface coverage. A modified Clausius-Clapeyron method is adopted to study the behaviour of isosteric heat of adsorption.

In Chapter 7, the thesis ends with the major findings where the originality and contribution of the author, and recommendations for future improvement have been made. It is concluded that RD silica gel with large particle size have better porous properties and specific heat capacity among all the studied silica gel samples. Among the investigated carbon samples, spherical phenol resin based sample is found to be superior. However, the possibility of using natural adsorbents and consolidated composite samples need to be explored. Pore shaping concept explained in chapter 5 is very effective to improve the quality of adsorbent. The method needs more research to get better selective removal. Finally, studied adsorption characteristics of biomass derived activated carbon with R32 refrigerant opens the door to design a high performance next generation cooling system.

Chapter 2

Literature review: Scientific advancement of cooling systems

High demand of heating, ventilation, air conditioning, and refrigeration (HVAC&R) system has created a highly competitive global market for the HVAC&R manufacturing industries. The technology is available for the past 200 years and each component of the system has already been grown to a matured stage because of its extremely potential business opportunity. Researchers have invented the most efficient heat exchangers, developed advanced compressors for wide-ranging applications, identified and characterized various refrigerants which are suitable for specific applications, introduced auxiliary circuits (e.g. subcooling, superheating) to increase the efficiency of the system. Therefore, current systems are very compact, sophisticated and energy consumption is also low (high COP). However, it possesses one major drawback – the system has negative impact on the environment. It produces huge amount of greenhouse gases by releaising high GWP refrigerants to the environment. The system also contributes indirectly to global warming by consuming electricity. Both the problems can be resolved to a great extent by replacing the mechanical compressor by a thermal compressor (also called adsorption bed) and by switching from high GWP synthetic refrigerants to natural refrigerants. However, the switching is not so straightforward, since the thermodynamic properties of the refrigerants are different. The compatibility of the functional pair must be verified before using in an adsorption cooling system. Adsorbents with superior porous and thermophysical properties is required to design an efficient adsorption cooling system. Hence, all the potential adsorbents should be characterized accurately and new high quality adsorbents could be synthesized. This chapter discusses about the historical development of conventional mechanical vapor compression system and adsorption cooling system. Moreover, a summary of the literatures related to this research work is also presented in this chapter.

2.1 Mechanical vapor compression refrigeration (MVCR) system

2.1.1 History

"Abortion of a Young Steam Engineer's Guide" – a book written by Oliver Evans and published in 1805, describes a closed refrigeration cycle which is able to produce ice by using ether under vacuum condition. However, he did not propose any system. Later, Jacob Perkins patented a design of cooling system in 1834 and John Hague made the design into a working model [4]. The working fluid of the system was ether. The schematic and photograph of first ever built freezing system is shown in Fig. 2.1. James Harrison made a practical vapor compression refrigeration system and patented in 1856 using ether, alcohol or ammonia. David Boyle (1871) and John Enright (1876) made MVCR system with NH_3; Linde (1882), Franz Windhausen (1886) and T.S.C. Lowe (1887) used CO_2 as working fluid; Raoul Pictet (1875) designed a system with toxic refrigerant SO_2; C. Vincet (1878) used anaesthetic methyl chloride as refrigerant; Palmer (1890) used ethyl chloride; Edmund Copeland and Harry Edwards (1920) used isobutene; dichloromethane (CARRENE) was commercially used by renowned manufacturer Carrier for their centrifugal compressors in 1926 – 1933 [4].

<div align="center">(a)   (b)</div>
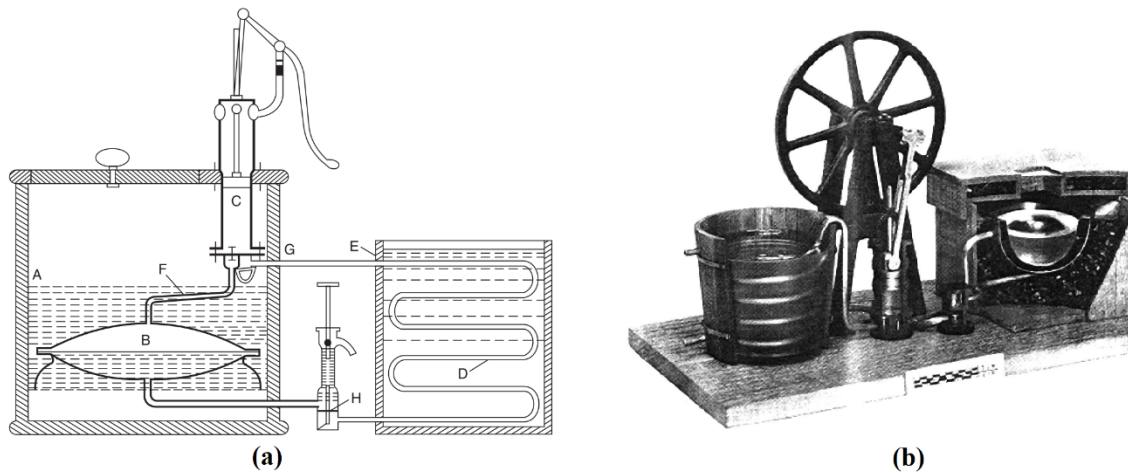
Fig. 2.1.   (a) Schematic of J. Perkins model (b) Perkins apparatus built by J. Hague [4].

2.1.2 Refrigerants

Selecting refrigerant is the most significant task before designing a cooling system. Table 2.1 shows the expected properties of a refrigerant with reasons.

Table 2.1. Expected properties in a refrigerant.

Desired property	Significance
● Low freezing and boiling point	Operation range depends on these points
● High COP	To reduce the power consumption cost
● Zero ozone depleting potential (ODP) and low global warming potential (GWP)	To ensure environmental safety
● High critical temperature and pressure	Power consumption depends on critical points
● High latent heat of vaporization	A high enthalpy of vaporization means more heat removal during cooling
● Temperature – pressure relation	To understand the refrigeration cycles and leakage probability.
● High vapor density	To reduce the size of the compressor
● High thermal conductivity	For efficient heat transfer
● Non-flammable, non-toxic, non-corrosive	To avoid health hazards and ensure safety
● Cost and availability	To reduce the manufacturing cost

People were not very concerned about the environment even few decades ago. Hence, they were using any refrigerant that was fulfilling their requirements. For example, CFCs and HCFCs such as R11, R12, R22, R113, R114, R115, R123, R124 are frequently used in the cooling applications. Most of these refrigerants have high ozone depleting potential and high global warming potential [5,6]. These refrigerants are gradually phasing out because of the regulations of Montreal and Kyoto protocol [2,7,8].

Current generation refrigerants are HFC and HFC blends such as R32, R134a, R152a, R404A, R410A, R507A [6]. These refrigerants do not have ODP but they have high GWP. Hence, many of them will be phasing out soon according to Montreal and Kyoto protocol. The refrigeration industries are trying to find very low GWP refrigerants such as HFOs and also trying to use natural refrigerants in their system. CO_2 system is commercially available in the market. However, they operate in very high pressure transcritical region. None of these refrigerants are perfectly meeting all the desirable

conditions of an ideal refrigerant. Therefore, the refrigeration industry is in a great crisis and they are unable to develop a vapor compressor cooling system that have very low environmental impact.

2.1.3 *Heat exchanger*

A heat exchanger is a medium that is used to transfer thermal energy (i.e. enthalpy) between two or more fluids. In heat exchangers, there are usually no external heat and work interactions [9]. A vapor compression refrigeration system requires heat exchanger in both evaporator and condenser. Heat exchanger design for cooling system is one of the most challenging task. The efficiency of the cooling system greatly depends on the material and geometry of the heat exchanger [10]. Heat exchanger classification according to their shape is shown in Fig. 2.2. A heat exchanger is typically made of heat transfer elements such as a core or matrix containing the heat transfer surface, and fluid distribution elements such as headers, manifolds, tanks, inlet and outlet nozzles, pipes, or seals. Shell and tube type heat exchanger is typically used in the evaporator and condenser [11]. Numerous researchers are designing new heat exchangers and testing the performance of their invented prototype [12] as shown in Fig. 2.3.
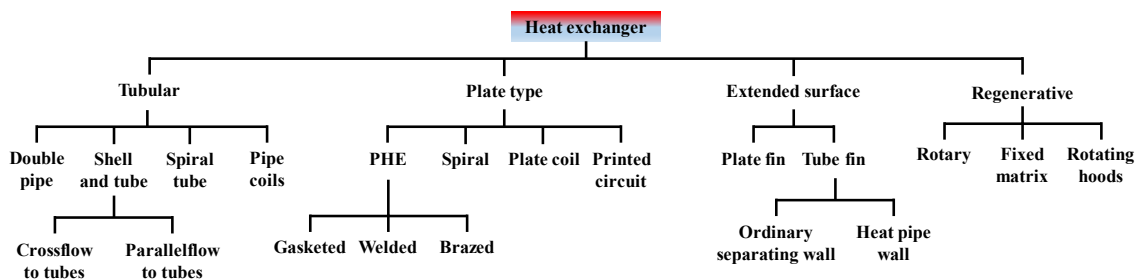
Fig. 2.2.   Classification of heat exchanger according to construction [9].

(a)

(b)
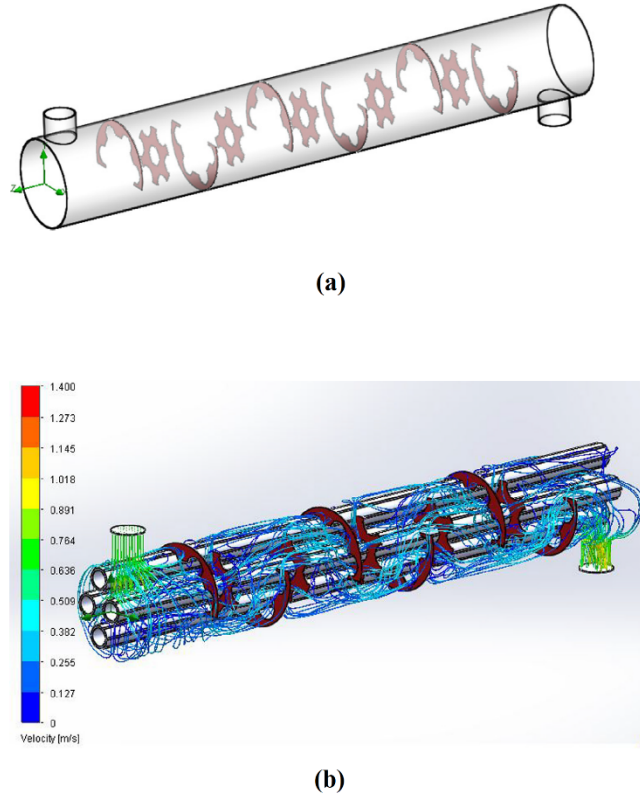
Fig. 2.3. (a) Modified shell and tube heat exchanger with combined segmental-disk baffle, (b) Simulation result of velocity path line [12].

2.1.4 Compressor

Compressor is that component of the conventional cooling system, which consumes about 90% of the electricity. Previous generation compressors had constant speed and hence they consumed more electricity [13]. Current generation advanced compressors are inverter type that is capable of varying speed according to the temperature requirement. They are highly efficient, have high COP and consume low power. Some modern compressors from renowned compressor manufacturer Bitzer is shown in Fig. 2.4.

1. R134a emergency system
2. LT compressors
3. MT/Parallel compressors
4. LT supply/return header
5. MT supply/return header
6. MT receiver
7. Oil separator & reservoir
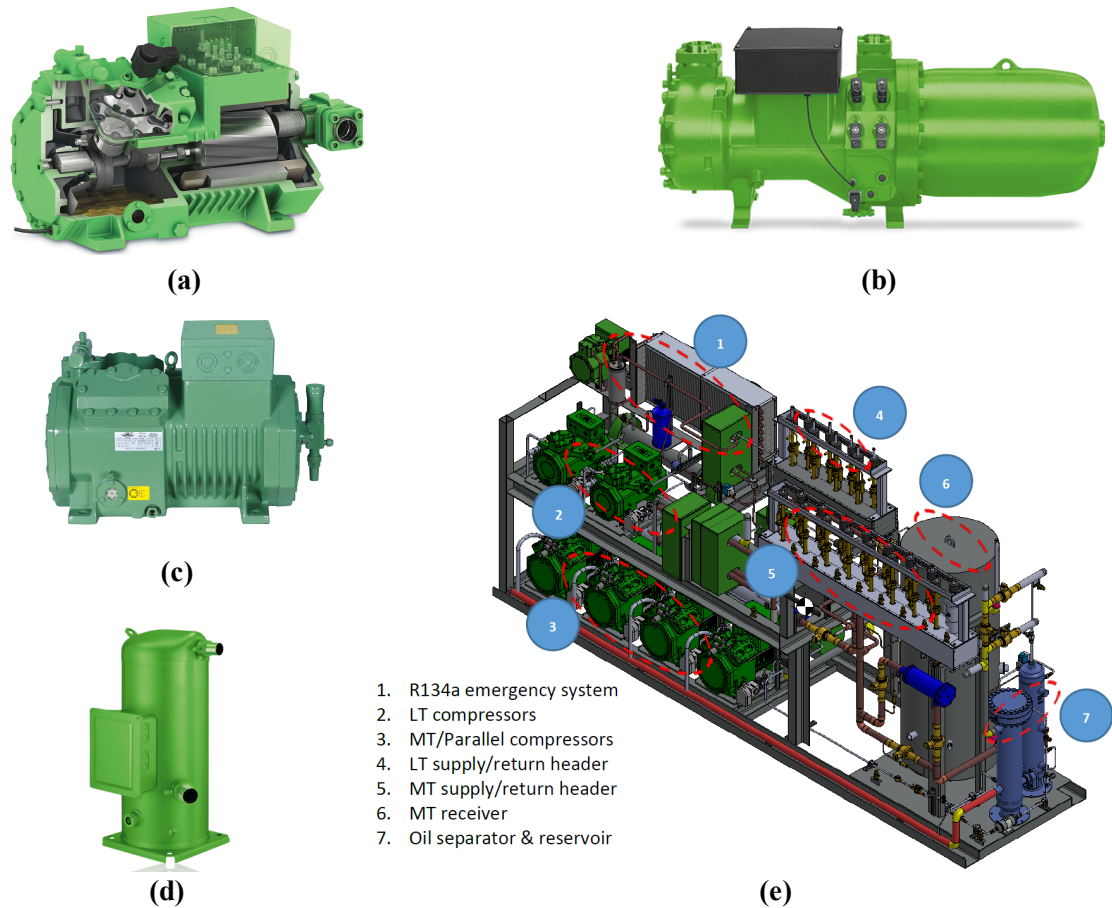
Fig. 2.4. Modern compressor models (a) Semi-hermetic reciprocating compressor, (b) Semi-hermetic screw compressor, (c) Open type reciprocating compressor, (d) Hermetic scroll compressor, (e) CO_2 booster rack [14].

2.2 History of adsorption cooling system

Faraday discovered the adsorption phenomena in 1848. He found that cooling could be obtained by adsorbing NH_3 onto AgCl. Later, G. E. Hulse (1920) proposed a cooling system with silicagel/SO_2 as working pair to preserve the food in train. The heat source of this system was from propane combustion and the heat exchanger fluid was air. The evaporation temperature could reach up to 12 °C. R. Plank and J. Kuprianoff proposed another adsorption cooling system with activated carbon/methanol pair. In 1930s, Freon is invented and the vapor compression became very popular. Hence, the development of adsorption cooling system halted for a very long time. In 1970s, energy crisis started to happen and in 1990, environmental pollution became very serious. Hence, the adsorption cooling technology again attracted the attention of researchers. In 1986, a commercial

adsorption chiller was marketed by Nishiyodo Kuchouki Co., Ltd. The working pair of that system was silica gel/water [15]. The schematic of that chiller is shown in Fig. 2.5. The chilling water temperature was 3 °C and heat source temperature was 50 – 90 °C.
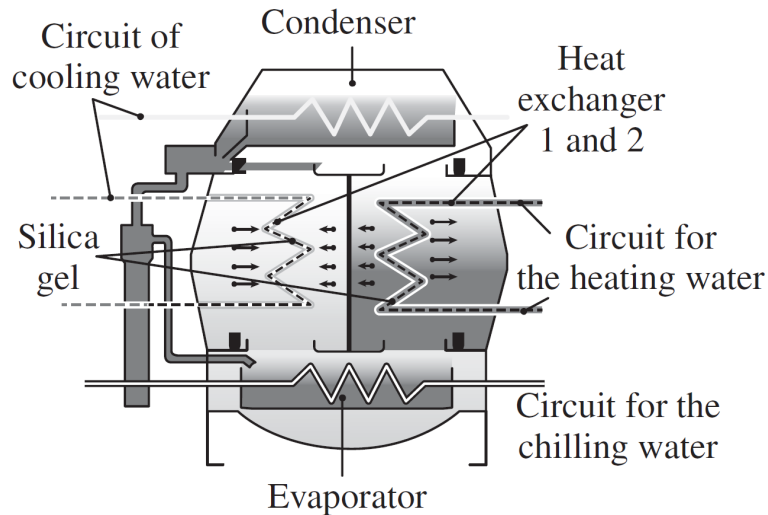
Fig. 2.5.   Silica gel/water adsorption system from Nishiyodo Kuchouki Co., Ltd.

In 2003, a Japanese company named Macom commercialized silica gel/water adsorption chiller. Chilling water output of that system was 14 °C, heat source temperature 75 °C with a COP of 0.6.

In 2003, Tokai Optical Co., Ltd. introduced an adsorption CCHP system powered by waste heat. They claimed that 10% energy consumption and 12% CO_2 emission could be reduced annually by installing such a system.

2.3   Material characterization

Silica gel (SG), activated carbon powder (ACP), activated carbon fiber (ACF), zeolite, metal oxide framework (MOF) are the most popular options to use as adsorbent. Many researchers are developing consolidated composites by using a small amount binders with these adsorbents [16–18]. The consolidation would increase the packing density and the adsorption bed would be smaller. The porous and thermophysical properties of these materials are very important to predict the performance of an adsorbent.

2.3.1 Porous properties measurement

Adsorption capacity and kinetics of an adsorbent mainly depends on the surface area, pore volume and pore size distribution of that material. The porous properties of some common adsorbents that are reported by the researchers are presented in Table 2.2. These information implicates which adsorbents are microporous and which are mesoporous. Adsorbate choice depends on the porous pore types. Surface area and pore volume indicates which sample would adsorb more amount of adsorbate. Hence, these data are very important before designing an adsorption cooling system.

Table 2.2. Porous properties of some common adsorbents.

Adsorbent Name	BET Surface area ($m^2 \, g^{-1}$)	Pore width (Å)	Pore volume ($cm^3 \, g^{-1}$)
Activated carbon (Maxsorb III) [19]	3045	11.20	1.70
Activated carbon from waste palm trunk [20]	2927	16.80	2.41
Activated carbon from Mangrove [20]	2924	14.70	2.13
Activated carbon fiber (A20) [21]	1900	21.60	0.765
Activated carbon fiber (A15) [21]	1400	21.75	1.028
Silica gel (RD) [22]	650	21.00	0.35
Silica gel (type A) [22]	650	22.00	0.36
Zeolite (AQSOA Z01) [23]	132	7.40	0.087
Zeolite (AQSOA Z02) [23]	590	3.70	0.2769
Natural zeolite [24]	29	4	–
MOF MIL-101 Cr [25]	4100	10, 16	2.0

2.3.2 Specific heat capacity

Specific heat capacity of an adsorbent is one of the key thermophysical parameter to design and optimization of an adsorption chiller. When the adsorption bed is designed, the equations contain the specific heat capacity term. Mitra et al. analysed the performance of

a two-stage air-cooled silica gel/water adsorption system. The following equation (2.1) is for the adsorption bed mentioned in their article.

$$\left[\left(Mc_p\right)^{I/II}_{bed} + \left(\phi M_{sg}\right)^{I/II}_{ads/des}\right]\frac{dT^{I/II}_{ads/des}}{dt} = \lambda M^{I/II}_{sg}\left(\frac{d\phi^{I/II}_{ads/des}}{dt}\right)h_{ads} - \dot{m}_{cw/hw}c_{p,w}\left(T^{I/II}_{cw/hw,out} - T_{cw/hw,in}\right) \quad (2.1)$$

Most of the researchers consider a constant value of specific heat capacity for their calculation [26–29]. Boelman et al.[30], Chihara & Mizuki [31] Saha et al. [32], Myat et al. [33], Thu et al. [34], Mitra et al. [35] and Ali & Chakraborty [36] have considered a constant specific heat capacity of silica gel in their investigations. Jribi et al. [37] used the specific heat capacity of Maxsorb III to be 1.375 kJ kg^{-1} K^{-1} to simulate an activated carbon/CO_2 based adsorption cooling system. Askalany et al. [38] assumed 0.930 kJ kg^{-1} K^{-1} for the specific heat capacity of granular activated carbon to estimate the performance of adsorption cooling system. Chan et al.[39] considered the specific heat capacity of zeolite 13X/$CaCl_2$ composite to be 0.836 kJ kg^{-1} K^{-1} for their system. However, the temperature of the beds is not always constant. Specific heat capacity of a material also varies with temperature. Hence, the calculation would be affected if a constant value is considered.

There are few literatures that present a detailed analysis of specific heat capacity with a function of temperature for the porous materials. Aristov [40] reported an approximation to present the specific heat of adsorbate-adsorbent pair and verified for $CaCl_2$/silica gel and zeolite 4A composite during water adsorption. Jiang et al. [41] measured the heat capacities and thermodynamic properties of powder MOF materials using temperature modulated differential scanning calorimetry (TMDSC). Kloutse et al. [42] measured specific heat capacity of five MOFs: MOF-5, Cu-BTC, Fe-BTC, MIL-53 (Al) and MOF-177 over a wide temperature range. They proposed polynomial fitting for their experimental data [43]. Uddin et al. measured the specific heat capacity of four types of activated carbon samples and two graphite samples within 30 – 150 °C temperature range. They correlated their experimental data with a temperature dependent specific heat capacity model, namely Green – Perry model.

18

2.4   Pore modification

The application area of adsorbents are very wide. Each application requires a certain set of characteristics. For example, activated carbon sample contains some percentage of ultramicropores (< 0.7 nm) and mesopores (> 2 nm) along with the regular micropores. In adsorption cooling applications, the ultramicropores do not participate in the adsorption due to their tiny size. Moreover, the mesopores slow down the adsorption rate. Hence, removal of these pores would definitely improve the performance of an adsorption cooling system.

Kawabuchi et al. [44] have investigated the chemical vapor deposition (CVD) of carbon from benzene and cyclohexane on a certain activated carbon fiber (ACF) sample. They varied the pyrolization temperature to find the optimum condition and obtained good result at 700 – 800 °C temperature. Sample mass increased about 11% due the pyrolysis of benzene and deposition of carbon in the pores. After a certain amount of deposition, reduction of pore size appeared to be limited by the thickness of the benzene plane and no further carbon deposit took place because the pore could no longer accept benzene. Their target application was molecular sieve separation of CH_4 from CO_2. The reshaped pores are capable of doing the task more efficiently and the target is fulfilled. Moreover, cyclohexane decomposed too rapidly and blocked all the pores. Thus, high molecular sieving selectivity could not be obtained with cyclohexane.

Verma et al. [45,46] observed the effect of heat treatment on activated carbon. The application is targeted to the gas separation. Their results shows that alteration of pore occurred and the sample is improved towards the targeted application. Kim et al. [47] investigated the decomposition of methane onto various types of activated carbon. The target application was CO_2 free hydrogen production. At 1123 decomposition temperature, most of the pores of activated carbon are blocked and the surface area becomes about 20 – 60 m^2/g. Sotowa et al. [48] modified a pitch-based activated carbon fiber by CVD of pyridine. Pyrolization temperature is varied from 500 to 725 °C. Surface area of parent sample (2149 m^2/g) decreased to 1265 m^2/g after the pyrolization. However, the pore size distribution of modified sample is not reported in that article. To the best of our knowledge,

pore modification of activated carbon was never targeted for the enhancement of the performance of adsorption cooling system.

2.5 Adsorption isotherm model

Adsorption isotherm of various functional pair is investigated and correlated with the well-established models. Dubinin–Astakhov [49,50], Tóth [51], Freundlich [52,53] and Langmuir [54,55] models are the widely used isotherm models which fits well with most of the functional pairs. Governing equation of D–A and Tóth models are represented by (2.2) and (2.6), respectively. The following Table 2.3 shows the fitting parameters of those model for various functional pairs investigated by the researchers.

D–A equation:
$$W = W_0 \exp\left[-\left\{\frac{RT \ln\left(\frac{P_s}{P}\right)^n}{ME}\right\}\right] \tag{2.2}$$

Here,
$$W = CV_m \tag{2.3}$$

$$V_m = V_t \exp\left[\alpha\left(T - T_t\right)\right] \tag{2.4}$$

$$\frac{P_s}{P_C} = \left(\frac{T_s}{T_C}\right)^k \tag{2.5}$$

Tóth equation:
$$C = C_0 \left[\frac{bP}{\left(1 + \left(bP\right)^t\right)^{\frac{1}{t}}}\right] \tag{2.6}$$

Here,
$$b = b_0 e^{\frac{Q_{st}}{RT}} \tag{2.7}$$

Table 2.3. Correlation coefficients of D–A and Tóth model from literature.

Functional pairs	Tóth isotherm parameters				D–A isotherm parameters			
	C_0	b_0	Q_{st}	t	k	W_0	E	n
Type A Silica gel/water [56]	0.4 kg kg^{-1}	(4.65 ± 0.9) $\times 10^{-10}$ kPa^{-1}	(2.71 ± 0.1) $\times 10^3$ kJ kg^{-1}	10	–	–	–	–
RD type Silica gel/ water [56]	0.45 kg kg^{-1}	(7.30 ± 2) $\times 10^{-10}$ kPa^{-1}	(2.693 ± 0.1) $\times 10^3$ kJ kg^{-1}	12	–	–	–	–
AQSOA-Z01 zeolite/water [23]	–	–	–	–	–	0.21 kg kg^{-1}	4 kJ mol^{-1}	5
AQSOA-Z02 zeolite/water [23]	–	–	–	–	–	0.31 kg kg^{-1}	7 kJ mol^{-1}	3
Natural zeolite/ water [24]	–	–	–	–	5.05	0.1219 kg kg^{-1}	–	1.4
Maxsorb III/ ethanol [57]	–	–	–	–	–	1.2 kg kg^{-1}	139 kJ kg^{-1}	1.8
KOH-H$_2$ treated Maxsorb III/ ethanol [57]	–	–	–	–	–	1 kg kg^{-1}	152 kJ kg^{-1}	1.9
H$_2$ treated Maxsorb III/ethanol [57]	–	–	–	–	–	1.2 kg kg^{-1}	138 kJ kg^{-1}	2
Maxsorb III/CO$_2$ [58]	2.3061 kg kg^{-1}	1.842 $\times 10^{-7}$ kPa^{-1}	19.297 kJ mol^{-1}	0.799	4.504	1.54 cm^3 g^{-1}	5.25 kJ mol^{-1}	1.326
Consolidated Maxsorb III/CO$_2$ [17]	2.05 kg kg^{-1}	6.67×10^{-5} kPa^{-1}	22.5 kJ mol^{-1}	0.6	4.844	1.109 cm^3 g^{-1}	5.42 kJ mol^{-1}	1.29
Spherical activated carbon SAC2/ HFC32 [59]	3.9981 kg kg^{-1}	2.2×10^{-7} kPa^{-1}	19.067 kJ mol^{-1}	1.8873	3.65	3.1344 cm^3 g^{-1}	3.4981 kJ mol^{-1}	1.0217

2.6   Isosteric heat of adsorption

Molecular interaction during adsorption and change in energy level of the adsorbate molecules is known as isosteric heat of adsorption (Q_{st}). The amount of released heat is partially absorbed by the adsorbent which causes a rise in adsorbent temperature and thus influences the rate of adsorption. Q_{st} depends on the functional pair. The isosteric heat of adsorption at constant uptake is evaluated from adsorption isotherm data using Clausious-Clapeyron (C-C) equation (2.8) written as:

$$\frac{-Q_{st(C-C)}M}{R} = \frac{\partial \ln P}{\partial \left(\dfrac{1}{T}\right)} \tag{2.8}$$

The numerical value of isosteric heat of adsorption (Q_{st}) might vary due to the adopted isotherm models. For low pressure refrigerant such as ethanol, the isosteric heat of adsorption can be expressed by equation (2.9). D–A model fitting parameters are used to determine the Q_{st}.

$$-Q_{st} = RT^2 \frac{\partial}{\partial T} \ln \left(P_s\right) + E \left\{ -\ln \left(\frac{W}{W_0}\right) \right\}^{\frac{1}{n}} \tag{2.9}$$

Chakraborty et al. [60] proposed a modified equation to determine the Q_{st} for high pressure gases. Equation (2.10) represents the equation of that model:

$$Q_{Chak,m(D-A)} = kRT + A + \frac{\alpha}{n} TE^n A^{1-n} + Tv_g \left(\frac{\partial P}{\partial T}\right) \tag{2.10}$$

Another well-known model to investigate the Q_{st} with surface coverage for high pressure gas using D–A fitting parameters is proposed by Rahman et al. model [61].

$$Q_{st} = h_{fg} + E \left[\left(-ln\,\Theta\right)^{\frac{1}{n}} + \frac{T\alpha}{n}\left(-ln\,\Theta\right)^{\frac{1-n}{n}} \right] \tag{2.11}$$

When the temperature is above critical, the equation takes the following form:

$$Q_{st} = kRT + E \left[\left(-ln\,\Theta\right)^{\frac{1}{n}} + \frac{T\alpha}{n}\left(-ln\,\Theta\right)^{\frac{1-n}{n}} \right] \tag{2.12}$$

Isosteric heat of adsorption for some commonly used adsorbent/adsorbate pair is presented in the Table 2.4.

Table 2.4. Isosteric heat of adsorption of some common adsorbents from articles.

Functional pair	Average isosteric heat of adsorption
Type A Silica gel/water [56]	2710 ± 100 kJ kg^{-1}
RD Silica gel/water [56]	2693 ± 100 kJ kg^{-1}
Natural zeolite/water [24]	2500 to 3800 kJ kg^{-1}
Maxsorb III/ethanol [62]	1002 kJ kg^{-1}
Spherical phenol resin based activated carbon (KOH6–PR)/ethanol [63]	995 kJ kg^{-1}
Activated carbon fiber (A–15)/ethanol [21]	1050 kJ kg^{-1}
Maxsorb III/CO_2 [58]	19.297 kJ mol^{-1}
Spherical activated carbon SAC2/HFC32 [59]	19.067 kJ mol^{-1}

Chapter 3

TEWI of cooling systems

Conventional cooling and refrigeration systems already evolved to efficient design, have higher COP and compact size. However, the compressor section of such system consumes a tremendous amount of electricity and contribute indirectly to global warming. The working fluids of these systems are typically HFC or HFC blends which possess very high global warming potential (GWP). A significant percentage of this working fluid is leaked from the high-pressure side of the system and directly contribute to global warming. The summation of indirect and direct warming impact namely, total equivalent warming impact (TEWI) of the vapour compression cooling systems are significantly high. Adsorption cooling system (ACS) is capable of resolving this critical issue.

In ACS, the mechanical compressor of the traditional cooling system is replaced by a thermal compressor, namely, a pair of adsorption beds. Highly porous adsorbent material (silica gel, activated carbon, zeolite and so forth) is the key component of an adsorption bed. These materials have the capability to capture and hold certain types of fluid. This phenomenon is known as adsorption. Upon heating, the adsorbed fluid is liberated from the pores (desorption process) and gets thermally compressed. Waste heat from industries, thermal power plants, brick fields, automobiles and solar thermal energy are the most prospective heat sources for the desorption process to occur. Since there is no mechanical compressor, the electricity consumption is deficient which significantly minimizes indirect warming impact. Moreover, natural or alternative refrigerants are used as the working fluid which has zero/negligible GWP. Hence, the direct warming impact is also shallow.

In this chapter, the working principle and governing equations of a waste heat driven adsorption cooling system will be elaborated. Besides, TEWI assessment procedure will be explained and compared for both vapour compression and adsorption cooling systems.

3.1 Background

The main objectives behind the invention of cooling systems are to attain thermal comfort during summer and to preserve various goods (fish, meat, vegetable, and so forth) that usually rots very fast at ambient conditions [4,64]. The conventional cooling systems have four major building blocks: evaporator, compressor, condenser and expansion device. A working fluid (namely refrigerant) flows through these components, changes its phase due to pressure variation and removes heat from a low-temperature source to a relatively higher temperature sink [65]. Electricity is required to run this cooling system, and the mechanical compressor consumes about 90% of that electricity. Electricity generation sources are mainly fossil fuel based and release greenhouse gases during electricity production [66–68]. Briefly, a cooling system indirectly contributes to global warming by using electricity. Moreover, refrigerant leakage is inevitable from joints and seals, mechanical failure or during servicing [69,70]. Currently employed refrigerants in the cooling systems have a very high global warming impact. Hence, the leaked refrigerant contributes directly to global warming. The summation of indirect and direct warming impact namely, total equivalent warming impact (TEWI) of the conventional cooling systems are significantly high [71–74]. Hence, the adsorption cooling system is becoming popular which can be driven by solar thermal energy or any other low-temperature heat sources [23,75–77]. Electricity consumption of this system is very low. Moreover, natural refrigerants can be used as working fluids which have zero or negligible global warming impact [78–80]. According to history, Faraday discovered the adsorption cooling phenomenon in 1948. He observed that NH_3 adsorption onto $AgCl$ could produce cooling. G. E. Hulse proposed an adsorption refrigeration system with silica gel as adsorbent and SO_2 as the refrigerant in the 1920s [15]. Nowadays, many renowned industries such as Mitsubishi [81], Tokyo Boeki Machineries [82], Bry-Air [3], Mayekawa [83], and SorTech [84] are commercially manufacturing high capacity adsorption chillers. TEWI is assessed and compared for both mechanical vapor compression system and adsorption cooling system in this chapter.

3.2   Calculation procedure

3.2.1 Operation principle

A simple vapour compression system with subcooling and superheating is shown in Fig. 3.1. Corresponding P-h diagram and the state of refrigerant in a refrigeration cycle is shown in Fig. 3.2. In this cycle, when the refrigerant leaves the evaporator (point a), a certain amount of superheat is applied to prevent damage and to increase the efficiency of the system. The refrigerant is then fed to the suction line of the compressor (point a'). Vapour refrigerant discharges from the compressor (point b") after a non-isentropic compression. The hot vapour refrigerant is then cooled and condensed in the condenser through an isobaric process. Released refrigerant from the condenser (point c) is subcooled to ensure that the entire refrigerant is in the liquid state. After subcooling (point c'), the refrigerant is collected into a reservoir. The refrigerant then goes through an expansion device, enter into the evaporator (point d'), evaporate isobarically until it reaches evaporator exhaust (point a) and the cycle continues to repeat.
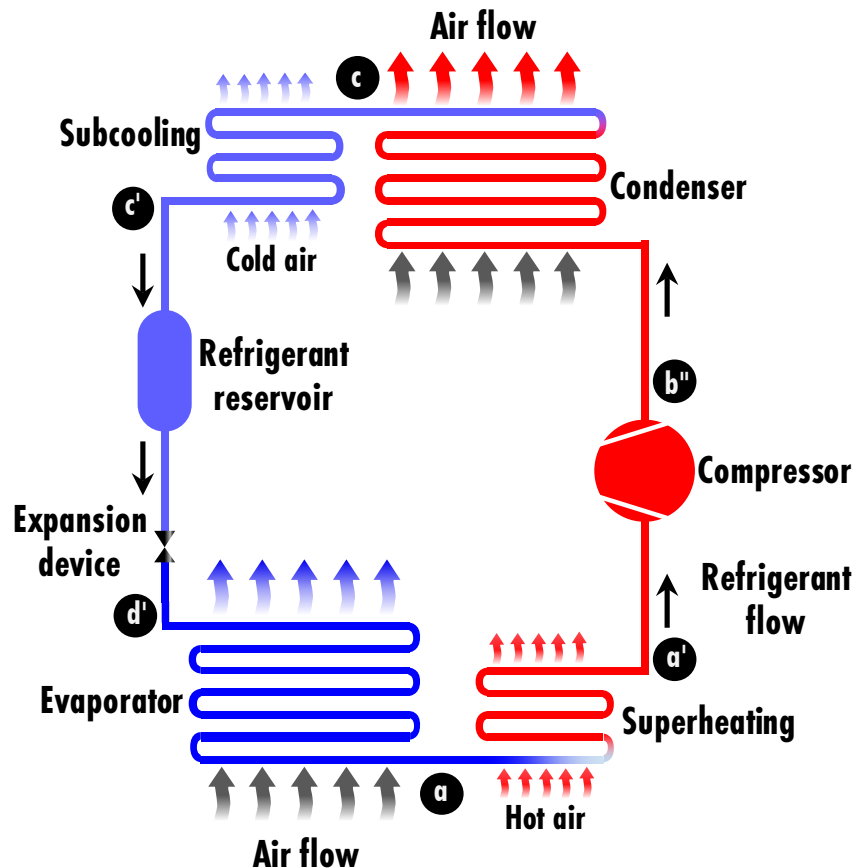
Fig. 3.1.   Schematic of a simple vapor compression refrigeration system.
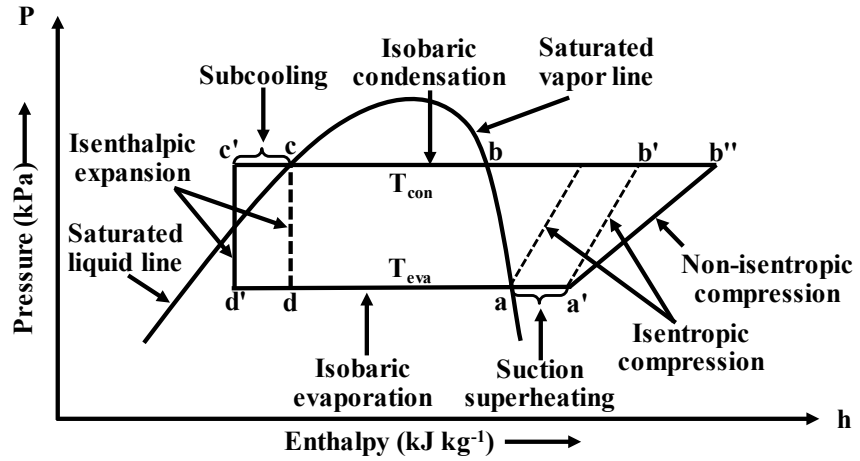
Fig. 3.2.   A typical P-h diagram and refrigeration cycle.

In a refrigeration cycle, the refrigerant encounters isobaric, isentropic, non-isentropic and isenthalpic processes as shown in Fig. 3.2. The following set of equations can be written from the state diagrams.

$$P_{d'} = P_d = P_a = P_{a'} \tag{3.1}$$

$$P_{b''} = P_{b'} = P_b = P_c = P_{c'} \tag{3.2}$$

$$T_a = T_{eva} \tag{3.3}$$

$$T_{a'} = T_{eva} + T_{sup} \tag{3.4}$$

$$h_{c'} = h_{d'} \tag{3.5}$$

$$S_{a'} = S_{b'} \tag{3.6}$$

$$T_b = T_c = T_{con} \tag{3.7}$$

$$T_{c'} = T_{con} - T_{sub} \tag{3.8}$$

$$\eta_{isen} = \frac{h_{b'} - h_{a'}}{h_{b''} - h_{a'}} \tag{3.9}$$

Unlike VCR, work input of an adsorption cooling system is thermal energy instead of electricity. The mechanical compressor of a VCR is replaced with a thermal compressor namely adsorption bed [85–92]. Other three components of the system are the same as

VCR. Some additional components are also required in the adsorption cooling system for the cooling to occur. The complete system schematic is shown in Fig. 3.3.
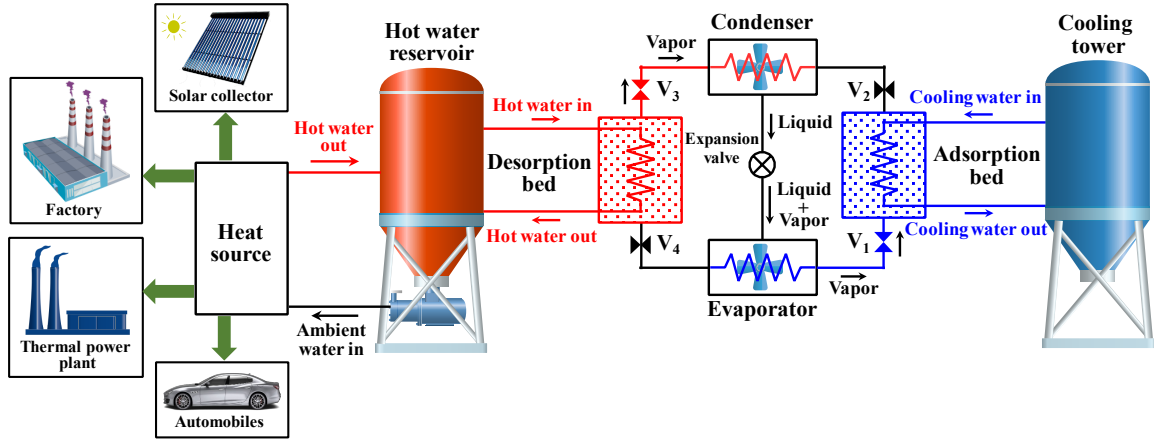
Fig. 3.3.   Adsorption cooling system by using waste heat/solar thermal energy.

A pair of beds alternately works as adsorption bed and desorption bed for uninterrupted cooling. State points and refrigeration cycle is similar for VCR and adsorption cooling system if the operating conditions are same. So the same set of equations can be used for the adsorption cooling system. Since, superheating and subcooling is not required for ACS, equation (3.4), (3.8) and (3.9) are irrelevant.

3.2.2 TEWI

Every refrigeration system contributes to global warming either directly or indirectly. TEWI is the overall quantity of direct and indirect GWP released from a system.

The compressor (desorption bed for an adsorption cooling system) and condenser sections operate at a high temperature and pressure than the atmospheric. Although all the sections are properly sealed, a significant amount of leakage (about 20%) can occur from joints and seals, due to mechanical failure or during servicing [69,93]. This leakage will lead to performance degradation and will increase energy consumption [94,95]. Moreover, the leaked refrigerants have high GWP which will eventually contribute directly to global warming [73].

Indirect emission occurs due to the electricity consumption of the refrigeration system since major share of the electricity is generated from fossil fuel.

A cooling system is mostly made with metals such as stainless steel, aluminium, copper. These materials production requires a lot of energy which indirectly contribute to global warming.

Hence, TEWI can be assessed from the following equation:

$$
\begin{aligned}
TEWI &= direct\ emission\ +\ indirect\ emission \\
&= (GWP_r \times L) \times y\ \ +\ \left[(E \times \varepsilon) \times y + m \times GWP_m \right]
\end{aligned}
\tag{3.10}
$$

Here,

GWP_r global warming potential of the selected refrigerant [kg-CO_2 eq.]

L annual leakage rate of charged refrigerant [%]

y duration to calculate TEWI [year]

E electricity consumption [kWh]

ε CO_2 emission factor for per unit electricity generation [kg-CO_2 eq./kWh]

m mass of the raw materials which are used for constructing the cooling system [kg]

GWP_m CO_2 emission factor for per unit raw material production [kg-CO_2 eq./kg]

3.2.3 TEWI of conventional cooling system

Operating conditions and assumptions are required to set before the TEWI assessment of a conventional VCR system. The complete set of parameters are listed in Table 3.1.

Electricity consumption amount is required to determine the indirect emission of the cooling system. Electricity consumption depends on the COP of the system which is ultimately obtained from the thermodynamic properties of the refrigerant by using REFPROP [96] and the equations from (3.1) to (3.9). Thermodynamic quantities of room air-conditioning system is listed in Table 3.2. A similar data set can be evaluated for medium and low-temperature system. These thermodynamic data of room air-conditioning system, medium temperature system and low-temperature system is used to draw refrigeration cycle which is shown in Fig. 3.4, Fig. 3.5, and Fig. 3.6, respectively.

Table 3.1. Operating conditions and assumptions to calculate TEWI of a VCR system.

Parameter	Quantity
Evaporation temperature for specific applications, T_{eva}	12 °C (room air-conditioning)
	–7 °C (medium temperature applications)
	–25 °C (low temperature applications)
Condensation temperature, T_{con}	40 °C
Selected refrigerants	R32 (Difluoromethane: CH_2F_2)
	R134a (1,1,1,2-Tetrafluoroethane: $C_2H_2F_4$)
	R404A(44% R125, 4% R134a, 52% R143a) [96]
GWP of the considered refrigerants, GWP_r	GWP_{R32} : 675 kg-CO_2 eq.[97],
	GWP_{R134a} : 1300 kg-CO_2 eq.[64],
	GWP_{R404A} : 3922 kg-CO_2 eq.[98]
Cooling load, Q_c	10 kW
Suction gas superheat, T_{sup}	8 °C
Degree of subcooling, T_{sub}	5 °C
Isentropic efficiency of the compressor, η_{isen}	70 % (room air-conditioning)
	65 % (medium temperature applications)
	60 % (low temperature applications)
Initial refrigerant charging amount	1 kg for per kW room air-conditioning cooling load
	2 kg for per kW medium temperature load
	3 kg for per kW room air-conditioning load [7]
Annual leakage rate of refrigerant, L_a	15 % [69,70]
GWP for electricity generation, ε	0.518 (kg-CO_2/kWh) [99]
Product weight (indoor + outdoor unit), m	60 kg (10 kW room air-conditioning) [100,101]
	80 kg (10 kW medium temperature system)
	100 kg (10 kW low temperature system)
Weight percentage of raw materials to build a cooling system	Stainless steel: 50 %
	Copper: 20 %
	Aluminium: 20 %
	Others (refrigerant, plastic, paint etc.): 10 %
GWP of per kg material production, GWP_m	Stainless steel: 2.13 kg-CO_2 eq. [102]
	Copper: 4.97 kg-CO_2 eq. [103]
	Aluminum: 9.17 kg-CO_2 eq. [103]
System lifespan	15 years
System runtime	12 hours/day
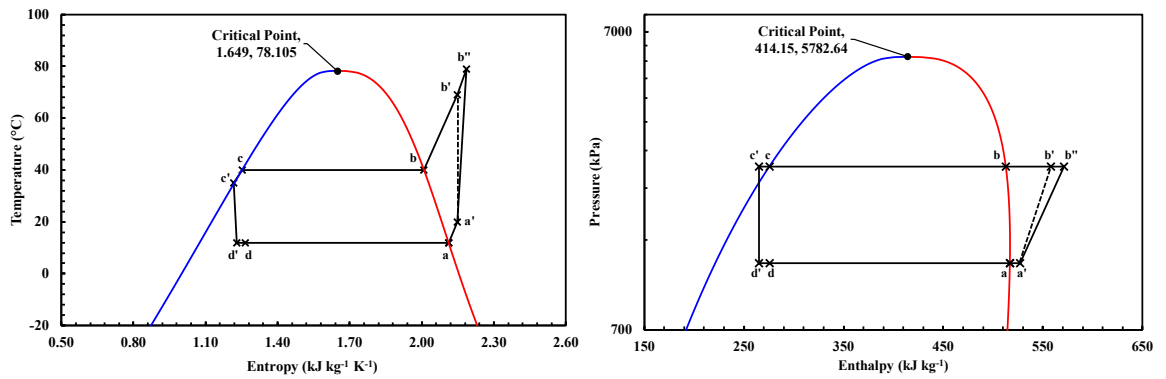
Fig. 3.4.   T-s and P-h diagram of room air-conditioning cycle with R32.
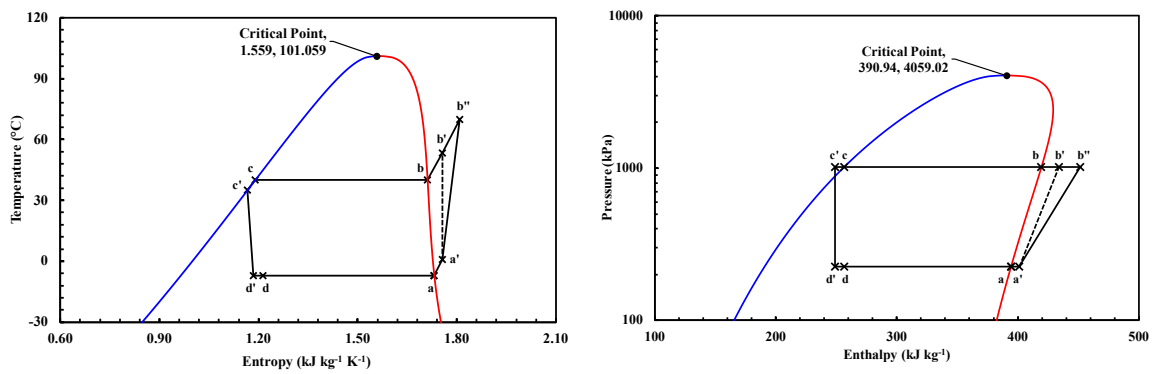
Fig. 3.5.   T-s and P-h diagram of Medium temperature (–7 °C) refrigeration cycle with R134a.
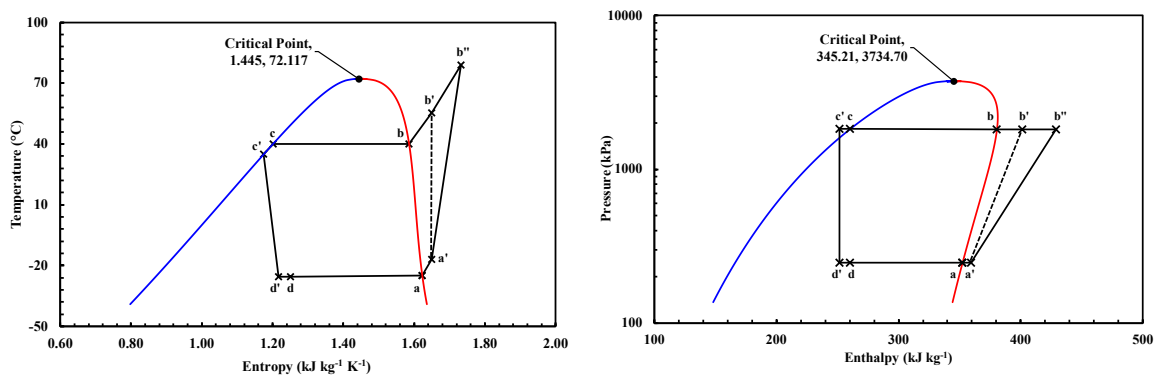
Fig. 3.6.   T-s and P-h diagram of low temperature (–25 °C) refrigeration cycle with R404A.

Table 3.2. Thermodynamic quantities at state points of room air-conditioning system.

State point	Explanation	Temp. T (°C)	Pressure P (kPa)	Enthalpy h (kJ kg^{-1})	Entropy s (kJ kg^{-1} K^{-1})
a	Saturated vapor	12.00	1174.18	516.80	2.111
a'	Superheated vapor	20.00	1174.18	527.36	2.148
b"	Hot vapor with non-isentropic compression	78.97	2478.31	571.15	2.186
b'	Hot vapor with isentropic compression	68.91	2478.31	558.02	2.148
b	Saturated vapor	40.00	2478.31	512.71	2.009
c	Saturated liquid	40.00	2478.31	275.61	1.252
c'	Subcooled liquid	35.00	2478.31	265.08	1.218
d'	Expanded two-phase refrigerant when subcooled	12.00	1174.18	265.08	1.229
d	Expanded two-phase refrigerant without subcooling	12.00	1174.18	275.61	1.266

Equations (3.11) to (3.14) are used to determine the maximum theoretical COP, actual COP, electricity consumption and required mass flow rate of refrigerant, respectively. The performance of a system can be estimated by these equations.

$$COP_{carnot} = \frac{273.15 + T_{eva}}{T_{con} - T_{eva}} \qquad (3.11)$$

$$COP = \frac{h_{a'} - h_{d'}}{h_{b"} - h_{a'}} \qquad (3.12)$$

$$E_p = \frac{Q_c}{COP} \qquad (3.13)$$

$$\dot{m} = \frac{h_{a'} - h_{d'}}{Q_c} \qquad (3.14)$$

Assessed system performance and environmental impact is summarized in Table 3.3. Apparently, the COP decreases for lower evaporation temperature requirement because of higher compression ratio. Hence, the electricity requirement and indirect warming impact both increases.

Table 3.3. Results of assessment: conventional cooling system.

Parameter \ System type	Room air-conditioning (R32)	Medium temperature refrigeration (R134a)	Low-temperature refrigeration (R404A)
COP_{carnot}	10.018	5.663	3.818
COP	5.989	3.029	1.660
Refrigerant flow rate, $\dot{m}$ (kg h^{-1})	137.257	236.251	143.344
Discharge temperature of refrigerant (°C)	78.971	69.950	160.416
Discharge pressure of refrigerant (kPa)	2478.310	1016.592	2478.31
Compression ratio	2.111	4.509	7.408
Annual electricity consumption (kWh)	7312.923	14462.196	26392.087
Annual indirect warming impact for electricity consumption (t-CO_2 eq.)	3.788	7.491	13.671
Total indirect warming impact for building the cooling system (t-CO_2 eq.)	0.234	0.311	0.389
Annual indirect warming impact for building the cooling system (t-CO_2 eq.)	0.016	0.021	0.026
Annual direct warming impact (kg-CO_2 eq.)	1.013	3.900	17.649
Annual TEWI (t-CO_2 eq.)	4.816	11.412	31.346

A small 10 kW conventional cooling system can produce 4.816 – 31.346 tonne equivalent CO_2 emission every year depending on the application. The emission amount could be higher if the system is situated in an underdeveloped or developing country where electricity is primarily generated from coal, gas and other fossil fuel based sources.

Additionally, TEWI would increase for tropical countries where the exterior temperature is higher than the considered temperature. Environmental impact would further increase, (i) for lower temperature applications because COP and isentropic efficiency is lower, (ii) with aging of the system because the system would be more prone leakage and will consume more electricity, (iii) if selected refrigerant have higher GWP or poor thermodynamic property in the operation condition.

3.2.4 TEWI of adsorption cooling system

Operating conditions and assumptions for the adsorption cooling system is summarized in Table 3.4. Same operating temperatures (T_{eva} and T_{con}), operation hours and cooling capacity have been set for the adsorption cooling system to compare the results with the conventional cooling system. Natural refrigerants (GWP = 0) have been chosen to decrease environmental impact. Three different functional pairs have been selected for three different applications. Silica gel/water pair is suitable for the temperature range of room air-conditioning systems. Moreover, medium temperature and low-temperature applications require different working fluids such as methanol and ammonia [104]. Activated carbon is suitable for the adsorption of these refrigerants.

COP of the adsorption cooling system can be expressed in two ways which are shown in equations (3.15) and (3.16). Thermal input is very high compared to cooling output for adsorption cooling system. Hence, thermal COP is usually very low. Moreover, electricity input is much lower for an adsorption cooling system, and therefore electrical COP is very high. Thermal COP of the chiller for room air-conditioning system is the range of 0.5 – 0.6 [3,105]. COP decreases for lower evaporation temperature. In this assessment, we have considered COP values 0.6, 0.4 and 0.2 for room air-conditioning, medium temperature and low-temperature cooling systems, respectively.

$$COP_{thermal} = \frac{Q_{eva}}{Q_{des}} \qquad\qquad (3.15)$$

$$COP_{elctrical} = \frac{Q_{eva}}{E_{in}} \qquad\qquad (3.16)$$

Here,

Q_{eva} evaporator cooling capacity [kJ]

Q_{des} required thermal input for desorption [kJ]

E_{in} required electrical power input [kWh] or [kJ]

The adsorption chillers require a small amount of electricity to run the pumps (chilled water, cooling water) and control the valves. A 10 kW chiller requires about 0.8 kW electricity according to the manufacturer's specification [3]. Medium and low-temperature applications require a considerably higher amount of electricity which is shown in Table 3.4. The required amount of adsorbent and refrigerant also increases for lower temperature applications.

An adsorption system has two or more beds. The frames of the beds are usually made of stainless steel. The beds contain adsorbent and heat exchangers. Hence, the weight of an adsorption system is about ten times or higher than the conventional system of the same cooling capacity. The weight of a 10 kW solar room air-conditioning cooling system is about 900 kg according to manufacturer's specification. Weight of medium and low-temperature systems have been considered higher due to the higher adsorbent and heat exchanger requirement. The weight percentage of steel, aluminium, copper and other materials have been modified due to the constructional differences with the conventional cooling system. The system has a higher lifetime and requires lower maintenance than the conventional systems because there are very few moving parts in this system.

Table 3.4. Operating conditions and assumption for adsorption cooling system.

Parameter	Quantity
Evaporation temperature for specific applications, T_{eva}	12 °C (room air-conditioning)
	–7 °C (medium temperature applications)
	–25 °C (low temperature applications)
Condensation temperature, T_{con}	40 °C
Selected refrigerants	R717 (Ammonia: NH_3),
	R718 (Water: H_2O),
	MetOH (Methanol: CH_3OH)
Functional adsorbent/adsorbate pairs	Silica gel/water (room air-conditioning) [3,82]
	Activated carbon/methanol (medium temperature applications) [106]
	Activated carbon/ammonia (low temperature applications) [107,108]
GWP of the considered refrigerants, GWP_r	GWP_{water} : 0 kg-CO_2 eq. [1],
	$GWP_{ethanol}$: 0 kg-CO_2 eq.[109],
	$GWP_{ammonia}$: 0 kg-CO_2 eq. [8].
Cooling load, Q_c	10 kW
$COP_{thermal}$	0.6 (room air-conditioning) [3,105]
	0.4 (medium temperature applications)
	0.2 (low temperature applications)
Electricity consumption (for pumps and valves)	0.8 kW (room air-conditioning) [3]
	1.4 kW (medium temperature applications)
	2.0 kW (low temperature applications)
Required adsorbent amount (two beds)	50 kg (room air-conditioning) [3]
	70 kg (medium temperature applications)
	90 kg (low-temperature applications)

Initial refrigerant charging amount	30 kg (room air-conditioning) [3]
	50 kg (medium temperature applications)
	70 kg (low-temperature applications)
Annual leakage rate of refrigerant, L_a	15 %
GWP for electricity generation, ε	0.518 (kg-CO_2/kWh) [99]
Product weight (only main module), m	900 kg (10 kW room air-conditioning) [3]
	1200 kg (10 kW medium temperature system)
	1500 kg (10 kW low-temperature system)
Weight percentage of raw materials to build a cooling system	Stainless steel: 60 %
	Copper: 10 %
	Aluminium: 10 %
	Others (refrigerant, adsorbent, cooling/ chilled water etc.): 20 %
GWP of per kg material production, GWP_m	Stainless steel: 2.13 kg-CO_2 eq. [102]
	Copper: 4.97 kg-CO_2 eq. [103]
	Aluminum: 9.17 kg-CO_2 eq. [103]
System lifespan	25 years [3]
System runtime	12 hours/day

The results of the assessment for the adsorption cooling system is summarized in Table 3.5. Thermal COP, electricity consumption, indirect emission due to electricity consumption, direct emission and TEWI of the considered solar cooling systems are lower than the conventional system. Since the weight of the adsorption cooling system is much higher, the indirect warming impact for building the cooling system is higher. However, TEWI of the solar cooling systems is much lower than the conventional systems.

Table 3.5. Results of assessment: adsorption cooling system.

System type / Parameter	Room air-conditioning (Silica gel/ water)	Medium temperature refrigeration (Activated carbon/ methanol)	Low temperature refrigeration (Activated carbon/ ammonia)
$COP_{thermal}$	0.6	0.4	0.2
$COP_{electrical}$			
Annual electricity consumption (kWh)	3504	6132	8760
Annual indirect warming impact for electricity consumption (t-CO_2 eq.)	1.815	3.176	4.538
Total indirect warming impact for building the cooling system (t-CO_2 eq.)	2.423	3.230	4.038
Annual indirect warming impact for building the cooling system (t-CO_2 eq.)	0.097	0.129	0.162
Annual direct warming impact (kg-CO_2 eq.)	0	0	0
Annual TEWI (t-CO_2 eq.)	1.912	3.306	4.699

3.3   Results comparison and discussions

The conventional vapour compression system is very compact in size and COP is also high. COP of adsorption cooling system is very low because of huge loss of thermal energy conversion during operation. Hence, COP of adsorption cooling system is often referred as thermal COP. Electrical COP (ratio of cooling capacity to electricity input) is much higher for the solar cooling system which is shown in Fig. 3.7. COP decreases for both conventional and solar cooling system when the evaporation temperature requirement is lower.

In Fig. 3.8, electricity consumption is compared between the conventional and solar cooling system. Inevitably the consumption is lower for the adsorption cooling system

since the desorption (often referred as thermal compression) is carried out by waste heat or solar thermal input.

Indirect and direct emissions are individually drawn in Fig. 3.9 for conventional and solar cooling system for three different applications. Last two bars of each application are the TEWI for that particular application which is obtained by aggregating the direct and indirect emissions.
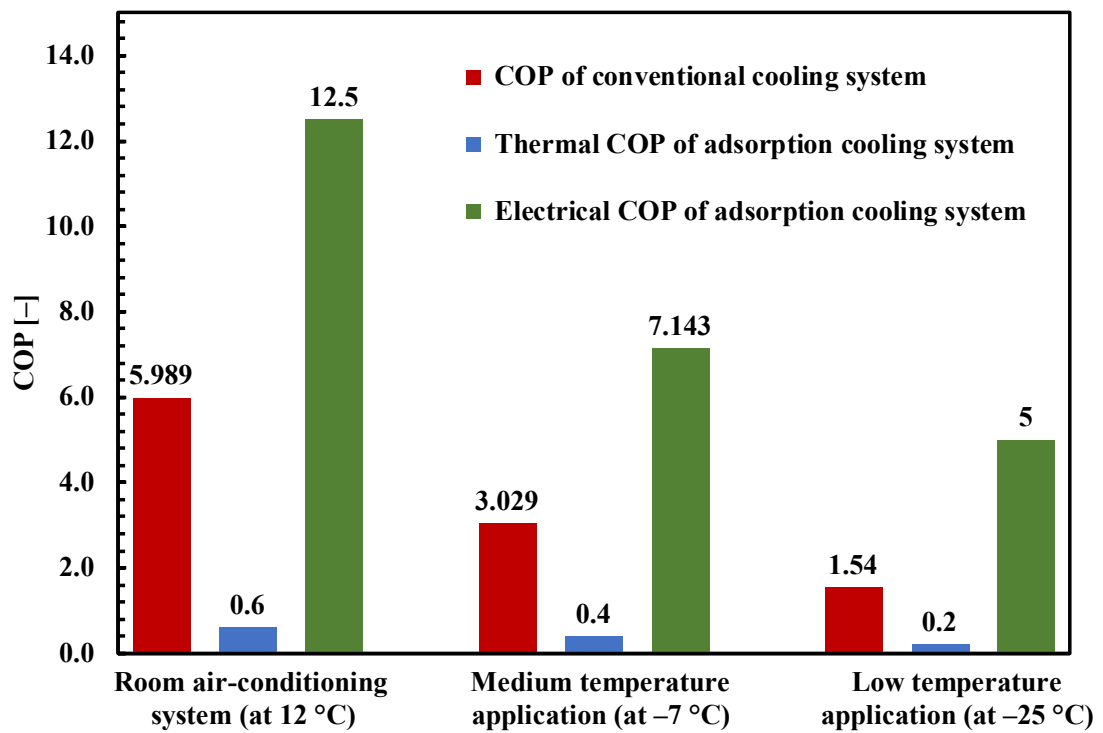
Fig. 3.7.   COP variation for different applications: conventional vs solar cooling system.
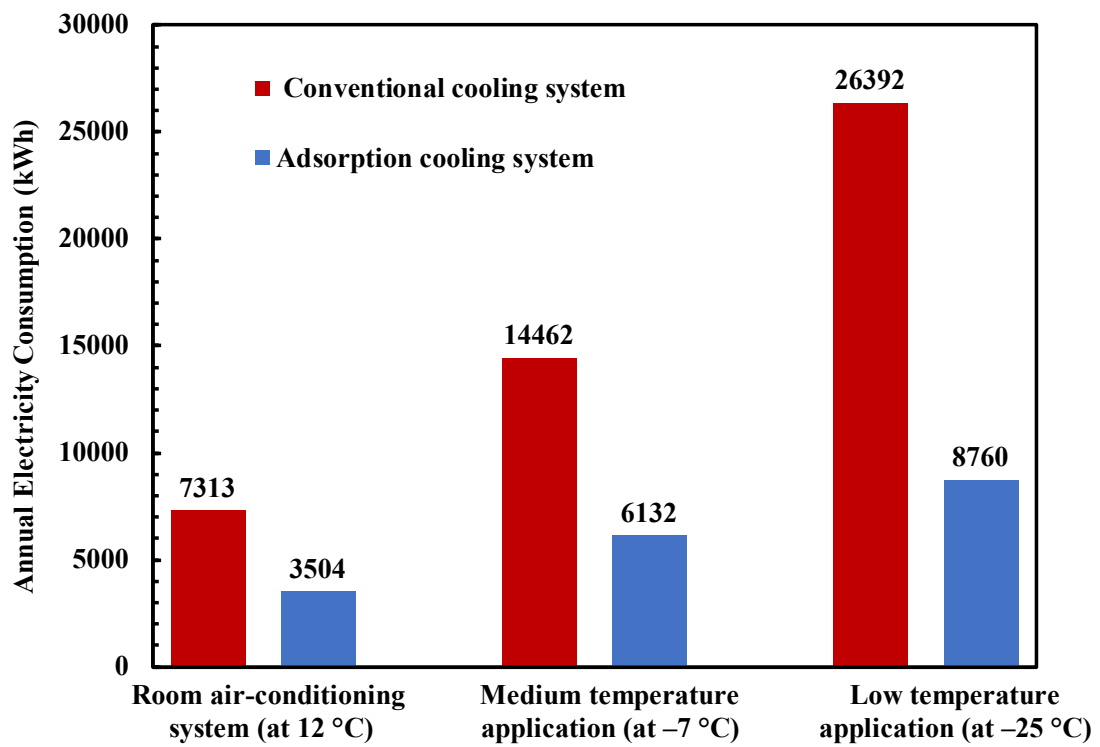
Fig. 3.8.   Electricity consumption: conventional vs adsorption cooling system.
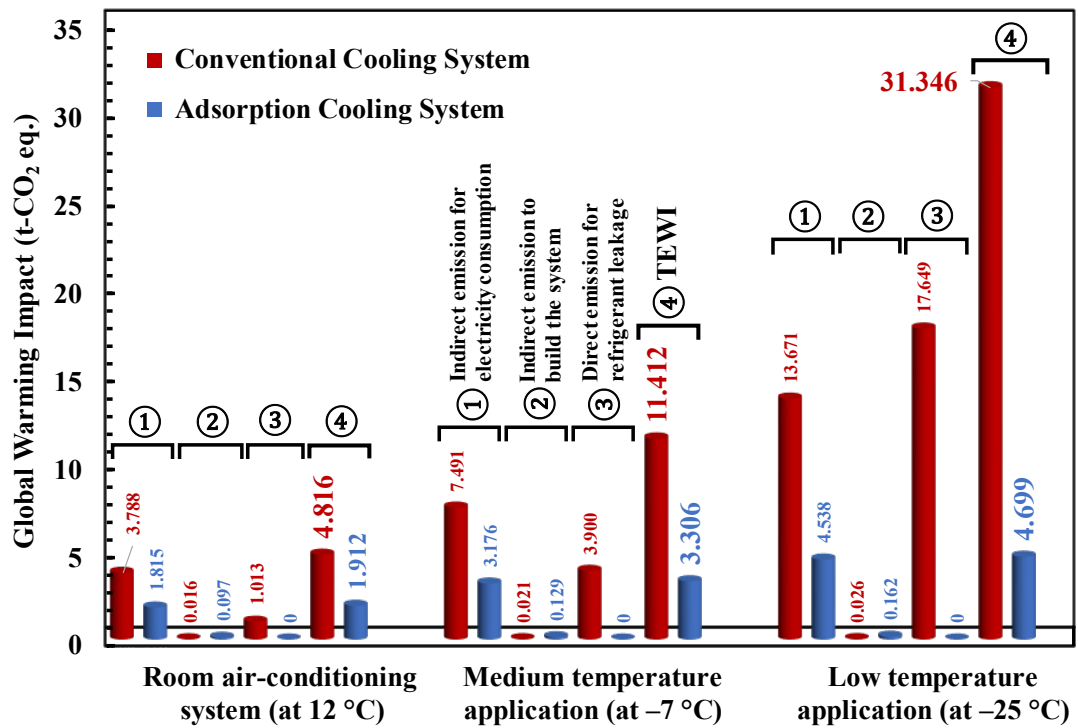
Fig. 3.9.   Indirect, direct and total equivalent warming impact comparison.

Since the solar cooling system has low electricity consumption, indirect emission is also lower for all three applications. However, the dimension and weight of the adsorption cooling system are much higher than the conventional system. Hence, indirect emission for raw materials production is higher for the adsorption cooling system. Additionally, direct emission for the adsorption cooling system is zero because of deploying natural refrigerants as working fluid.

3.4   Conclusions

In this assessment, performance and environmental impact of conventional and solar cooling system have been evaluated and compared. Three different applications: room air-conditioning (T_{eva} at 12 °C), medium temperature application (T_{eva} at –7 °C) and low-temperature applications (T_{eva} at –25 °C) have been considered for both the systems. R32, R134a and R404A have been selected as working fluid for the conventional VCR system. Whereas, silica gel/water, activated carbon/methanol and activated carbon/ammonia pairs have been considered for the adsorption cooling system. A constant cooling load of 10 kW is considered for all the applications. The results indicate that COP of the conventional cooling system is much higher than thermal COP of the solar cooling system. However, electrical COP of the solar cooling system is considerably high due to the thermal input for desorption (thermal compression).

Indirect emission for electricity consumption is considerably higher for the conventional cooling system. It happens due to the huge electricity consumption by the mechanical vapor compressor. However, the weight of the used raw materials is very high that build the adsorption cooling system. Hence, annual indirect warming impact to build the system is relatively higher for the adsorption cooling system. In the case of direct emission, the adsorption cooling system is better because it uses natural refrigerants and the GWP of those refrigerants are zero. Currently deployed refrigerants (R32, R134a, R404A etc.) in conventional VCR systems have high GWP and hence the direct warming impact is higher. However, the situation might change if low GWP refrigerants are introduced in conventional systems.

Currently, TEWI (summation of indirect and direct emissions) is very high for conventional cooling systems. Therefore, now is the appropriate time to switch from conventional systems to adsorption cooling technology.

Chapter 4

Specific heat capacity and porosimetry measurement of potential adsorbents

Silica gel, activated carbon and zeolites are the most commonly used adsorbents for adsorption cooling, dehumidification, and gas separation applications. Porosimetry (e.g. surface area, pore volume, pore size distribution) and thermophysical properties (e.g. specific heat capacity) determination are very significant to simulate the performance when the material is employed in a real application. For example, porous properties of the adsorbent are required to find a suitable adsorbate for that adsorbent and to predict adsorption isotherm of that adsorbent-adsorbate pair. Moreover, specific heat capacity data of an adsorbent is very siginificant to design an adsorption bed. Generally, the researchers consider a constant value of specific heat capacity when they determine the performance of an adsorption bed. However, the bed temperature varies during adsorption/desorption and the specific heat capacity also changes with temperature. Hence, the precise bed performance determination requires the accurate specific heat capacity value for that particular temeparture. Specific heat capacity for a particular temperature range and porosimetry measurement of silica gel and carbon based materials have been performed and reported in this chapter.

4.1 Silica gel

Silica gel (SG) has been extensively using as an adsorbent in dehumidifying applications, separation process, purification of gases, cryocooler design and adsorption cooling systems (ACS) in the last few decades. Material properties such as the specific heat capacity, surface area, pore volume, pore size distribution are critical parameters in adsorption simulation and system design. This chapter discusses about the experimental investigation of the porous properties and specific heat capacity of several types (RD, type A, type B, type A indicator, home SG, high purity Chromatorex SG) of silica gels. Type B silica gels are found to have the lowest surface area and the highest total pore volume. RD silica gels of large particle size (above 0.7 mm) have the highest surface area. Pore

size distribution result shows that type B and home silica gels have comparitvely larger mesopores than the other samples. The specific heat capacity of these materials is measured employing a heat flux type differential scanning calorimeter (DSC). Since the decomposition temperature of most silica gels is about 120 °C, the specific heat capacity of the samples is measured within 30 °C to 100 °C. The specific heat capacity of the measured samples varies between 0.8 to 1.10 kJ kg^{-1} K^{-1} in the measurement temperature range. RD silica gel of the smallest particle size shows highest and indicator type silica gel shows the lowest specific heat capacity. Specific heat capacity model proposed by Green and Perry is employed to fit the experimental data. The model fits well with experimental data with less than 0.4% error in the measurement range.

4.1.1 Introduction

Silica gel has an incompletely dehydrated polymeric structure of colloidal silicic acid which exhibits an excellent capacity for adsorption of water. It is frequently used for commercial applications like adsorption cooling [30,110,111], dehumidification [112–114], separation [113,114], and recently desalination [115–118]. The adsorption refrigeration technology employing silica gel is escalating in recent decades because it is environment-friendly and it requires a low-grade heat source to drive the system [22,118–121]. In the design and optimization of such adsorption cycles, surface area, pore volume, pore size distribution and the specific heat capacity of the silica gel are key thermo-physical parameters to measure. In general, higher surface area and smaller specific heat capacity of silica gel is desired to design an efficient adsorption cooling system. Adsorbents with higher surface area increases the adsorption uptake. Besides, lower specific heat capacity material retains smaller amount of heat during desorption and requires lower thermal input. It is obvious that the adsorption cycles involve rapid thermal fluctuation due to alternate heating and cooling [122–124]. Hence, it is logical to perceive that specific heat capacity of the adsorbent is not constant instead a function of temperature. Yet it is found that many researchers adopted the average value of specific heat of adsorbent in their simulation models of adsorption processes [30–35]. On the other hand, Aristov [40,125] proposed an approximation to calculate the specific heat of dry adsorbent $CaCl_2$/silica gel KSK as a function of temperature at various water uptake. Author considers specific heat capacity of water in the liquid state and found it is closer to

the experimental value. However, detailed analyses of specific heat capacity of porous silica gel at various temperatures are not available in open literature.

There are two methods to measure the specific heat capacity, which are indirect methods and direct methods. Indirect methods require other physical properties, like thermal diffusivity and thermal conductivity to calculate the specific heat capacity. The flash method and laser flash method can be used to measure the thermal diffusivity, heat capacity and thermal conductivity if the density of both the specimen and reference material are known [126–129]. The desirability of direct calorimetric information rather than indirect thermometric data has been recognized by advanced workers in differential thermal analyzer for many years. For the direct methods, the specific heat capacity measured by calorimeters, e.g. adiabatic calorimeters, reaction calorimeters, bomb calorimeters and differential scanning calorimeters (DSC) [130,131]. Specific heat capacity measurement by DSC is a powerful and accurate method with relatively simple working process. The DSC can measure the specific heat capacity of milligram level sample correctly and the results can be obtained in wide range of temperature rather than a single temperature condition. Several works on the development and measurement techniques using DSC have been reported. Watson and O'Neill [132,133] described the advantages of DSC over the traditional thermal analyzer especially the use of differential temperature amplifier to adjust the sample and reference signal. The effect of sample mass and rate of heating does not influence so much to measure the heat capacity [134,135]. It was found that the heating rate and sample geometry influence the DSC thermograms and the apparent specific heat capacity during melting process [136]. The reduction of instrument baseline defects resulting from the imbalances using comprehensive heat flow was achieved by Danley [131,137]. In the present study, porous properties and the specific heat capacities of several types of silica gel have been measured using a 3Flex and heat flux type DSC, respectively.

4.1.2 Experimental

4.1.2.1   Materials

Six different types of silica gel (total 13 samples including subcategories) are experimentally investigated in this study.Table 4.1 summarizes the common properties of all the samples. This information is obtained from the specification data sheet of the silica gel manufacturer.

Table 4.1. Physical properties of silica gel samples.

Sample Type	Particle shape	Particle diameter (mm)	Sample name	Bulk density (kg m^{-3})	Manufacturer
RD type	Spherical	D ≥ 3.3	RD on 6	730	Fuji Silysia
	Spherical	D ≥ 1.0	RD on 18	730	Fuji Silysia
	Spherical	D ≈ 0.7 to 1.18	RD 14–24	730	Fuji Silysia
	Granular	D ≈ 0.25 to 1.0	RD 2060	730	Fuji Silysia
	Granular	D ≈ 0.075 to 0.25	RD	730	Fuji Silysia
Type A	Granular	D ≈ 1.7 to 4.0	A 5–10	730	Fuji Silysia
	Granular	D ≤ 0.5	A thru 40	730	Fuji Silysia
Type B	Spherical	D ≈ 1.7 to 4.0	B 5–10	500	Fuji Silysia
	Granular	D ≤ 0.5	B thru 40	500	Fuji Silysia
High purity Chromatorex silica gel	Spherical	D ≈ 0.075 to 0.5	MB3A 30–200	730	Fuji Silysia
Indicator type A	Spherical	D ≥ 3.3	A on 6 F	730	Fuji Silysia
	Spherical	D ≈ 1.7 to 4.0	A 5–10	730	Fuji Silysia
Home silica gel	Granular	D ≥ 0.5	B on 40	500	Fuji Silysia

4.1.2.2   Porosimetry analysis

Porosimetry measurement (surface area, pore volume, and pore size distribution) have been performed using a "3FLEX – high resolution surface characterization analyzer" apparatus from Micromeritics Instrument Corporation (Fig. 4.1). This apparatus is ideally suited for the characterization of silica gels, MOFs, zeolites, activated carbons, and a wide

variety of porous and nonporous materials. Relative pressure (P/P$_0$) can be as low as 1.3 ×
10^{-9} and up to 1.0. Minimum surface area that can be measured by N$_2$ adsorption at liquid
nitrogen boiling temperature (77 K) is 0.01 m^2/g. 3FLEX contains several software
advancements including a new advanced dosing method that allows the user to mix both
pressure and volume increments [138].
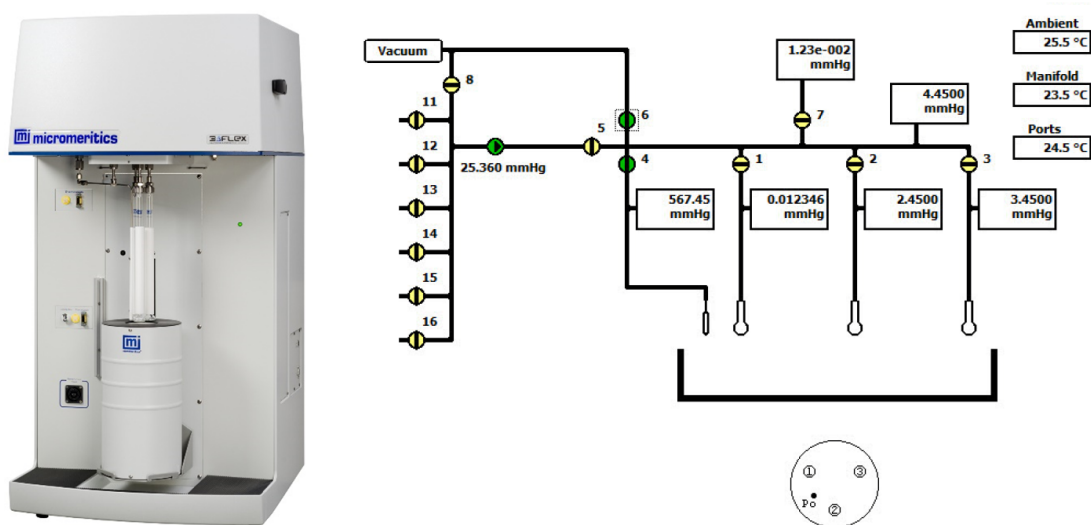
Fig. 4.1. Photograph and internal schematic diagram of 3FLEX apparatus [138].

4.1.2.3   *Differential scanning calorimetry*

Schematic diagram of the differential scanning calorimeter (DSC–60A from
Shimadzu Corporation) apparatus is shown in Fig. 4.2. The heart of the apparatus is the
DSC unit, which is depicted in Fig. 4.3. The furnace section of the DSC unit has two slots
to put samples.
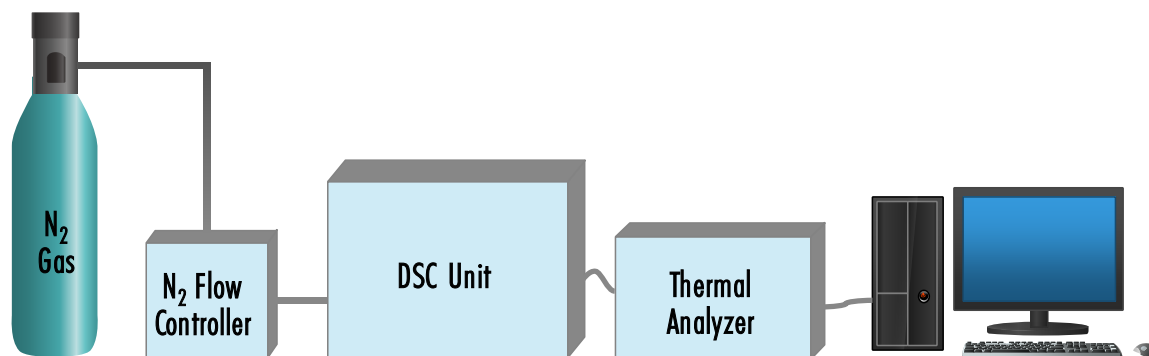
Fig. 4.2.   Schematic diagram of a differential scanning calorimetry (DSC) apparatus.
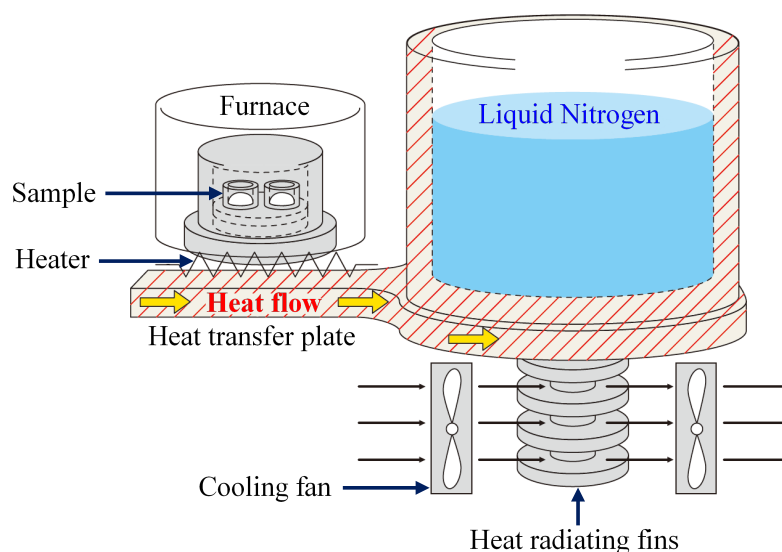
Fig. 4.3.   Schematic diagram of the DSC furnace unit [139].

An empty pan is always placed on the left slot and the sample to be measured is placed on the right slot of the furnace. Both the slots have thermocouples at the bottom to track, record and control the temperature change. When the measurement starts, a metallic cover encloses the furnace which prevents foreign elements to enter inside. Moreover, dry N_2 gas is flown to the sample at 50 ml/min rate to remove the water vapor and other contaminants that are released from sample during the measurement. The temperature ranges to measure specific heat capacity of this apparatus is from –140 °C to 600 °C. Moreover, heating/cooling rate of the apparatus can be programmed from ±0.01 °C/min to ±99.9 °C/min.

4.1.3 Measurement procedure

4.1.3.1   Porosimetry measurement

The silica gel samples have been degassed for at least six hours in vacuum condition at 100 °C prior to the measurement. The sample amount is about 100–200 mg. Since the sample amount is small, precise mass measurement is an important prerequisite. Hence, mass of each sample have been measured at least 5 times using a microbalance (AND BM–22) which has a resolution of ±1 μg. The N_2 adsorption/desorption isotherm have been obtained at 77 K by employing liquid nitrogen. Pore size distribution and pore volume have been determined by DFT method whereas, surface area have been calculated by BET method.

4.1.3.2   Specific heat capacity measurement

About 25–50 mg silica gel is placed inside the Aluminium sample pan. The opening is then sealed with an Aluminium lid by providing marginal pressure so that the silica gel particles are not crushed inside. Silica gel have high affinity to water vapor and the samples already contain the water vapor along with other foreign materials. These unwanted substances need to be removed before the measurement to acquire precise specific heat capacity data. Hence, the prepared sample is parched in a typical oven at 100 °C overnight. Subsequently, the sample is dried in a vacuum oven at 100 °C for 4 hours to eliminate remaining water vapor and other foreign elements. Mass measurement is done immediately after bringing out the sample from the heater so that no foreign elements can influence the measurement. Experimental conditions of the specific heat capacity measurement is summarized in Table 4.2.

Table 4.2. Experimental conditions of specific heat capacity measurement.

Sample degassing duration	$\geq$ 12 hours
Heating/cooling rate	10 °C/min
Number of thermodynamic–isothermal cycles	3
Isothermal time	60 min
Mass of aluminium pan and lid [mg]	$\approx$ 30 mg
Dimension of aluminium pan [mm]	5.6 mm $\times$ 2.8 mm
Dimension of aluminium lid [mm]	5.2 mm $\times$ 1.4 mm
Mass of sample	25 – 50 mg
Temperature range of measurements	30 – 100 ºC

Final specific heat capacity data calculation requires three DSC data: (a) Baseline data/DSC of blank pan: empty pan with sealed lid is placed on the both slots of the furnace and DSC data is collected for the measured temperature range; (b) DSC of standard sample: an empty pan with sealed lid is placed on the left slot and a sealed pan containing standard sample (α-Alumina) is put on the right slot of the furnace. The amount of the standard sample should be close to the chosen sample mass. (c) DSC of chosen sample:

previously prepared and dried sample is put on the right slot of the furnace while a sealed empty pan is kept on the left slot.

Three cycles of heating/cooling have been performed and the final data to calculate C_p is taken from third heating phase. First two cycles are to remove the foreign materials which has been again adsorbed in the meantime. In Fig. 4.4, first heating phase have a large spike in the DSC signal. This indicates power consumption by the water vapor and other impurities. Second and third heating phase do not have such unusual spike which points out that all the impurities are removed in the first heating phase with nitrogen flow.
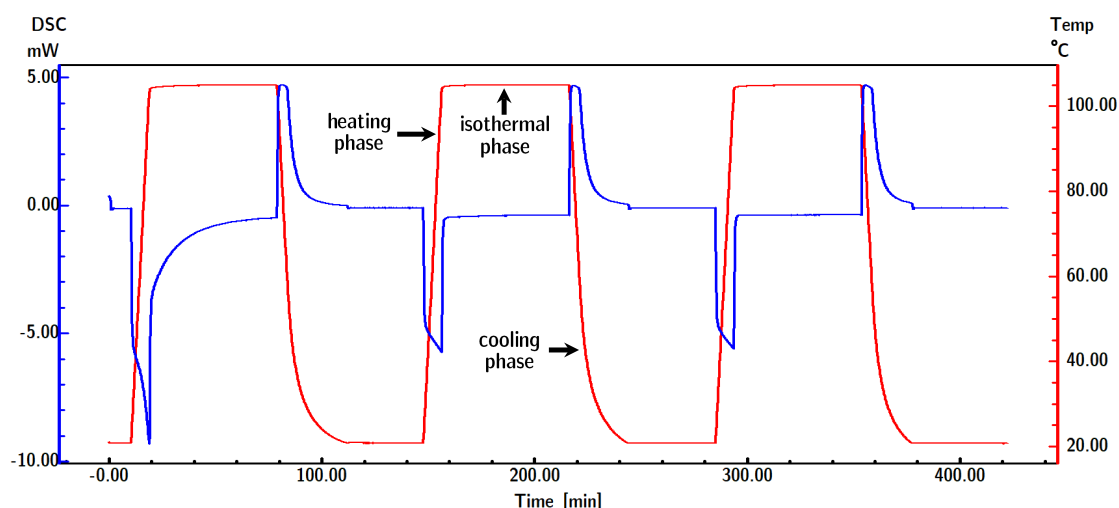
Fig. 4.4.   Temperature program and corresponding DSC signal.

4.1.4 Results and discussion

4.1.4.1   Porosimetry

Experimentally measured data of surface area and total pore volume is summarized in Table 4.3. Selected RD type silica gel have five different particle sizes. Surface area and total pore volume is similar for the first three samples (large particle size). Moreover, remaining two smaller particle sized samples have comparatively lower surface area and lower total pore volume. PSD plot of the RD type silica gel samples are shown in Fig. 4.5. All the RD silica gel samples contain both micropores and mesopores. First two samples (large particle) have sharp peak at about 1.18 nm and 1.25 nm pore width, respectively. However, the smaller particle samples have two peaks – one is at about 0.74 nm and

another is at about 1.20 nm. Hence, the PSD indicates that smaller particle samples have smaller micropores than the larger particle samples.

Both the samples of type A silica gels have almost similar surface area and pore volume. The difference is in the PSD as shown in Fig. 4.6. Smaller particle (D ≤ 0.5 mm) samples have small micropores, regular micropores and also mesopores. Pores are in the range of 0.69 – 0.86 and 1.1 – 5.13 nm width. However, the large particle sample (D ≈ 1.7 to 4.0 mm) have pores in the range from 1.09 – 5.03 nm width with a sharp peak at 1.18 nm.

Porosimetry of Type B silica gels are different from all the other samples. These samples have lower density according to manufacturers' specification (Table 4.1). Their surface area is lowest and pore volume is highest among all the samples. The PSD are also interesting of these samples (Fig. 4.7). These samples also contain micropores and mesopores. However, the amount of mesopores are much higher and the size of mesopores are larger than the other samples (2.4 – 14 nm).

Chromatorex silica gel has high surface area like large particle RD and type A silica gels. However, their pore volume is comparably higher than those samples. There are two peaks in PSD (Fig. 4.8) at the same position like RD and type A silica gels. However, the pore width range of Chromatorex silica gel is relatively wider than type A silica gels.

Two indicator type samples have almost equal surface area and total pore volume (approximately 710 m^2/g). The PSD of these samples in Fig. 4.9 shows that higher particle diameter sample have one sharp peak at 1.18 nm and the pores are in the range of 1.00 – 6.25 nm width. However, the smaller diameter sample (D ≈ 1.7 to 4.0 mm) have another peak at 0.8 nm which means smaller micropores are present in this sample.

Home silica gel have low surface area and high pore volume like type B silica gels. They also have more mesopores like type B silica gel which is in the range of 2.40 – 9.80 nm (Fig. 4.10).

Table 4.3. Porous properties of the selected silica gel samples.

Silica gel type	Particle diameter (mm)	BET surface Area (m^2/g)	Total pore volume (cm^3/g)	Pore size distribution	
				Peak (nm)	Range (nm)
RD type	D ≥ 3.3	769.0582 ± 7.0300	0.38078	1.18	1.06 – 5.43
	D ≥ 1.0	776.4119 ± 10.4633	0.36586	1.25	1.00 – 5.53
	D ≈ 0.7 to 1.18	774.8605 ± 9.0833	0.39184	0.74, 1.18	0.68 – 0.86, 1.09 – 5.18
	D ≈ 0.25 to 1.0	621.5522 ± 4.7102	0.27096	0.75, 1.21	0.68 – 0.86, 1.02 – 4.07
	D ≈ 0.075 to 0.25	630.6937 ± 4.3943	0.26378	0.73, 1.20	0.60 – 0.86, 1.00 – 4.20
Type A	D ≈ 1.7 to 4.0	740.3478 ± 6.0242	0.36177	1.18	1.09 – 5.03
	D ≤ 0.5	747.2496 ± 8.8508	0.36523	0.74, 1.18	0.69 – 0.86, 1.10 – 5.13
Type B	D ≈ 1.7 to 4.0	486.6904 ± 1.7464	0.80323	1.40, 6.90,	1.20 – 1.70, 2.40 – 14.0
	D ≤ 0.5	556.8693 ± 2.1949	0.79211	1.40, 6.10	1.20 – 1.80, 2.40 – 12.0
High purity Chromatorex silica gel	D ≈ 0.075 to 0.5	752.5088 ± 6.0601	0.42233	0.73, 1.18	0.68 – 0.85, 1.10 – 6.98
Indicator type A	D ≥ 3.3	710.9865 ± 5.1527	0.38623	1.18	1.00 – 6.25
	D ≈ 1.7 to 4.0	704.0182 ± 6.0323	0.37793	0.80, 1.24	0.73 – 0.85, 1.10 – 5.58
Home silica gel	D ≥ 0.5	564.9241 ± 1.8672	0.70015	1.40, 5.40	1.20 – 1.80, 2.40 – 9.80
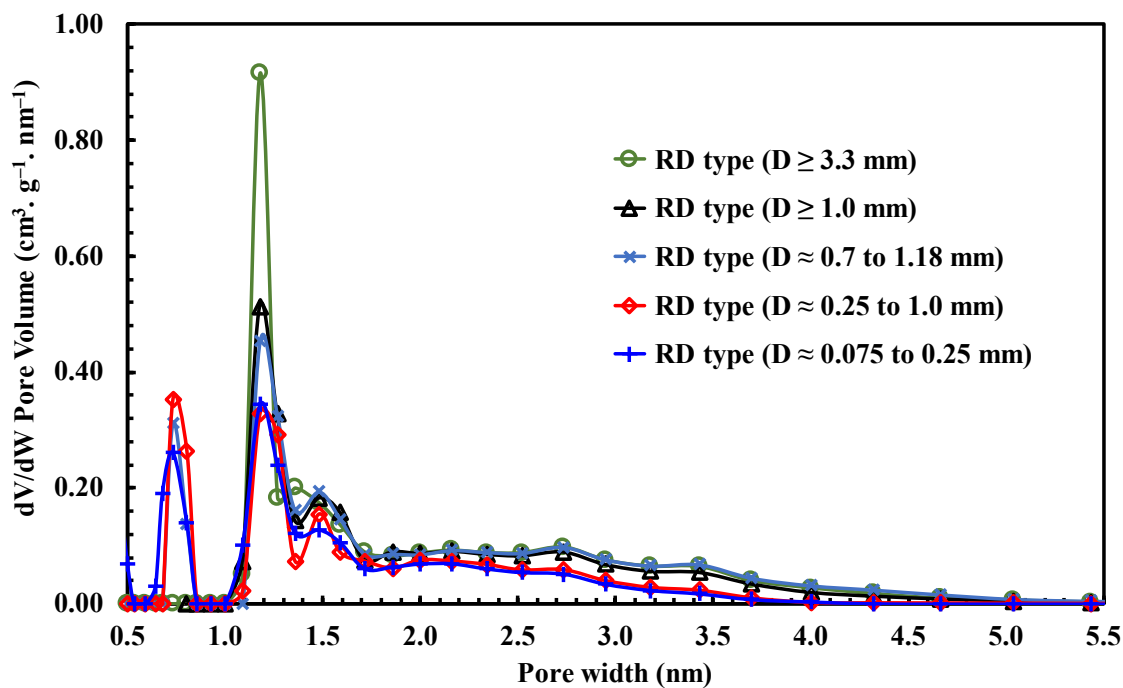
Fig. 4.5.   Pore size distribution of RD silica gels.
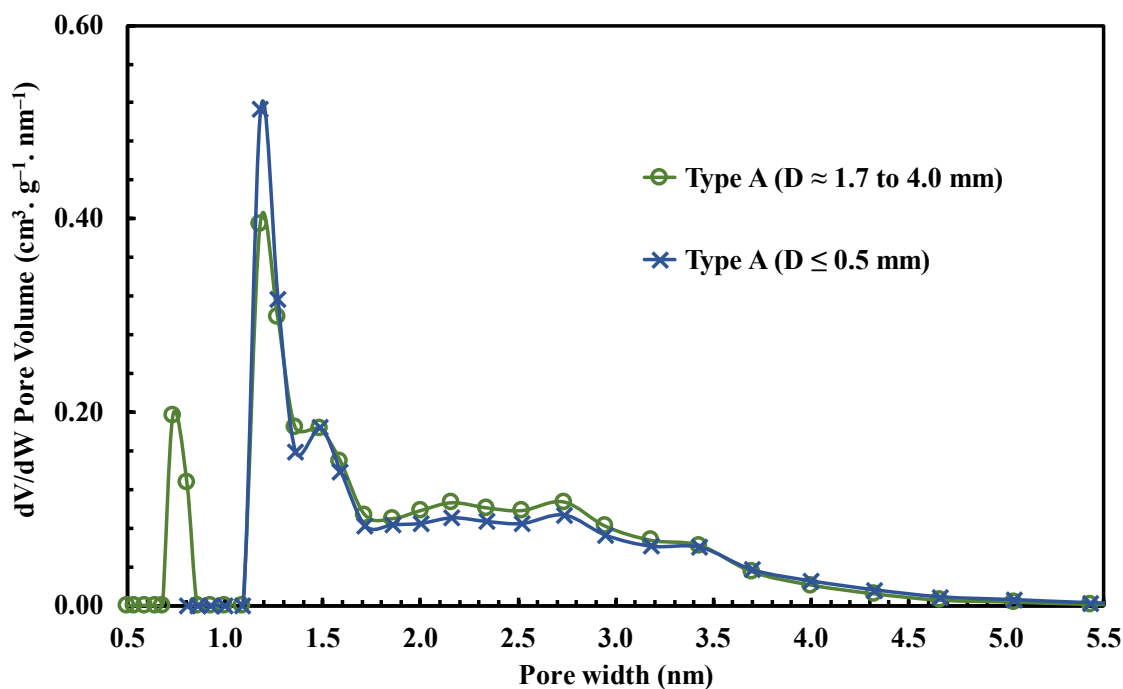
Fig. 4.6.   Pore size distribution of type A silica gels.
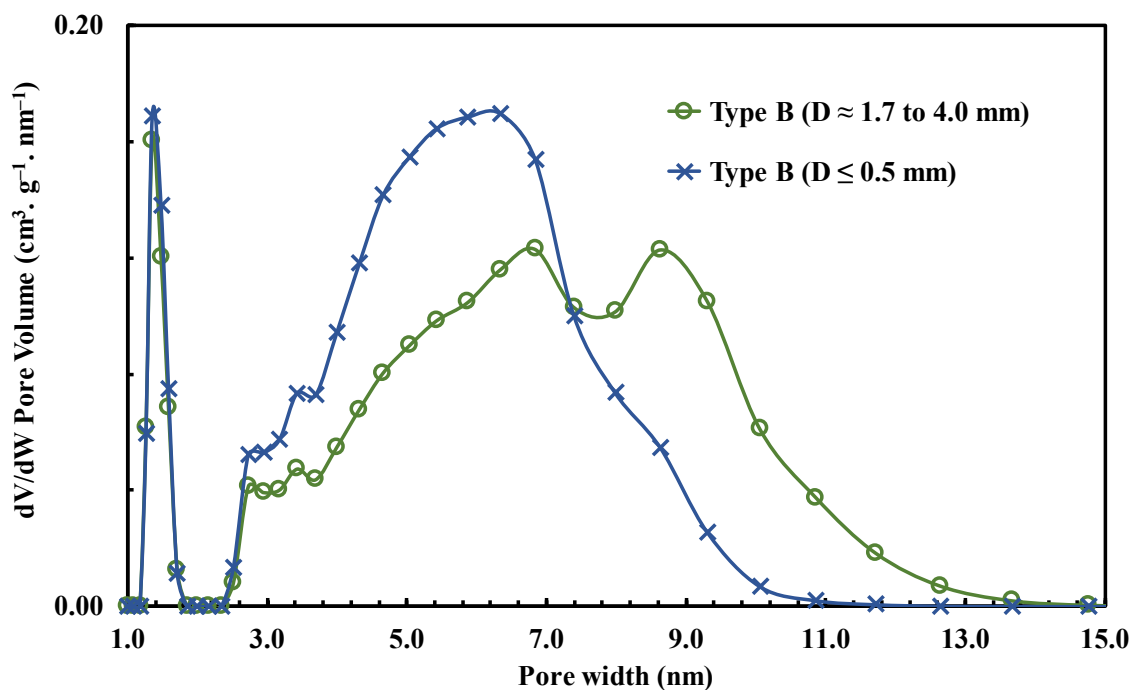
Fig. 4.7.   Pore size distribution of type B silica gels.
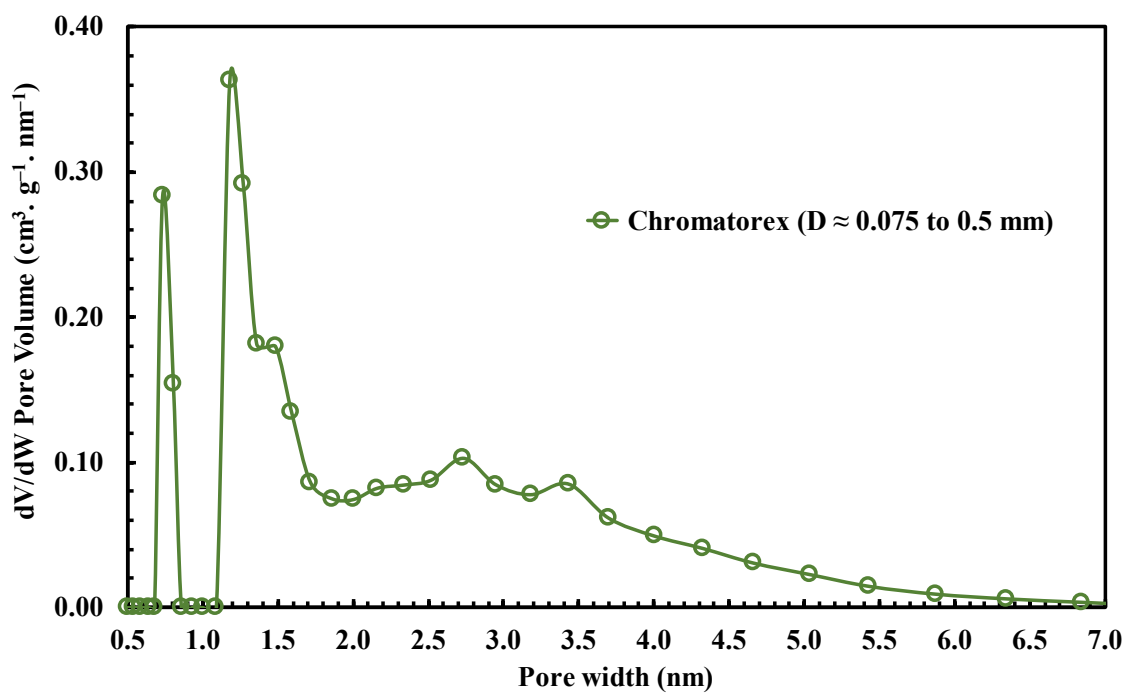
Fig. 4.8.   Pore size distribution of high purity chromatorex silica gel.
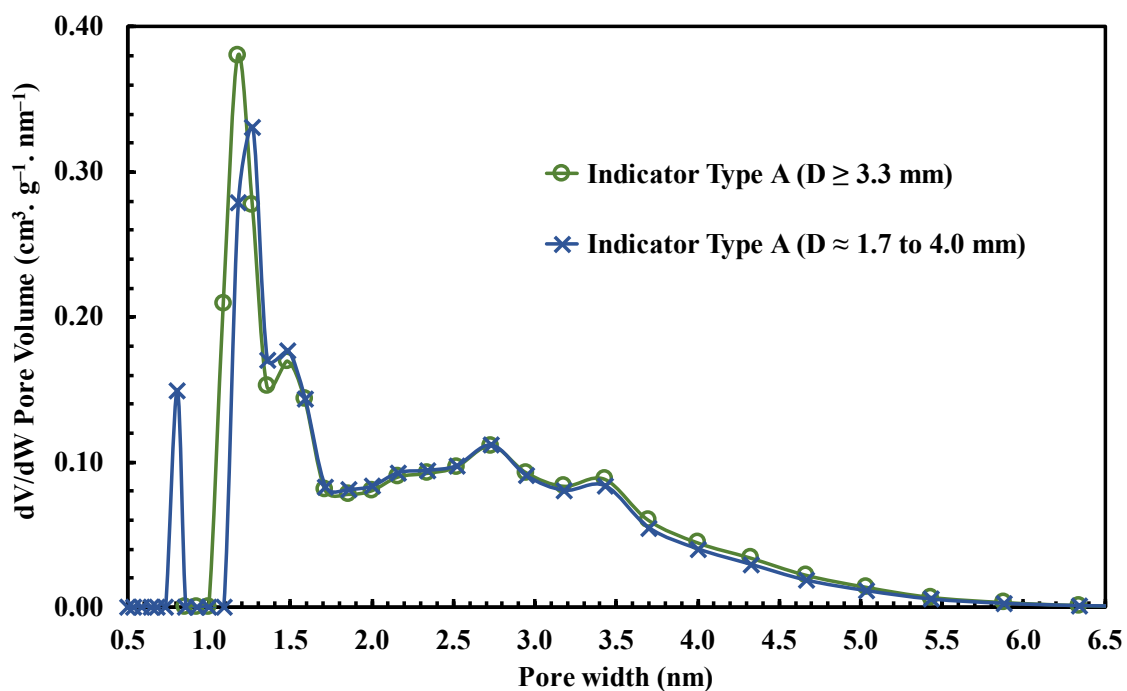
Fig. 4.9.   Pore size distribution of indicator type A silica gels.
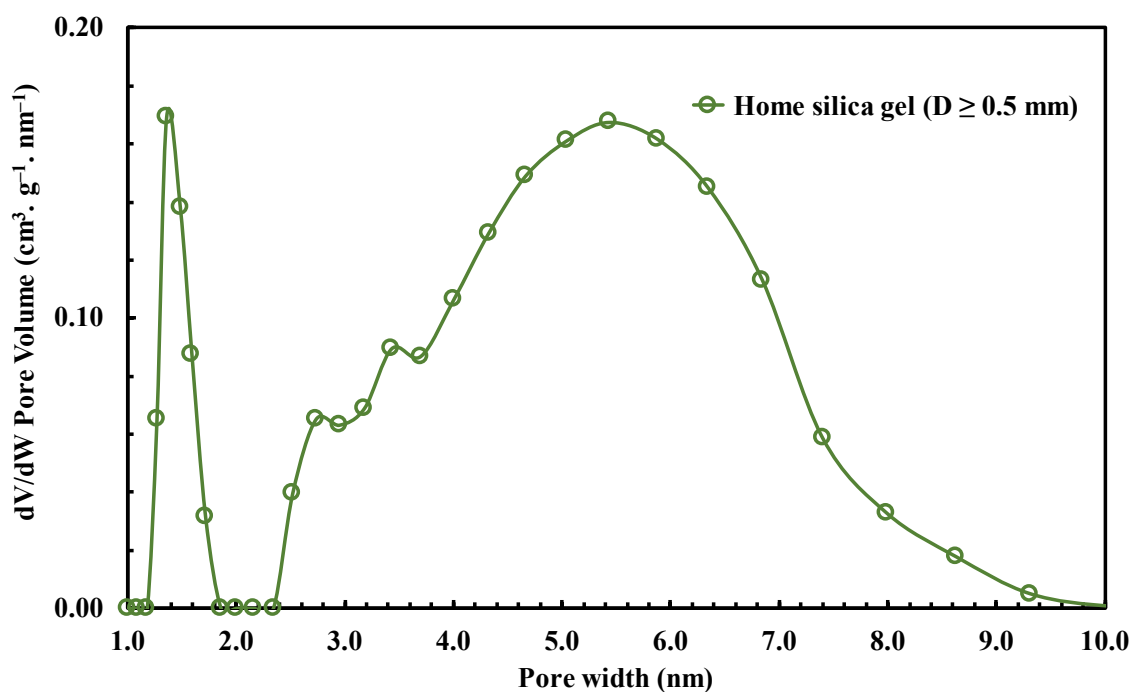
Fig. 4.10. Pore size distribution of home silica gel.

4.1.4.2 Specific heat capacity

Specific heat capacity of all the previously mentioned samples have been measured and illustrated in the following sections. Experimental data of all the samples is listed in Table 4.4.

4.1.4.2.1 RD type

There are five samples of RD type silica gel with different particle sizes. The largest particle size (D ≥ 3.0 mm) shows smaller specific heat capacity value. In Fig. 4.11, it can be clearly seen that specific heat capacity tends to increase when the particle diameter decreases. This could be due to the internal structural difference when they were manufactured.
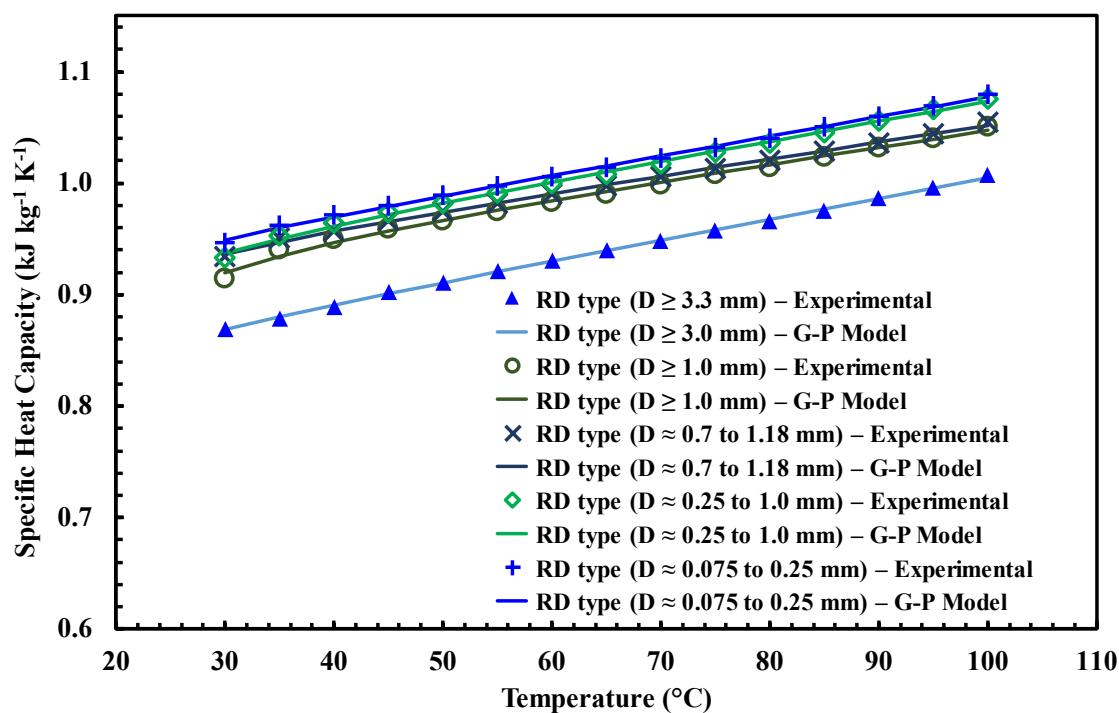
Fig. 4.11. Specific heat capacity of RD type silica gels.

4.1.4.2.2 Type A

Specific heat capacity of type A silica gel samples with two different particle sizes have been measured and shown in Fig. 4.12. The one with smaller particle diameter (D ≤ 0.5 mm) has a slightly lower C_p value than the larger particle sized (D ≈ 1.7 to 4.0 mm) one.
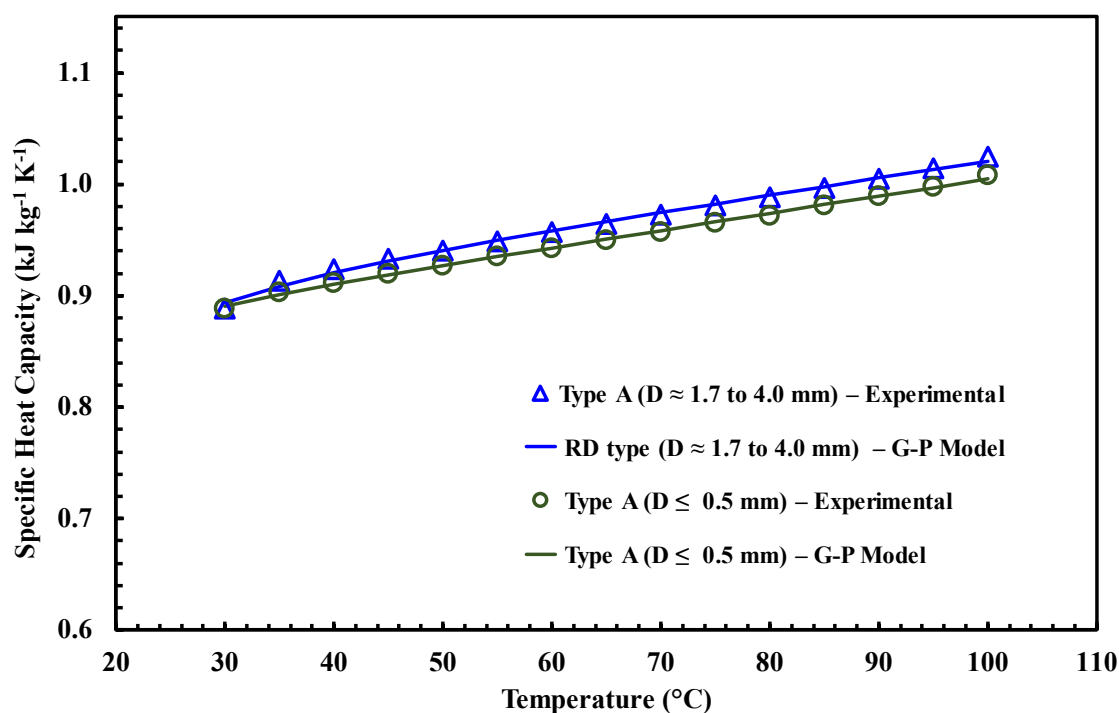
Fig. 4.12. Specific heat capacity of type A silica gels.

4.1.4.2.3 Type B

Type B silica gels also have two samples like type A. Their particle sizes are also similar. The specific heat capacity of these samples are similar as indicated in Fig. 4.13. However, type B silica gels have lower specific heat capacity value than type A silica gels.

4.1.4.2.4 Chromatorex – high purity silica gel for chromatography

Chromatorex silica gel particles are very fine and the diameter is 0.075 to 0.50 mm. The specific heat capacity is 0.888 kJ kg K^{-1} at 30 °C and increases up to 0.966 at 100 °C (Fig. 4.14).
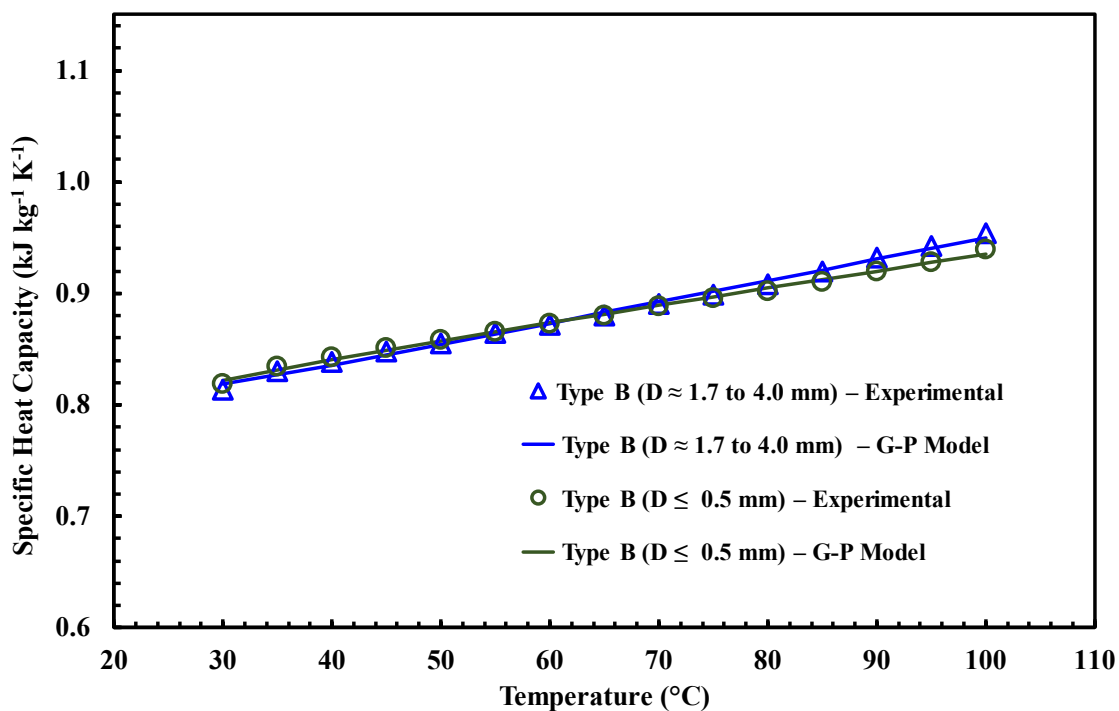
Fig. 4.13. Specific heat capacity of type B silica gels.
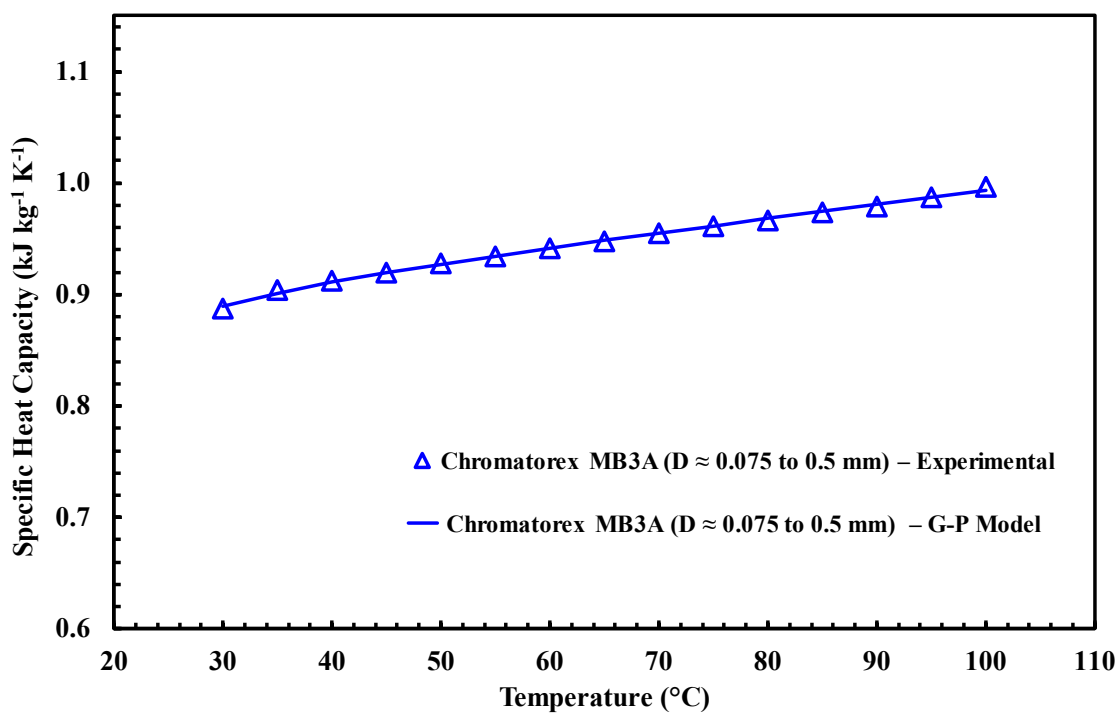
Fig. 4.14. Specific heat capacity of high purity chromatorex silica gel.

4.1.4.2.5 Indicator – type A silica gel of green color

Specific heat capacity of two samples with different particle sizes of indicator type silica gels have been measured and shown in Fig. 4.15. These types of silica gels are actually type A. However, they are transparent when dehydrated and change the color to green after vapor adsorption. C_p value of the samples almost overlap for lower temperature and relatively high for the large particle sample in the high temperature region.
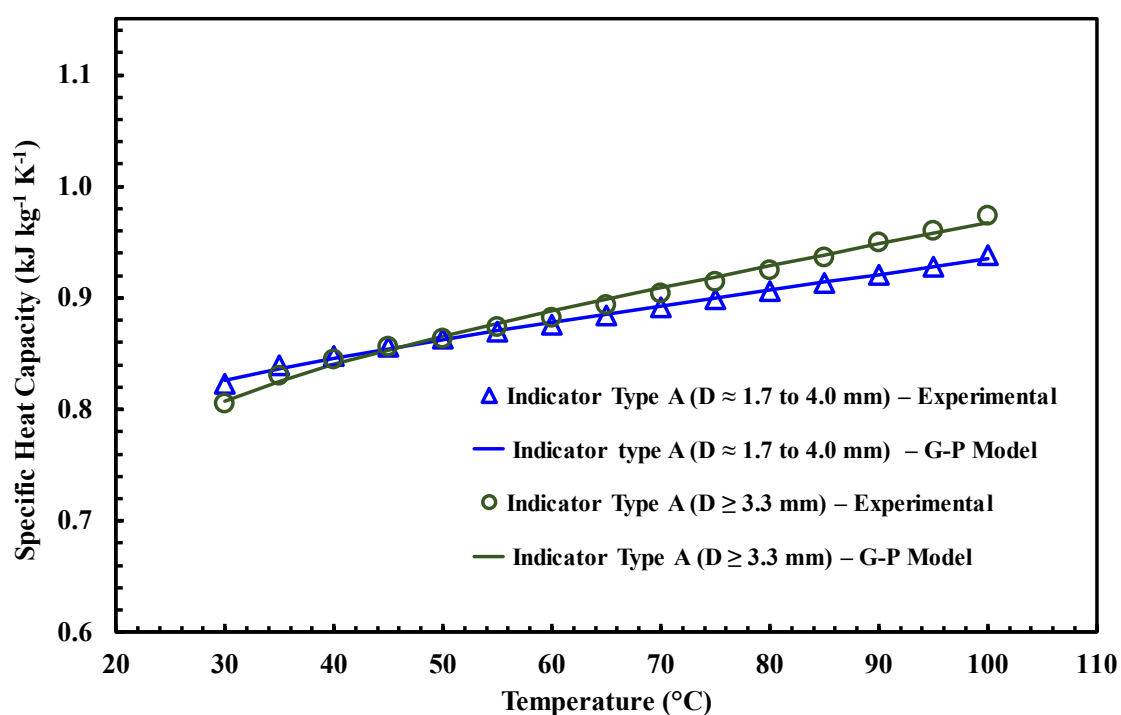
Fig. 4.15. Specific heat capacity of indicator type A silica gels.

4.1.4.2.6 Home silica gel

Continual high humidity can damage the internal structure of a building. Home silica gel is a dry desiccant which is used to control the humidity and prevent shabbiness of a building. Specific heat capacity of home silica gel is shown in Fig. 4.16.
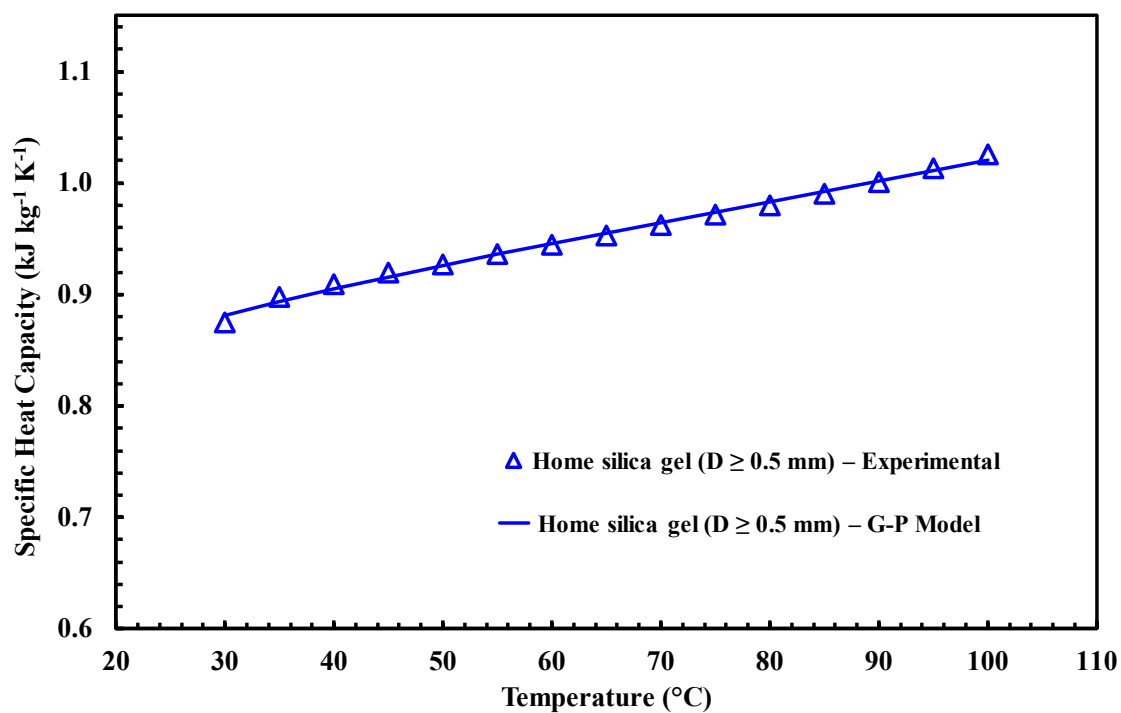
Fig. 4.16. Specific heat capacity of home silica gel.

Table 4.4. Experimental specific heat capacity data of silica gels.

Specific heat capacity (kJ kg⁻¹ K⁻¹)													
Sample name and particle size (mm) / Temp. (°C)	RD type					Type A		Type B		Chromatorex	Indicator type A		Home
	$D \geq$ 3.3	$D \geq$ 1.0	$D \approx$ 0.7 to 1.18	$D \approx$ 0.25 to 1.0	$D \approx$ 0.075 to 0.25	$D \approx$ 1.7 to 4.0	$D \leq$ 0.5	$D \approx$ 1.7 to 4.0	$D \leq$ 0.5	$D \approx$ 0.075 to 0.5	$D \approx$ 1.7 to 4.0	$D \geq 3.3$	$D \geq 0.5$
30	0.870	0.915	0.934	0.934	0.946	0.889	0.889	0.814	0.822	0.888	0.823	0.805	0.875
35	0.879	0.940	0.951	0.953	0.963	0.914	0.903	0.830	0.832	0.904	0.840	0.830	0.898
40	0.889	0.950	0.958	0.964	0.971	0.924	0.911	0.839	0.841	0.912	0.848	0.845	0.909
45	0.902	0.959	0.966	0.974	0.980	0.933	0.920	0.848	0.849	0.920	0.856	0.856	0.919
50	0.911	0.967	0.974	0.982	0.989	0.941	0.927	0.855	0.858	0.928	0.863	0.864	0.927
55	0.921	0.975	0.982	0.991	0.997	0.949	0.936	0.864	0.866	0.935	0.870	0.874	0.936
60	0.931	0.983	0.990	1.000	1.006	0.957	0.943	0.872	0.874	0.942	0.876	0.883	0.944
65	0.940	0.991	0.997	1.008	1.015	0.965	0.950	0.880	0.881	0.948	0.884	0.893	0.953
70	0.949	0.999	1.006	1.017	1.023	0.972	0.958	0.890	0.889	0.955	0.892	0.904	0.962
75	0.958	1.008	1.013	1.027	1.032	0.981	0.965	0.899	0.897	0.961	0.899	0.914	0.972
80	0.966	1.015	1.020	1.036	1.040	0.988	0.972	0.909	0.905	0.966	0.906	0.925	0.980
85	0.976	1.023	1.029	1.046	1.051	0.997	0.981	0.920	0.912	0.973	0.913	0.936	0.991
90	0.986	1.032	1.037	1.056	1.060	1.005	0.989	0.932	0.920	0.979	0.920	0.950	1.001
95	0.996	1.040	1.045	1.066	1.069	1.014	0.998	0.942	0.927	0.988	0.928	0.960	1.013
100	1.008	1.051	1.055	1.076	1.079	1.025	1.008	0.954	0.935	0.996	0.939	0.973	1.025

Green and Perry (1997) [140] proposed a thermodynamic equation to express the specific heat capacity. Experimental data have been fitted with that well-known equation.

$$c_p = \alpha + \beta T + \frac{\gamma}{T^2}$$
(4.1)

The adjustable parameters α, β, and γ of the equation are determined and summarized in equation (4.1). G-P model fitting error (RMSD) is less than 0.4% for all the silica gel samples.

Table 4.5. List of adjustable parameters for G–P model fitting.

Sample name and particle size		α	β	γ	Fitting error
RD type	D ≥ 3.3	0.81968	0.00186	−6.039580	0.11%
	D ≥ 1.0	0.90328	0.00146	−24.32286	0.27%
	D ≈ 0.7 to 1.18	0.90310	0.00150	−10.47861	0.14%
	D ≈ 0.25 to 1.0	0.91269	0.00179	−12.70729	0.19%
	D ≈ 0.075 to 0.25	0.90461	0.00173	−6.675290	0.15%
Type A	D ≈ 1.7 to 4.0	0.87783	0.00145	−24.94680	0.27%
	D ≤ 0.5	0.85473	0.00151	−8.273520	0.14%
Type B	D ≈ 1.7 to 4.0	0.75558	0.00194	4.0729700	0.27%
	D ≤ 0.5	0.78585	0.00150	−8.259000	0.20%
Chromatorex	D ≈ 0.075 to 0.5	0.87437	0.00121	−18.71797	0.14%
Indicator type A	D ≈ 1.7 to 4.0	0.79843	0.00138	−12.09580	0.18%
	D ≥ 3.3	0.78465	0.00186	−30.33435	0.39%
Home	D ≥ 0.5	0.84120	0.00180	−13.12172	0.31%

4.1.5 Conclusions

BET surface area, total pore volume, pore size distribution and specific heat capacity of six different silica gel samples (13 samples including all the subcategories) have been measured and reported in this chapter. Type B silica gel samples have the lowest surface area and highest pore volume among all the samples. Home silica gel also have similar porous properties. Highest surface area is found for RD type (large particle) silica gels and lowest pore volume is found for RD type (small particle) silica gels. All the silica gels have both micropores and mesopores. However, type B and home silica gels have more

mesopores and the size of mesopores are also larger for these samples. Specific heat capacity increases with temperature. Specific heat capacity is highest for RD silica gel (smallest particle) and lowest for indicator type silica gels. Specific heat capacity data of all the samples are fitted with G-P model and the adjustable parameters were determined for each sample. The fitting error for all the samples are less than 0.4%. Hence, specific heat capacity of a particular sample at any unknown temperature can be predicted using the G-P equation and the fitting parameters unless any structural change occurs to the sample. These porosimetry and specific heat capacity data is very significant to design and simulate adsorption cooling systems (ACS).

4.2   Carbon materials

The studied carbon samples include (i) parent Maxsorb III with different particle sizes, (ii) surface treated Maxsorb III (H_2 and KOH-H_2) (iii) recently developed spherical activated carbon (KOH treated phenol resin, KOH6-PR), and (iv) expanded graphite. Details information about the samples are summarized in Table 4.6. The specific heat capacity of these materials is measured at temperatures ranging from 30°C to 150°C using a heat flux type differential scanning calorimeter (DSC). The specific heat capacity measurement procedure is same as silica gel which is mentioned in the previous sections.

Table 4.6. Adsorbent materials used in the experiment.

Sample name	Sample type	Supplier/ Source	Particle diameter D_{50} (µm)
Maxsorb III [62]	Activated carbon (AC) powder	Kansai Coke & Chemicals Co. Ltd., Japan	105
H_2 treated Maxsorb III [62]	Surface treated AC powder	Materials Chemistry & Eng. Kyushu University	107
KOH-H_2 treated Maxsorb III [141]	Surface treated AC powder	Materials Chemistry & Eng. Kyushu University	100
Spherical Phenol resin (KOH6) [142]	Surface treated AC powder	Materials Chemistry & Eng. Kyushu University	23
EC-1000	Expanded graphite Powder	Ito Graphite Co., Ltd., Japan	15
EC-1500	Expanded graphite Powder	Ito Graphite Co., Ltd., Japan	7

4.2.1 Results and discussion

To minimize the impact of heating rate and sample weight, many test measurements have been performed in order to optimize it considering the volume of the sample holder and the density of powder adsorbents. It is noteworthy to mention that the heating rate of 10 ºC/min and sample weight 4-5 mg is found appropriate for the present measurement

because it can reproduce data with highest precision. To avoid edge effects in the calculated results, specific heat capacity values are furnished for temperature range of 30–150 ºC. This temperature range represents the typical operating condition of adsorption heat pump systems. The numerical values of specific heat capacities of some adsorbents are shown in Table 4.7.

Table 4.7. Specific heat capacity of adsorbent materials.

Specific heat capacity [kJ kg^{-1} K^{-1}]					
Temperature [ºC]	Maxsorb III	H$_2$-treated Maxsorb III	KOH-H$_2$ treated Maxsorb III	Phenol resin (KOH6)	Expanded graphite (EC-1500)
30	0.844	0.949	1.060	0.751	0.738
40	0.857	0.961	1.075	0.755	0.768
50	0.876	0.969	1.098	0.756	0.794
60	0.896	0.981	1.120	0.758	0.818
70	0.914	0.994	1.135	0.768	0.842
80	0.931	1.007	1.164	0.774	0.862
90	0.950	1.023	1.184	0.783	0.880
100	0.969	1.035	1.200	0.789	0.899
110	0.984	1.054	1.215	0.788	0.920
120	0.998	1.084	1.237	0.795	0.947
130	1.019	1.105	1.262	0.823	0.974
140	1.042	1.142	1.289	0.860	0.999
150	1.068	1.181	1.324	0.942	1.029

Specific heat capacity of reference sample (α-Al$_2$O$_3$) is measured and verified with literature [143]. It can be seen from Fig. 4.17 that the measured values of α-Al$_2$O$_3$ agrees well over the entire temperature range whilst the deviation is within ±0.3%. The heat flow calibration of the system is done by using reference indium and a good agreement was found with the standard value [144].
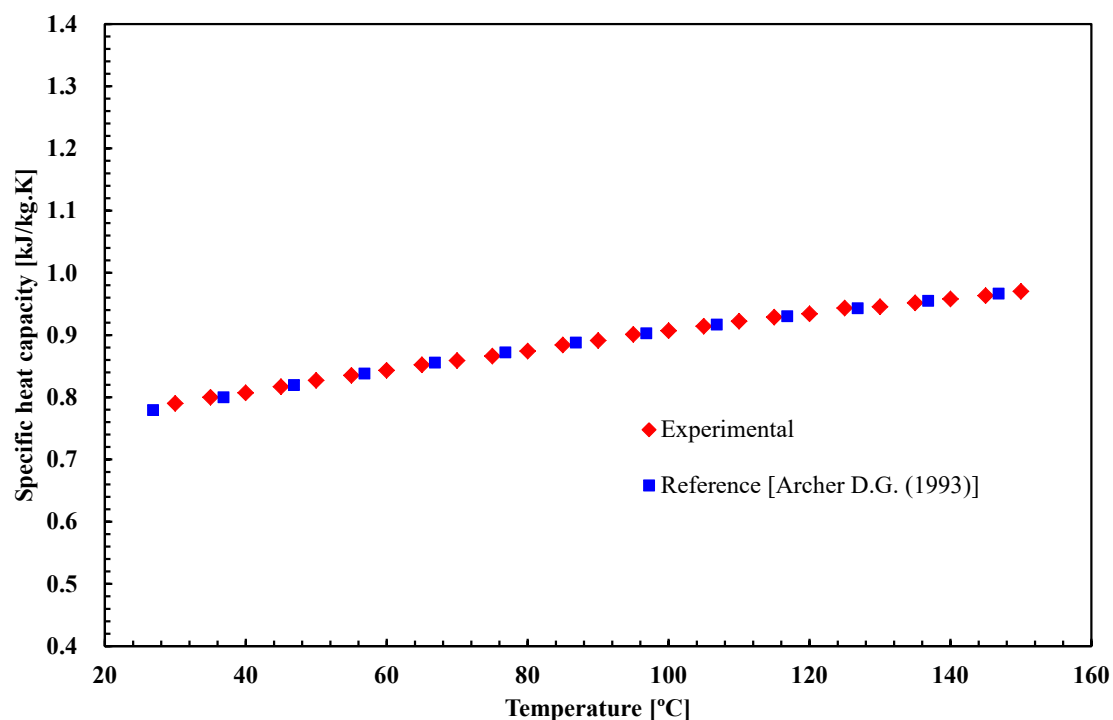
Fig. 4.17. Results of DSC measurements for the reference material (α-Al$_2$O$_3$).

Fig. 4.18 shows the specific heat capacity of the parent Maxsorb III, H$_2$ treated Maxsorb III and KOH-H$_2$ treated Maxsorb III at selected temperature range. It is found that KOH-H$_2$ treated Maxsorb III shows the highest specific heat capacity among the Maxsorb III-based adsorbents. This might be attributed to the contribution of surface functional group (–COOH) which is formed during surface treatment. The details of surface treatment and functional group formation can be found elsewhere (Kill et al.[145] 2013, El-Sharkawy et al. [141]). The average value of specific heat capacity of parent Maxsorb III, H$_2$ treated Maxsorb III and KOH-H$_2$ treated Maxsorb III is found to be 0.89, 0.98 and 1.11 kJ kg^{-1} K^{-1}, respectively. These findings agree well with fitted correlation for the specific heat of the activated carbon reported by Xiao et al. [146]. The computed value using the correlation is 0.98 kJ kg^{-1} K^{-1} for the same temperature range.
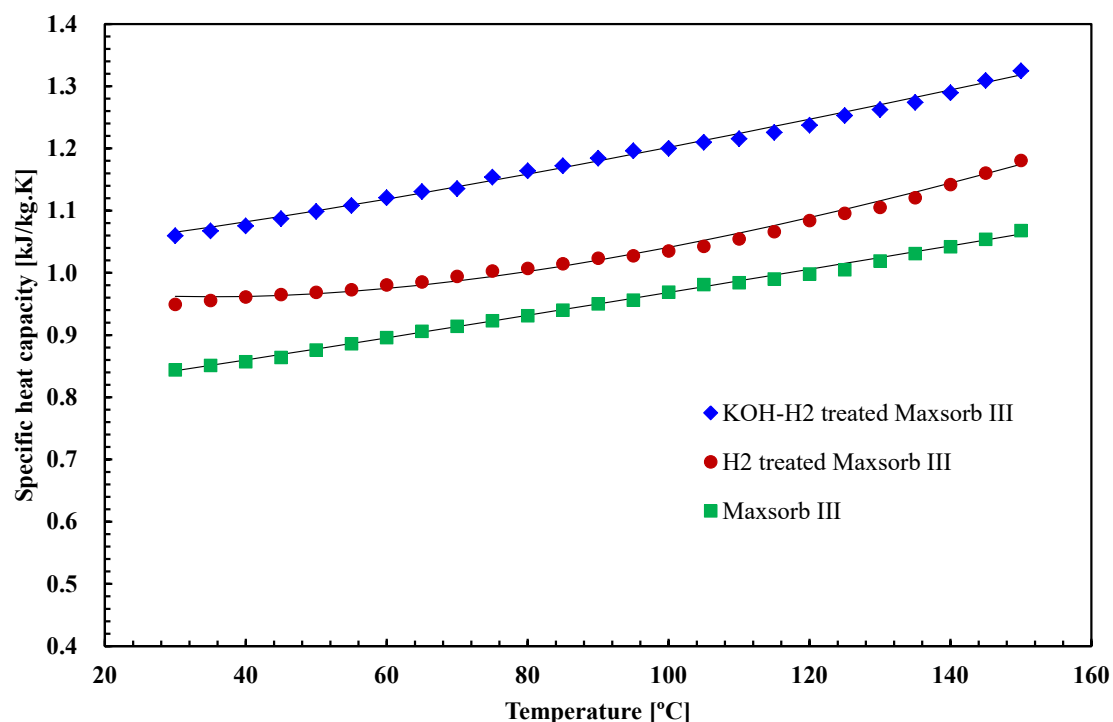
Fig. 4.18. Comparison of specific heat capacity of parent Maxsorb III, H_2 treated Maxsorb III and KOH-H_2 treated Maxsorb III.

The effect of particle size on specific heat capacity is also investigated and the results for Maxsorb III are depicted in Fig. 4.19. Again, it is noted that the data provided here are the mean values of four successive measurements. It is found that the specific heat capacity increases with increase in particle size. This finding might be attributed to lack of homogeneity of the adsorbent sample with respect to particle size. Furthermore, it should be mentioned that even though utmost care was taken to ensure uniform spreading of the powder samples, it was not possible to ensure close packing. There might still be trace amount of trapped gases in between the solid particles which could result in variable heat flow, eventually causing uncertainties in the specific heat measurements.
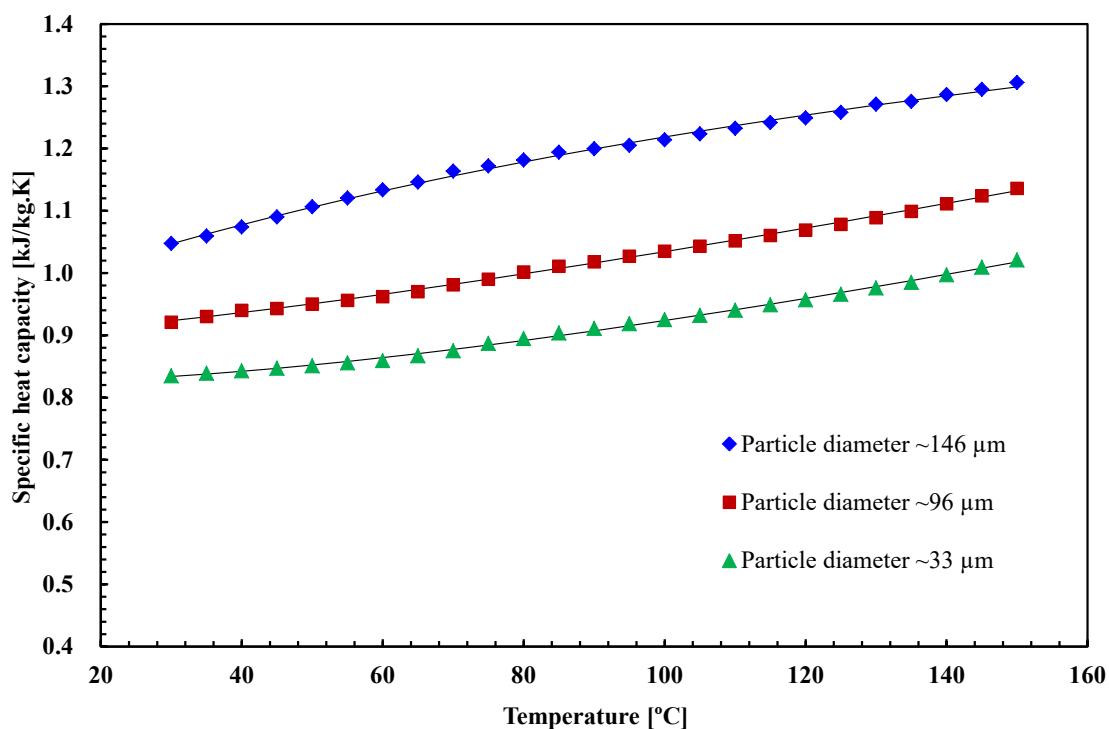
Fig. 4.19. Specific heat capacity of different particle size Maxsorb III.

Newly developed adsorbent based on KOH treated phenol resin (KOH6-PR) is reported to have high adsorption capacity, nearly 2 kg of ethanol/kg of adsorbent [142]. The specific heat capacity of such material is shown in Fig. 4.20. Similar to above results, an increase in specific heat at higher temperature is observed for this adsorbent. Interestingly, specific heat capacity of the KOH6-PR is found to be the lowest among all the selected porous adsorbents.
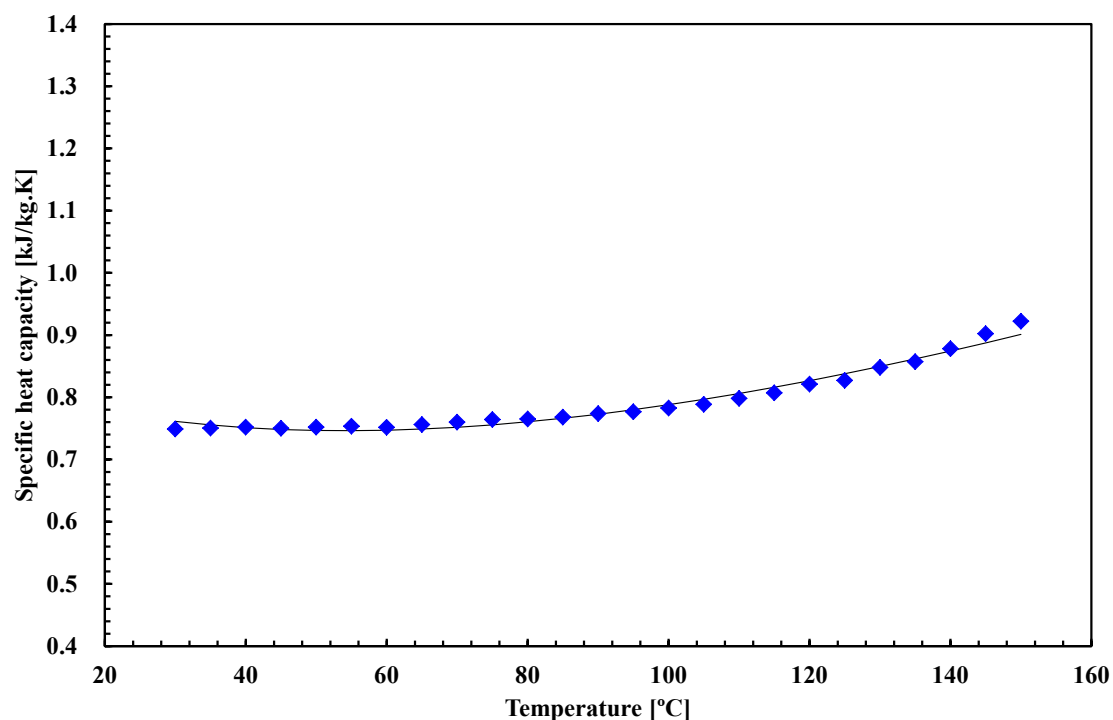
Fig. 4.20. Specific heat capacity of phenol resin based and KOH6 activated carbon.

Expanded graphite, even though not an adsorbent, has been a popular thermal conductivity enhancer in several composite adsorbents. Hence, its specific heat capacity is also of interest in addition to the carbonaceous adsorbents discussed above. In this study two types of expanded graphite namely EC-1500 and EC-1000 are evaluated in Fig. 4.21. It is again evident that the specific heat capacity of the sample increases in a continuous manner within the experimental temperature range. The marginal difference in specific heat capacity observed for different samples might be attributed to different particle size similar to the case of Maxsorb III discussed earlier.
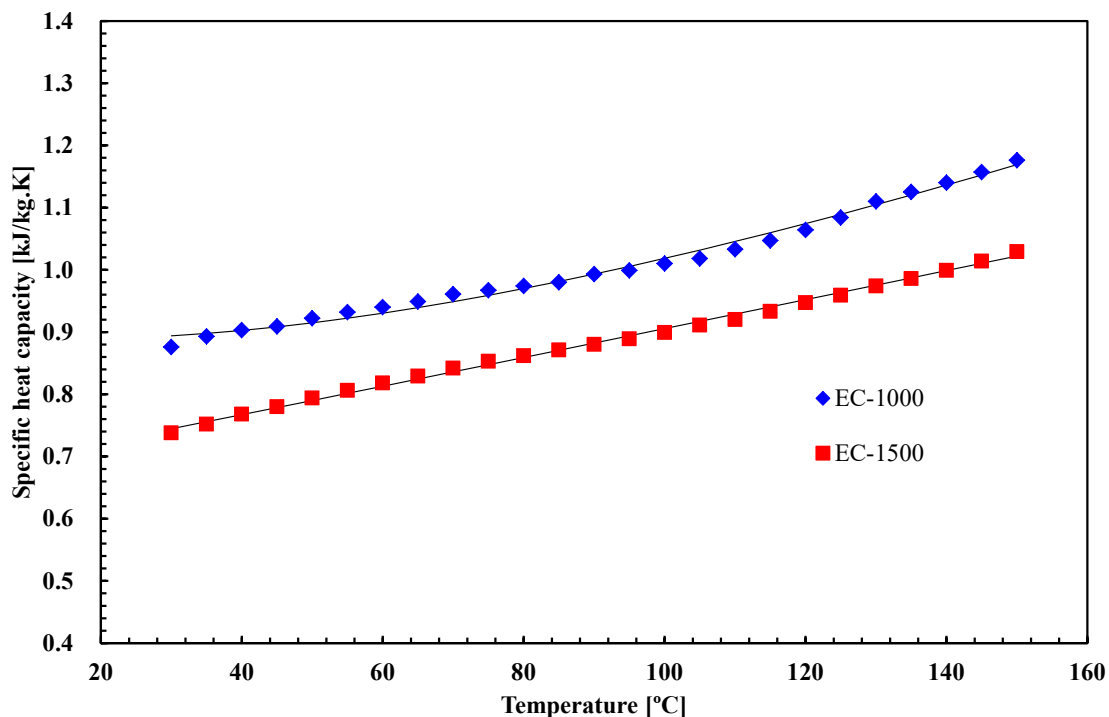
Fig. 4.21. Comparison of specific heat capacity of expanded graphite.

Furthermore, it is evident from the results that specific heat capacity of adsorbents measured in this study show significant dependency on temperature. For example, KOH-H_2 treated Maxsorb-III shows an increase of more than 13% in specific heat capacity for rise in temperature from 30 ºC to 100 ºC. Such conditions are typically encountered in adsorption systems wherein the heat input to the adsorber beds depend significantly on the specific heat capacity of the adsorbent used. Due to lack of data, several simulation models assume constant specific heat, which may eventually lead to inaccuracy in energy calculations. Therefore, it is necessary to formulate a temperature dependent correlation for specific heat capacity which can be beneficial for such thermal calculations in adsorption applications.

The measured specific heat capacities of all the selected samples are again fitted with the G-P model of equation (4.1). The values of constant α, β and γ for the carbonaceous materials studied in this study are summarized in Table 4.8.

Table 4.8. Coefficients of specific heat capacity correlation fitting.

Sample name	α	β	γ
Maxsorb III	0.20008	0.00199	3605.41
H$_2$ treated Maxsorb III	−1.36136	0.00502	73677.53
KOH-H$_2$ treated Maxsorb III	−0.01482	0.00291	18193.19
Maxsorb III (D~146 μm)	1.39449	0.00031	−40609.74
Maxsorb III (D~96 μm)	−0.03810	0.00253	17870.74
Maxsorb III (D~33 μm)	−0.32708	0.00280	28676.45
Spherical phenol resin (KOH6)	−1.77159	0.00513	89854.07
Expanded graphite (EC–1000)	−1.23137	0.004895	58943.45
Expanded graphite (EC–1500)	−1.10813	0.00239	1758.57

4.2.2 Conclusions

The specific heat capacities of various carbon-based materials employed in adsorption processes have been evaluated experimentally. Widely known activated carbon i.e., parent and surface treated Maxsorb III, recently developed KOH treated spherical phenol resin (KOH6-PR) and carbon based thermal conductivity enhancer (expanded graphite) for composite adsorbents have been investigated for the first time. The specific heat capacities for such materials have been measured using a wide range of temperature (30 to 150ºC) which is the practical operation range of adsorption cycles for cooling, dehumidification and desalination. It is observed that surface treated adsorbents show higher specific heat capacity values which might be contributed to the surface functional group. Some notable findings are: (i) the specific heat capacities of all the selected adsorbents exhibit increasing trend with temperature, (ii) KOH-H$_2$ treated Masxorb III shows the highest specific heat capacity (1.11 kJ/kg·K) and (iii) KOH6-PR possess the lowest specific heat capacity (0.792 kJ/kg·K). The influence of particle size on the specific heat capacity has been investigated wherein higher particle size were found to possess higher value. A temperature dependent correlation is used to model the experimental data. This fitting equation can be utilized for thermal calculations of practical adsorption systems and is essential for precise system design and performance evaluation.

Chapter 5

Pore shaping to enhance the quality of adsorbents

Activated carbon is widely used as an adsorbent because it is highly microporous. The pore size distribution of commercial and synthesized activated carbons contain a significant percentage of pores which are less than 0.7 nm (ultramicropores) size. There are some mesopores in the parent samples (2 – 4 nm). In adsorption cooling applications, commonly used refrigerant molecule clusters are unable to enter into such tiny ultramicropores and no adsorption occurs there. Hence, these ultramicropores degrade the performance of an adsorption cooling system (ACS). Moreover, another essential property of a good adsorbent is high thermal conductivity and lower specific heat capacity. Trapped air molecules and foreign elements inside these pores cause a reduction of the thermal conductivity and increase the specific heat capacity. Additionally, the presence of mesopores might cause slower kinetics. The objective of this research work is to remove those unusable pores by chemical vapor deposition (CVD) and enhance the quality of commercial activated carbon namely Maxsorb III. Pyrolysis of methane gas and liquid benzene on Maxsorb III have been performed to block the unusable pores. Pyrolysis temperature range is from 800 °C to 1000 °C for various time duration (5 min to 30 min) and flow rate (5 ml/min to 50 ml/min). Porosimetry change of the pyrolyzed samples have been compared with the parent Maxsorb III. Pyrolization of methane (T_{pyr} = 1000 °C, $\dot{m}$ = 50 mL/min, t = 30 min) and benzene (T_{pyr} = 800 °C, $\dot{m}$ = 25 mL/min, t = 10 min) removes the ultramicropores and most of the mesopores which might improve the quality of activated carbon.

5.1 Background

Adsorption based systems appear to be the next generation of refrigeration and heat pump applications because of the viewpoint of minimal electricity usage, driven by low temperature waste heat, global warming impact and ozone layer depletion (ODP) problems [19,77,147]. Selection of appropriate adsorbent/refrigerant pair is prerequisite to build an

efficient adsorption cooling system (ACS). Because of the microporous structure, large surface area (approximately 3140 m^2/g) [148] along with huge pore volume and easy availability, activated carbon (AC) is the utmost potential element for ACS [19]. However, commercial Maxsorb III contains ultramicropores which might degrade the performance of the system. Hence, removal of these ultramicropores would enhance the adsorbent quality and performance of the system.

Researchers are trying to control the pore size of carbon for various applications [44,45,149–154]. Kawabuchi et al. [44] controlled pore size of activated carbon fiber (ACF) by CVD of carbon from benzene and cyclohexane. They found that 700 – 800 °C temperature is very effective and about 11% weight increases because of the carbon deposition. They also found that Cyclohexane decomposes rapidly in the operating temperature range and thus inferior to benzene as a carbon precursor. The objective was to enhance the molecular sieve separation of CH_4 from CO_2 which was explicitly achieved in this work. Subsequently, Kawabuchi et al. [48] used three heterocyclic compounds: pyridine, pyrrole, and thiophene to control the porosity and surface functionality of the active carbon fiber (ACF). Interestingly, they found improved selectivity during gas separation application by adsorptions of CO_2/CH_4 and O_2/N_2. Verma et al. [45] investigated heat treatment at 1100 K and carbon gasification on various carbon molecular sieve (CMS) and activated (AC). They found that the net effect of carbon gasification was shrinkage of pores in a particular size range, which introduced interesting possibilities for production of highly selective CMS. Afterwards, Verma [46] improved molecular sieving behavior of carbon by heat treatment, carbon gasification and chemisorption of propylene. Kinetic separation of O_2 from Ar was improved because of this treatment which was the main objective of this research work.

However, there is few research works until now which was targeted to enhance the performance of ACSs by pore shaping. In adsorption cooling system, activated carbon/ethanol, activated carbon/methanol, activated carbon/ammonia pairs are frequently used because of the high adsorption uptake and faster kinetics. However, the adsorbate molecules are unable to enter into the ultramicropores (<0.7 nm). Selective removal of those unusable pores will increase adsorption uptake, faster kinetics can be achieved

thermal conductivity and specific heat capacity will improve. Thus, the objective of this research work is to find the appropriate material and operating conditions of pyrolysis for pore size modification.

Current research has been carried out with pyrolization material methane and benzene. Maxsorb III is pyrolyzed by CH_4 and C_6H_6 for various pyrolization temperature, flow rate and time. The experiment has been conducted in an inert environment by flowing Argon at 100 sccm/min rate.

5.2 Theory

Commercial activated carbon contains ultramicropores ($0.1 \leq r < 0.7$ nm), regular micropores ($0.7 \leq r < 2$ nm) and few percentages of mesopores ($2 \leq r \leq 4.4$ nm) [148]. The concept of pore modification is illustrated in Fig. 5.1 (a) and (b). Pyrolization is done at much higher temperature than the boiling point of a material. At this high temperature, the pyrolization material decomposes inside the ultramicropores and block those unusable pores.
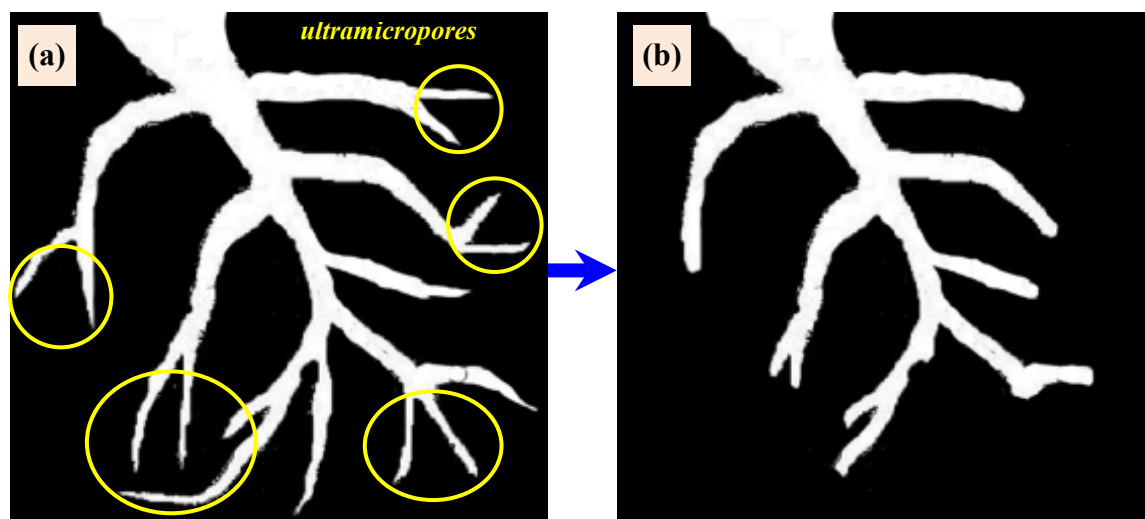
Fig. 5.1.   (a) An overview of pores before pyrolysis; (b) modified pores after pyrolysis.

SEM image of Maxsorb III depicted in Fig. 5.2 (a) shows the existence of pores. The length of benzene molecule is 0.7 nm and width is 0.34 nm. Hence, these molecules can

enter into the pores which are greater than 0.34 nm. After pyrolization, carbon atoms of those benzene molecules are deposited on the pore wall and block those pores (Fig. 5.2 (b)).
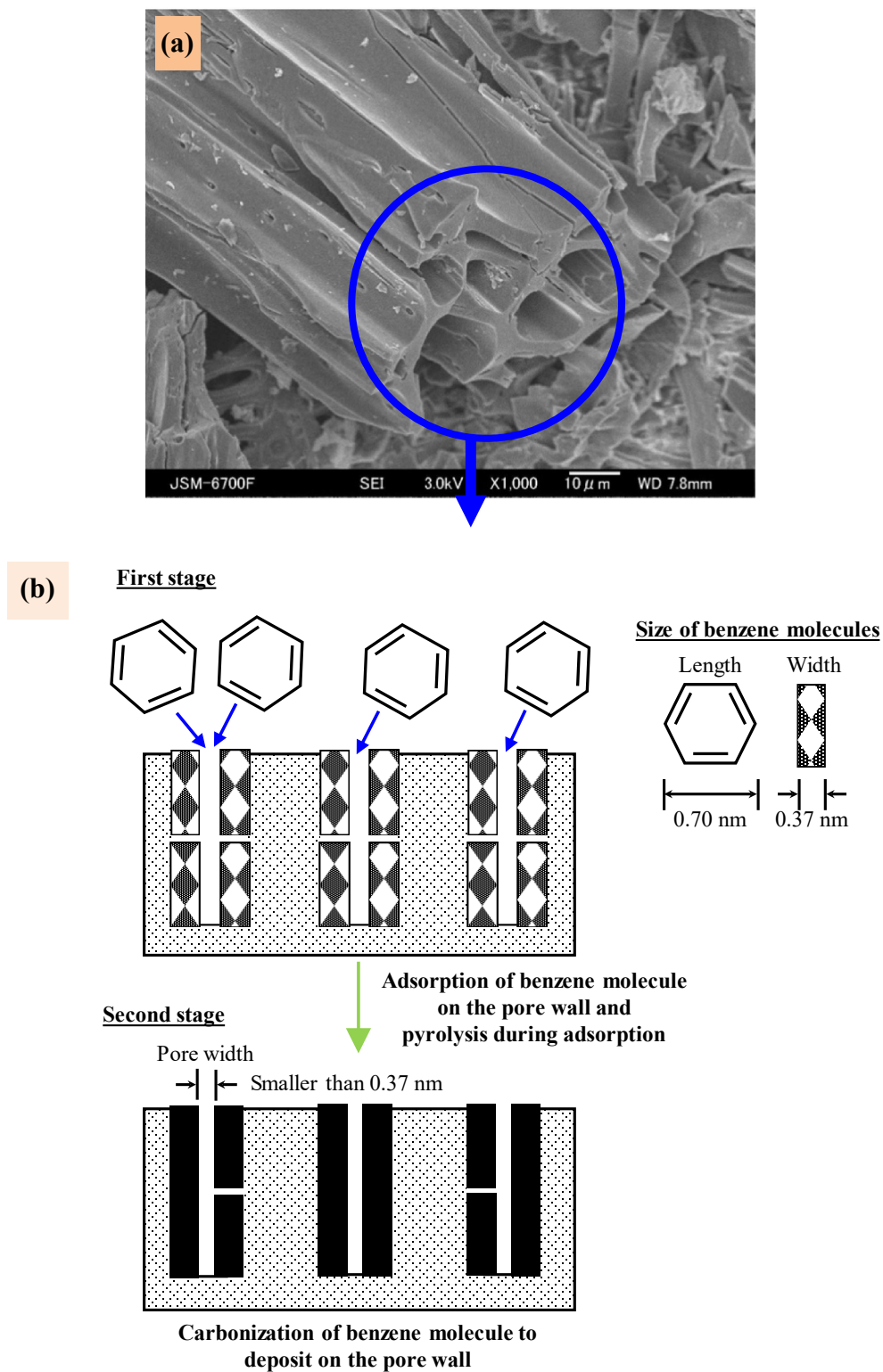
Fig. 5.2. (a) SEM image of Maxsorb III; (b) benzene pyrolization mechanism.

5.3   Experimental

5.3.1 Materials

5.3.1.1   Maxsorb III

The following Table 5.1 shows the thermophysical properties of the commercial activated carbon. Pore structure of this sample is modified using various pyrolization materials.
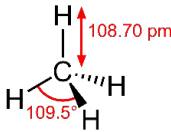
Table 5.1. Thermophysical properties of Maxsorb III [16,43,148].

Manufacturer	Kansai Coke & Chemical Company Ltd., Japan.
Surface area	3140 m^2/g
Micropore volume	1.70 ml/g
Total pore volume	2.01 ml/g
Apparent density	0.31 g/ml
pH	4.1
Average particle diameter	72 μm
Mean pore diameter	2.008 nm
Pore size distribution	0.1 – 4.4 nm
Specific heat capacity	0.844 kJ kg^{-1} K^{-1} (at 30 °C)
Thermal conductivity	0.066 W m^{-1} K^{-1}(at room temperature)

5.3.1.2 Methane

Methane gas has been used as a pyrolization substance for the pore modification. The common properties of methane is shown in Table 5.2.
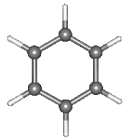
Table 5.2. Properties of methane [96,155].

Chemical formula	CH_4
Structural formula	
Molecular weight	16.043 g·mol^{-1}
Melting point	−182.5 °C
Boiling point	−161.48 °C
Flash point	−188 °C
Density	656.88 kg m^{-3} (at 25 °C and 1 atm)
Chemical safety	Flammable
Critical temperature	−82.586 °C
Critical pressure	4599.2 kPa

5.3.1.3 Benzene

Another pyrolization material that is used for the pore modification is benzene. Benzene is liquid at room temperature. The common properties are depicted in Table 5.3.

Table 5.3. Properties of benzene [96,155].

Chemical formula	C_6H_6
Structural formula	
Molecular weight	78.114 g·mol^{-1}
Melting point	5.558 °C
Boiling point	80.069 °C
Flash point	−11 °C
Liquid density	873.59 kg m^{-3} (at 25 °C)
Safety and hazard	Flammable, irritant, health hazard
Critical temperature	288.87 °C
Critical pressure	4907.3 kPa

5.3.2 Furnace

The core part of the furnace unit is made of ceramic. A pictorial view of the unit is shown in Fig. 5.3 and the technical specification is presented in Table 5.4.
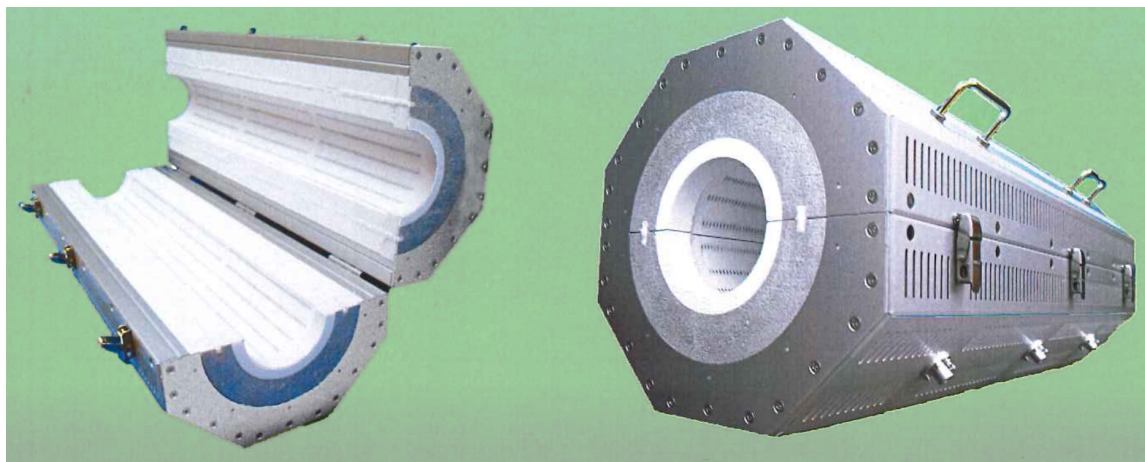
Fig. 5.3.   Photograph of the ceramic furnace unit.

Table 5.4. Specification of the furnace unit [156].

Manufacturer	Asahi Rika Corporation
Model no	ARF−50 KC
Furnace body	Ceramic
Temperature maximum limit	1200 °C
Supply voltage	100V AC
Electrical capacity	700 W
Ambient humidity	35 to 85%
Sensors	K, J, R, B, N, PL−II, Pt100, JPt100
Selected sensor	K
Scale range	−200 °C to 1370 °C
Control	PID

5.3.3 Temperature controller

Temperature controller of the furnace unit is made by Shinko Technos Co., Ltd. The schematic of the controller is shown in Fig. 5.4 and the technical specification is summarized in Table 5.5.
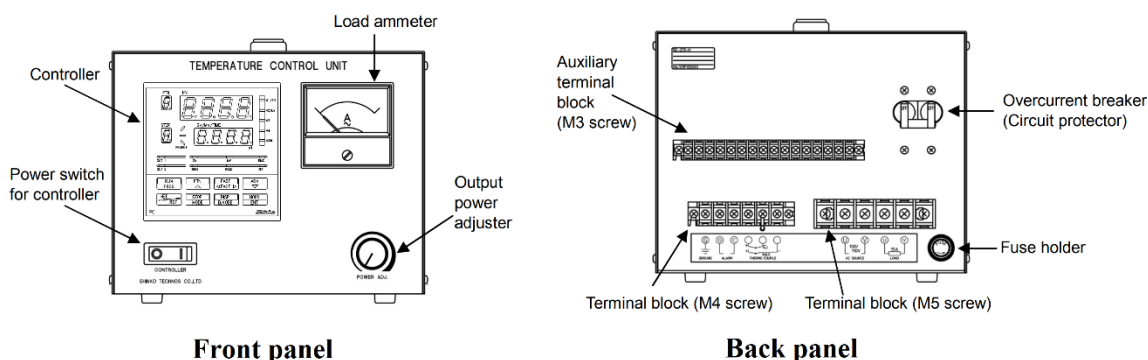
Fig. 5.4.   Schematic of temperature control unit.

Table 5.5. Specification of the temperature control unit.

Manufacturer	Shinko Technos Co., Ltd.
Model no	BC−230−H
Controller model	PC−935
Supply voltage	100/110V AC or 200/220V AC, 50/60Hz
Control current	Max 30A
Ambient temperature	0 to 40 °C
Ambient humidity	35 to 85%
Sensors	K, J, R, B, N, PL−II, Pt100, JPt100
Selected sensor	K
Scale range	−200 °C to 1370 °C
Control	PID

5.3.4 Procedure

The first step is to prepare the sample for pyrolysis. A boat made of Al_2O_3 is used to hold the sample during degassing and pyrolization. Alumina is used because it has high melting point (2072 °C) and do not react with Maxsorb III or pyrolization material. Maxsorb III contains many foreign elements which needs to be removed before the pyrolysis. Hence, the sample is heated in a vacuum oven at 100 °C for 12 hours. A small amount of sample is used (≈ 0.2g) for the experiment. Thus, the precise mass measurement is very important. The sample mass is measured at least five times to minimize any mass related errors. The sample boat is then pushed in the middle of a clean quartz tube. The tube was then inserted into the pyrolization oven. Both end of the quartz tube was covered with rubber stopper and Teflon. It was ensured that there was no leakage. Argon gas was

then flown into the quartz tube at 100 sccm rate from one end through the stopper. Target temperature, rising rate and holding time has been set to the temperature controller. After reaching the target temperature, methane gas has been flown at same rate. Ar and methane was flowing at the same time from the same end of quartz tube. Exhaust gas is discharged by a tube through the other end of quartz tube. A cooling bath is used to reduce the temperature before releasing the gas to environment. Unlike CH_4, benzene is liquid at room temperature. When pyrolyzed with benzene, an HPLC column is used to precisely control the flow of liquid benzene. The liquid benzene is introduced into the quartz tube from the same end where Ar is flowing. A tape heater is wrapped around that end of quartz tube to evaporate the benzene. Argon acts as carrier gas and push the vapor benzene into the pores. When the pyrolization is finished, both the Argon and pyrolization material flow is stopped. The sample is kept inside the quartz tube until it reaches the room temperature by natural cooling. The complete setup and procedure is shown in Fig. 5.5.
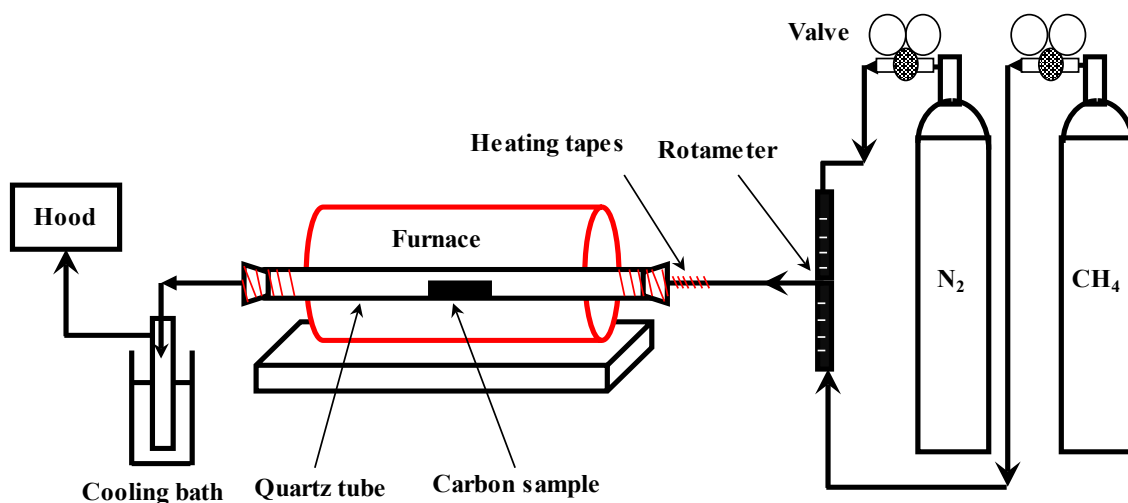
Fig. 5.5. Schematic diagram of the experimental setup for pyrolysis.

5.4   Results and discussion

Commercial Maxsorb III is pyrolyzed with methane and benzene at 800 to 1000 °C for various mass flow rate, temperature and time. The conditions and effect of pyrolization is summarized in Table 5.6 and Table 5.7. The table also contain the data of porosimetry analysis. Fig. 5.6 and Fig. 5.7 shows the plot of nitrogen adsorption isotherm and pore size distribution of parent and methane pyrolyzed Maxsorb III. Likewise, Fig. 5.8 and Fig. 5.9

shows the plot for benzene pyrolyzed samples. The PSD curves are drawn by minimizing the roughness of distribution so that all the peaks can be seen clearly. NLDFT model for N_2 at 77 K on carbon slit pores is considered to evaluate the PSD. The regularization value is considered 0.0001 for this model.

Methane is in gaseous phase at room temperature. The flow rate of carrier (Argon) gas and methane is considered constant in this experiment. The time of pyrolization is also considered fixed and only the temperature varied. Mass of the yield increased with pyrolization temperature. Surface area, pore volume and PSD peaks decrease with the pyrolization temperature. At 1000 °C, the PSD peak of 0.8 nm is completely vanished (Fig. 5.7). This indicates that the most of the unusable pores are removed. However, the usable pores also decreased at this temperature.

Benzene is in liquid phase at room temperature. In order to achieve similar flow rate of methane pyrolization experiment, the liquid benzene flow rate have to be very low. Hence, an HPLC pump is used to precisely control the flow rate. Vapor benzene flow rate can be calculated from the liquid flow rate by the following equation (5.1).

$$\dot{m}_{vap} = \left(\frac{\rho_{liq} \times \dot{m}_{liq}}{M} \right) \times 22.4 \qquad (5.1)$$

Here, the unit of mass flow rate, molecular weight and density is mL/min, g/mol and g/L respectively.

Pyrolysis at 900 °C for 30 minutes at 50 mL/min gas benzene flow rate remove all the pores from Maxsorb III and the surface area becomes zero. N_2 adsorption do not occur (Fig. 5.8) and there is no peak in the PSD plot (Fig. 5.9). When the temperature is decreased to 800 °C keeping the pyrolization time and flow rate constant, similar incident occurs. This indicates that pyrolization time and flow rate should be decreased too.
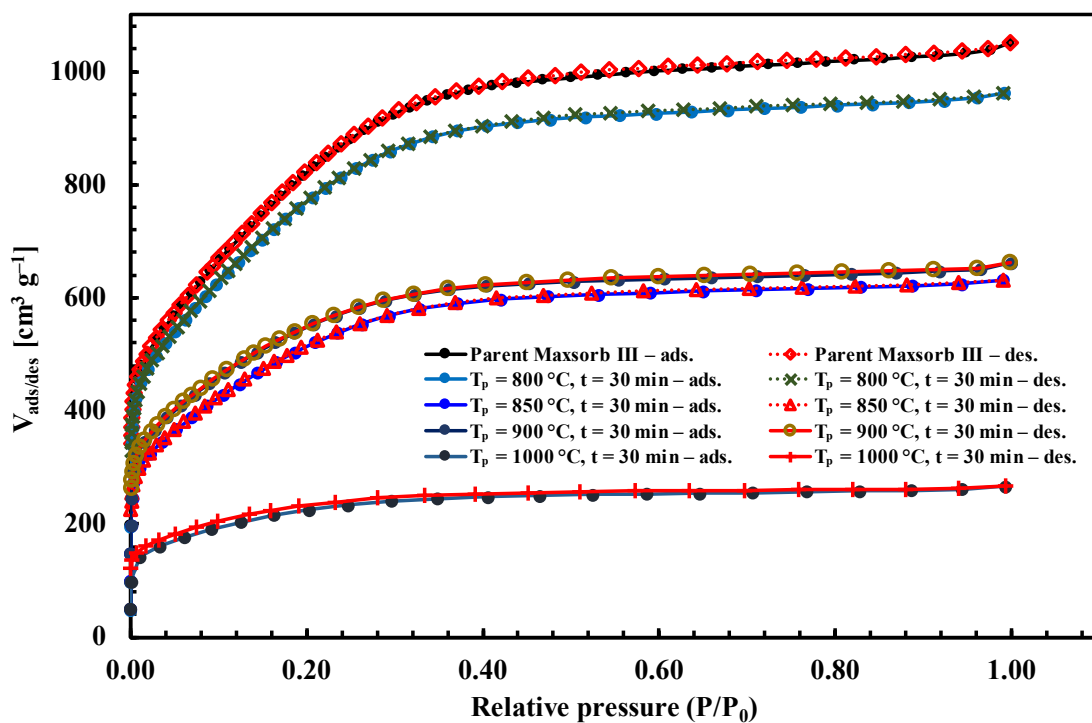
Fig. 5.6.   Ad/desorption isotherm of N_2 onto parent and CH_4 pyrolyzed Maxsorb III.
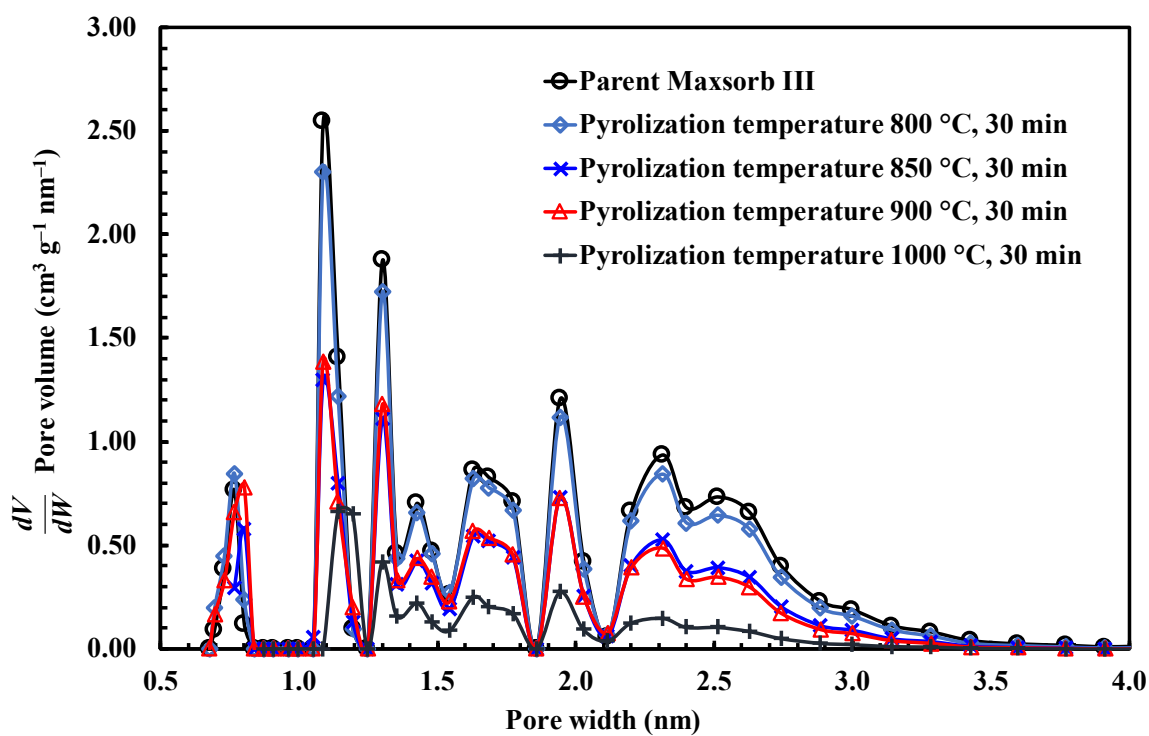
Fig. 5.7.   Comparison of PSD among parent and methane pyrolyzed Maxsorb III.

Table 5.6. Maxsorb III pyrolization with methane (CH_4).

Initial mass before degassing [g]	Initial mass after degassing [g]	Pyr. temp. [°C]	Gas flow rate [mL/min]		Pyr. time [min]	Final mass after pyrolysis [mg]	Mass increase [%]	BET Surface area [m²/g]	Total pore volume (cm³/g)	Pore size distribution	
			Ar	CH₄						Peak (W, dV/dW) [nm, cm³ g⁻¹ nm⁻¹]	Range [nm]
Parent Maxsorb III								3140	2.01	(1.67, 1.6)	0.1 – 4.4
0.2223	0.2004	800	50	50	30	0.2027	1.15	2762.07 ± 19.15	1.37	(0.77, 0.85), **(1.08, 2.30)**, (1.30, 1.72), (1.42, 0.67), (1.63, 0.82), (1.94, 1.13), (2.30, 0.85), (2.53, 0.64)	0.68 – 3.60
0.2000	0.1885	850	50	50	30	0.2355	24.27	1786.63±25.31	0.90	(0.80, 0.57), **(1.08, 1.23)**, (1.30, 1.10), (1.41,0.43), (1.63, 0.56), (1.94, 0.73), (2.30, 0.53), (2.53, 0.39)	0.76 – 3.57
0.2044	0.1879	900	50	50	30	0.2511	33.63	1916.21 ± 18.67	0.94	(0.80, 0.78), **(1.08, 1.38),** (1.30, 1.18), (1.41, 0.44), (1.63, 0.57), (1.94, 0.73), (2.30, 0.49), (2.53, 0.34)	0.68 – 3.52
0.2116	0.1897	1000	50	50	30	0.3318	74.91	760.68 ± 17.33	0.39	**(1.17, 0.66)**, (1.30, 0.42), (1.41, 0.22), (1.63, 0.25), (1.94, 0.28), (2.30, 0.15), (2.52, 0.10)	1.09 – 3.50

Table 5.7. Maxsorb III pyrolization with benzene (C_6H_6).

Initial mass before degassing	Initial mass after degassing	Pyr. temp.	Liquid C_6H_6 flow rate	Gas flow rate [mL/min]		Pyr. time	Final mass after pyrolysis	Mass increase	BET Surface area	Total pore volume	Pore size distribution	
				Ar	C_6H_6						Peak (W, dV/dW) [nm, cm³ g⁻¹ nm⁻¹]	Range [nm]
[g]	[g]	[°C]	[mL/min]			[min]	[mg]	[%]	[m²/g]	[cm³/g]		
Parent Maxsorb III									3140	2.01	(1.67, 1.6)	0.1 – 4.4
0.2107	0.1972	900	0.20	50	50	30	0.4341	120.13	0.1104 ± 0.0387	0.0012	**(19.2, 0.0016)**, (21.0, 0.00014), (25.0, 0.00009), (29.9, 0.00007)	17.5 – 33.9
0.2018	0.1998	800	0.20	50	50	30	0.4721	136.29	0.2739 ± 0.0423	0.0022	(9.91, 0.00032), **(12.9, 0.0016)**	9.49 – 21.9
0.2127	0.2047	800	0.10	50	25	10	0.3572	74.50	975.75 ± 17.51	0.5005	(1.09, 0.70), **(1.3, 0.77)**, (1.41, 0.31), (1.63, 0.34), (1.94, 0.40), (2.3, 0.26)	1.05 – 3.76
0.2073	0.1692	800	0.02	50	05	05	0.2221	31.26	2587.47 ± 26.02	1.2811	(0.77, 0.78), **(1.08, 2.01)**, (1.3, 1.64), (1.42, 0.63), (1.63, 0.78), (1.94, 1.06), (2.30, 0.77)	0.67 – 3.76
0.2043	0.1951	800	0.02	50	05	10	0.2450	25.58	2165.79 ± 22.47	1.0770	(0.77, 0.72), **(1.08, 1.49)**, (1.30, 1.42), (1.41, 0.53), (1.63, 0.67), (1.94, 0.89), (2.30, 0.63)	0.69 – 3.76
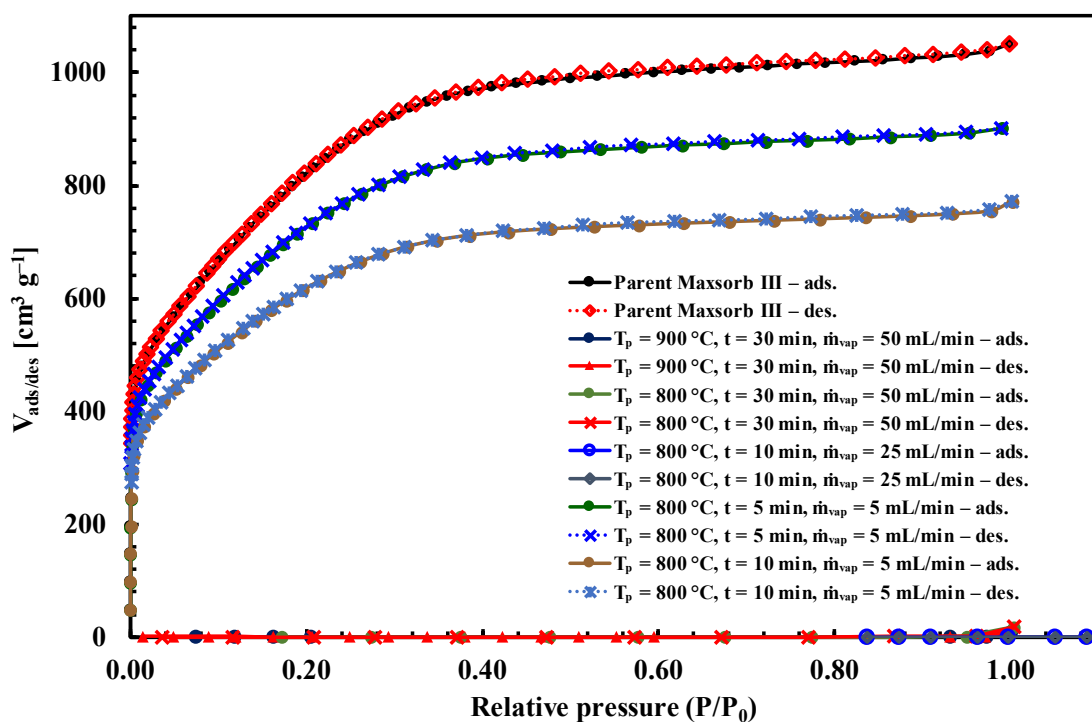
Fig. 5.8. Ad/desorption isotherm of N_2 onto parent and C_6H_6 pyrolyzed Maxsorb III.
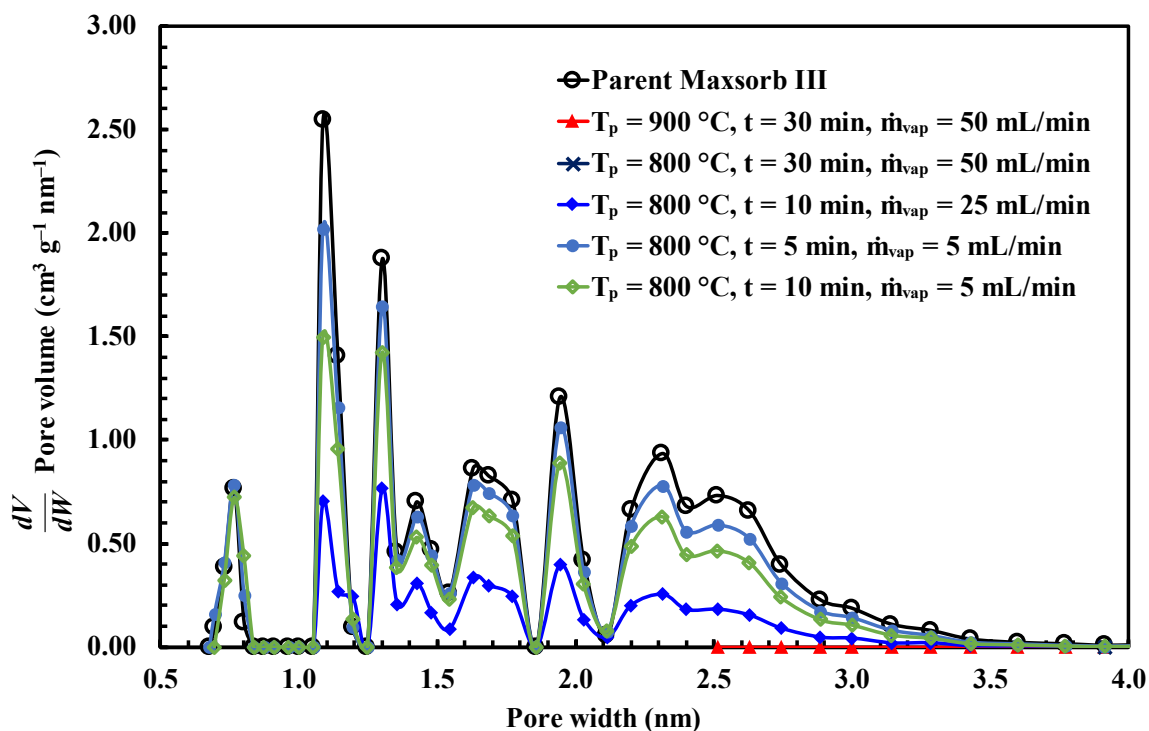
Fig. 5.9. Comparison of PSD among parent and benzene pyrolyzed Maxsorb III.

At this point, the pyrolysis temperature is set to 800 °C, the flow rate is decreased to half (0.25 mL/min) and the pyrolysis time is one third (10 min). For this conditions, all the pores were not blocked. However, the yield amount is still high and surface area is about one third of parent Maxsorb III. Smaller micropores around 0.8 nm were completely blocked and a lot of usable pores are decreased too.

At same pyrolysis temperature, the flow rate (5 mL/min) and pyrolization temperature is further decreased. At this conditions, surface area and pore volume change is not so significant. Smaller micropores still remains and the improvement is not so significant. Hence, the pyrolization time is increased to 10 min keeping all the other conditions unchanged. Some of the regular micropores and mesopores were removed at this condition.

5.5   Conclusions

In this work, the pore structure of commonly used activated carbon (AC) have been reshaped using organic compounds. The AC variant is commercially available Maxsorb III and the pyrolization fluids are methane and benzene. For both the fluids, an increase in pyrolization temperature – increase the yield amount; decrease the surface area and pore volume. Since methane atom have only one carbon, it requires higher temperature to get the same effect as benzene when all the other conditions are similar. Pyrolysis at 1000 °C with methane for 30 min at 50 mL/min flow rate, most of the smaller micropores and mesopores were removed. This might increase the quality of adsorbent. However, some usable pores are also decreased. Similar pore removal phenomenon happens for benzene pyrolysis temperature at 800 °C for 10 min pyrolization time at 25 mL/min flow rate. The removal of useable pores are lower in this case.

Chapter 6

Adsorption characteristics of biomass derived activated carbon/R32 Pair

Activated carbon (AC) is widely used for adsorption heat pump applications due to the higher uptake, faster kinetics, high surface area and pore volume. Raw materials of commercially available ACs are typically petroleum coke, mosaic coke, phenol resin and so on. Recently developed biomass derived activated carbon from mangrove (M–AC) and waste palm trunk (WPT–AC) have superior surface properties than commercial ACs. They are abundantly available in the nature and low-cost. Adsorption characteristics of low GWP HFC refrigerant R32 onto M–AC and WPT–AC have been experimentally investigated. At adsorption temperature 30 °C, the uptake of M–AC/R32 and WPT–AC/R32 pairs are 2.04 and 2.392 kg kg^{-1}, respectively. These values are remarkably higher than most of the available adsorbent/adsorbate pairs available for cooling applications. Two well-known isotherm models (D–A and Tóth) are employed to fit R32 adsorption isotherms of assorted pairs. Isosteric heat of adsorption for both the pairs have also been assessed with Clausius-Clapeyron model and D–A fitting parameters.

6.1 Background

The regulations set by Montreal (1987) and Kyoto (1997) protocols have already phased out the chlorofluorocarbons (CFCs) and most of the hydrochlorofluorocarbons (HCFCs) [8,157–159]. HFCs and natural refrigerants are most promosing to replace the existing ones [160,161]. Most of the adsorption cooling applications uses natural refrigerants as adsorbate. For example: silica gel/water [30,56,90,92], zeolite/water [39,162,163], activated carbon/ethanol [19,21,77], activated carbon/methanol [106,164], activated carbon/ammonia [165–167], activated carbon/CO$_2$ [58,168,169]. Most of these pairs have lower adsorption uptake or limited operation range (temperature and pressure). Pure HFC refrigerants (R32, R134a, R152a) and HFC blends (R404A, R410A, R507A etc.) have wider opreation range. However, the HFC blends have very high GWP (R404A: 3922; R410A: 2088, R507A: 3985) and unsuitable for using in the adsorption heat pump

system [64,170]. Hence, one of the pure HFCs with moderate GWP could be the potential candidate to use with activated carbon if it has higher adsorption uptake. Saha et al. [171] investigated the activated carbon/R134a pair and found that the maximum uptake could be 0.926 kg kg^{-1}. Ghazy et al. [172] carried out an experiment on Maxsorb III/R152a and their results shown a maximum uptake of 1.3 kg kg^{-1}. Sultan et al. [59] and Askalany et al. [173] investigated the activated carbon/R32 and found that the maximum uptake could be as high as 2.25 kg kg^{-1}. Among these three refrigerants, GWP of R152a is the lowest, R32 possess moderate (675) and R134a has the highest (1430) value. Since, R152a have flammability issue and uptake is also moderate, R32 is the best choice for AHP.

Biomass derived activated carbons synthesized by Pal et al. [20] have been employed to carry out this experiment. Some crucial contributions in study are:

- Experimental investigation of adsorption isotherms of R32 onto two biomass derived ACs.
- Dubinin Astakhov (D–A) and Tóth equations are employed to correlate R32 adsorption isotherms of assorted pairs.
- Determination of the isosteric heat of adsorption for both the pairs.

6.2 Experimental

6.2.1 Materials

6.2.1.1 M–AC and WPT–AC

Indonesian mangrove wood and Malaysian waste palm trunk are used as raw materials to prepare the activated carbons. Activation of these carbons are performed at high temperature using potassium hydroxide (KOH) at a ratio of 1:6 (carbonized sample: KOH). The details procedure is illustrated by Pal et al. in their article [20]. The physical properties of the adsorbents are depicted in Table 6.1.
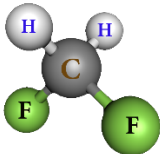
Table 6.1. Physical and adsorption properties of the selected adsorbents [20].

	M–AC (activated carbon from mangrove wood)	WPT–AC (activated carbon from waste palm trunk)
Total surface area $[m^2 \ g^{-1}]$	2924	2927
External surface area $[m^2 \ g^{-1}]$	34.19	62.52
Total pore volume $[cm^3 \ g^{-1}]$	2.18	2.51
Micropore volume $[cm^3 \ g^{-1}]$	2.13	2.41
Average pore width [nm]	1.47	1.68
Carbonization temperature [°C]	600	600
Activation temperature [°C]	900	900
Carbonized sample : KOH	1:6	1:6
Activation yield [%]	37.54	27.27
Average particle size range [μm]	42.70	31.19
Particle size range [μm]	23.07 – 71.52	16.94 – 55.70
Thermal conductivity at RT $[W \ m^{-1} \ K^{-1}]$	0.052 ±0.003	0.044 ± 0.003
Maximum ethanol uptake $[kg^{-1} \ kg^{-1}]$	1.65	1.9
Isosteric heat of adsorption $[kJ \ kg^{-1}]$	1092	1086

6.2.1.2   R32

The adsorbate of this experiment is R32. The refrigerant is chosen due to its wider operation range over natural refrigerants and moderate GWP value. Common properties of this refrigerant is listed in Table 6.2.

Table 6.2. Properties of the selected refrigerant.

Refrigerant or adsorbate	R32
Refrigerant type	Hydrofluorocarbon (HFC)
Alternate names	Difluoromethane; Freon 32; Methylene difluoride; Carbon fluoride hydride; Genetron 32; HFC 32 [174]
Chemical formula	CH_2F_2
Structural formula	
Molecular weight [g mol^{-1}]	52.024
GWP$_{100 \text{ years}}$ [kg–CO$_2$–eq.]	675 [59]
ODP	0
Critical pressure (MPa)	5.782 [96]
Critical temperature (°C)	78.105 [96]
Normal boiling point (°C)	–51.651 [96]
ASHRAE safety group	A2L [175]
ASHRAE flammability	Yes (mild) [175]
ASHRAE toxicity	No [175]

6.2.2 Instrumentation and procedure

The schematic diagram of the experimental apparatus is shown in Fig. 6.1. This is a magnetic suspension adsorption measurement unit (MSB-GS-100-10M) manufactured by Bel Japan, Inc. Sample mass is recorded with an accuracy of 20 µg. The pressure transducer model is PAA-35X made by Keller. The measurement range is up to 10 MPa (absolute)

with an uncertainty of ±0.1% of full scale. Tubes containing R32 gas are inside an air chamber with a controlled temperature to prevent condensation.
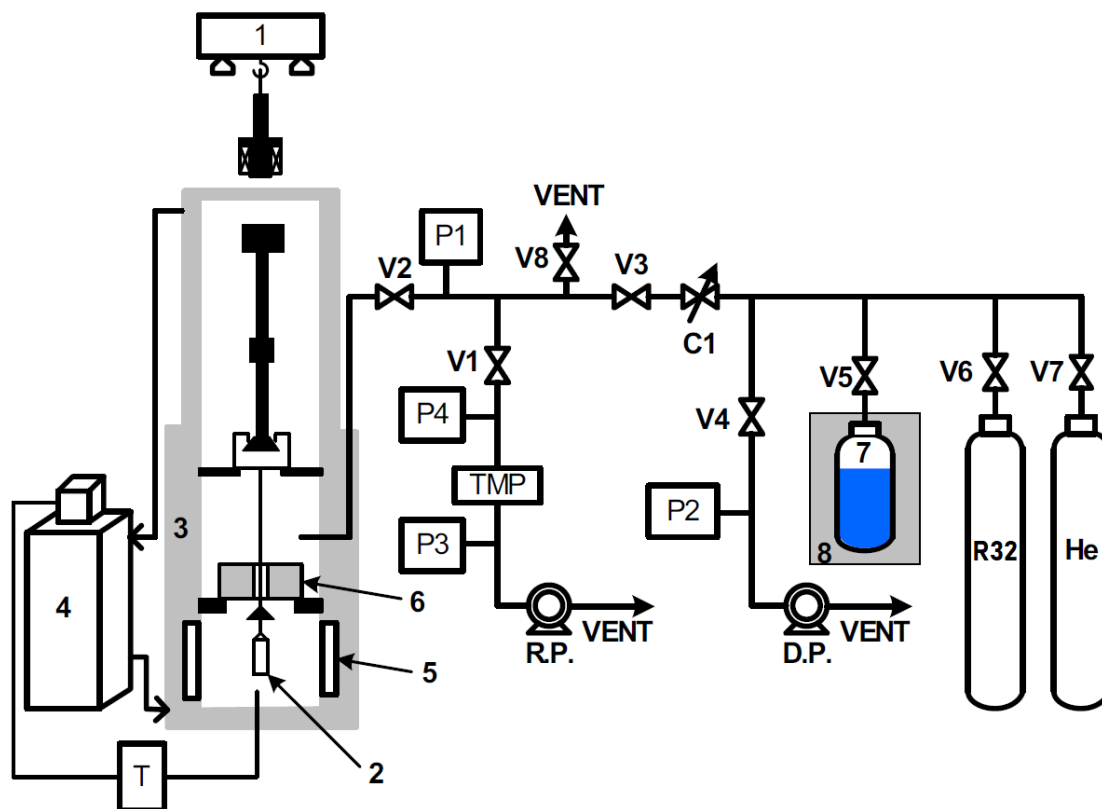
1: Magnetic suspension balance; 2: Sample holder basket; 3: Oil jacket; 4: Isothermal oil bath and circulator; 5: Sheathed heater; 6: Sinker; 7: Liquid refrigerant reservoir; 8: Isothermal oil bath; D.P.: Diaphragm pump; R.P.: Rotary pump; T.M.P.: Turbo molecular pump; P1–P4: Pressure gauges; T: Thermocouple; V1–V8: Valves; C1: Controlled valve.

Fig. 6.1.   Schematic diagram of magnetic suspension adsorption measurement unit [58].

About 50 – 60 mg sample (M–AC or WPT–AC) is inserted into the basket and hanged on the hook of the magnetic balance. The basket is then covered by the metal jackets and other supplemental tools to make the whole arrangement leak-proof. Vacuum and high pressure leakage test is performed to ensure the accuracy of the experiment. The sample is then regenerated at 130 °C in vacuum condition for several hours.

The oil circulator of the liquid refrigerant reservoir temperature is set to –6 °C. Gas refrigerant of room temperature is introduced into the reservoir. Since the reservoir temperature is low, R32 changes its phase to liquid. The liquid reservoir is filled only for

two minutes to prevent overflow. Both the adsorption chamber and liquid refrigerant cell temperature is then set to adsorption temperature. The valve C1 is used to precisely control the introducing pressure to the adsorption chamber. For example, to get enough data points of an adsorption isotherm at 30 °C adsorption temperature, evaporation temperature of liquid refrigerant reservoir unit is also set to 30 °C. Saturation pressure of R32 at 30 °C is 1927.5 kPa. For the first point of the isotherm, the C1 valve is slightly open to insert R32 gas into the tube (until the valve V2) at 500 kPa pressure. If overcharged, the vacuum pump removes the extra amount. This 500 kPa pressure corresponds to the evaporation temperature –14.33 °C, which means, a certain target pressure can be reached without lowering evaporator cell temperature. When the target pressure is reached, valve V2 is opened to start the adsorption. The mass of the sample starts increasing during adsorption. The mass change is detected by the magnetic balance and recorded in the computer. When the balance reaches equilibrium (mass change < 20 µg, pressure change < 300 Pa), V2 is closed. The tube is then charged again with a predefined amount for the second point of the adsorption isotherm. The process continues to repeat and all the data points are obtained up to saturation condition.

6.3 Adsorption isotherms

Adsorption isotherms of R32 onto M–AC and WPT–AC samples have been experimentally determined at temperatures of 30, 50, 70, 90 °C and pressure ranging from 0 to 3 MPa. D–A and Tóth isotherm models have less information loss from the statistical point of view [176] and hence, these two models are used in this study to fit the experimental data.

6.3.1 D–A adsorption isotherms

The Dubinin–Astakhov (D–A) adsorption isotherm model has been adopted by the researchers since the model can successfully predict the adsorption uptake for various refrigerant–adsorbent pairs. The governing equation of D–A isotherm model can be expressed by equation (6.1) [17,53,177]:

$$W = W_0 \exp\left[-\left\{\frac{RT\ln\left(\frac{P_s}{P}\right)^n}{ME}\right\}\right] \qquad (6.1)$$

Here,

$$W = CV_m \qquad (6.2)$$

$$V_m = V_t \exp\left[\alpha(T - T_t)\right] \qquad (6.3)$$

The numerical value of V_t at triple point of R32 (–136.81 °C) can be found in REFPROP which is 0.69966 cm³ g⁻¹. Besides, the thermal expansion coefficient α has been considered constant (0.0025 K⁻¹) in the articles [17,58,178]. However, some researchers have proposed the value of α as temperature dependent (1/T) [179,180].

Thermal expansion occurs during adsorption and a volume correction to the DA model is required. The specific volume of the adsorbed phase (V_m) is estimated using the equation (6.3) for a wide range of temperatures for high pressure gases.

Since, the phase of a fluid is unknown at $T > T_C$, P_s is calculated at this region by pseudo-saturated vapor pressure equation (6.4).

$$\frac{P_s}{P_C} = \left(\frac{T_s}{T_C}\right)^k \qquad (6.4)$$

Critical pressure (P_c) of R32 is 5.782 MPa as mentioned in Table 6.2. The parameter k is a heterogeneity parameter which can be obtained from the correlation fitting of D–A model. Hence, four adjustable parameters W_0, E, n and k are determined from the correlation fitting of experimentally obtained data.

6.3.2 Tóth adsorption isotherms

Adsorption isotherm model proposed by Tóth is another renowned model which can be expressed by the following equation:

$$C = C_0 \left[\frac{bP}{\left(1+(bP)^t\right)^{\frac{1}{t}}} \right]$$ (6.5)

Here,

$$b = b_0 e^{\frac{Q_{st}}{RT}}$$ (6.6)

where C and C_0 are equilibrium adsorption uptake [kg kg^{-1}] and saturated adsorption amount, respectively. P is the equilibrium pressure, t is heterogeneity constant and an adjustable fitting parameter of the Tóth model. It is noteworthy to mention that, for $t = 1$, the equation of Tóth model expresses Langmuir equation. Besides, b_0 [kPa] is adsorption affinity at infinite temperature, R is the universal gas constant [J mol^{-1} K^{-1}]; Q_{st} is isosteric heat of adsorption [J mol^{-1}]; and T is adsorption temperature [K].

6.3.3 Isosteric heat of adsorption

The heat release during the adsorption process as a result of change in energy level of the adsorbate molecules is known as heat of adsorption. Isosteric heat of adsorption signifies the strength of interactions between refrigerant and adsorbent [181]. Basically, this parameter can be expressed by the function of adsorption uptake [171,182]. However, numerous studies have shown that it is also dependent on adsorption temperature [20,62,142]. Several models have been proposed by the researchers and Rahman et al. model [61] is adopted in this study. The model is based on the Clausius–Clapeyron model. Following two equations (6.7) and (6.8) express the isosteric heat of adsorption for below and above critical temperatures, respectively.

For $T < T_C$,

$$Q_{st} = h_{fg} + E\left[(-ln\,\Theta)^{\frac{1}{n}} + \frac{T\alpha}{n}(-ln\,\Theta)^{\frac{1-n}{n}} \right]$$ (6.7)

For $T \geq T_C$,

$$Q_{st} = kRT + E\left[\left(-ln\,\Theta\right)^{\frac{1}{n}} + \frac{T\alpha}{n}\left(-ln\,\Theta\right)^{\frac{1-n}{n}}\right] \qquad (6.8)$$

Here, Θ is surface coverage and can be expressed by equation (6.9).

$$\Theta = \frac{W_0}{W} = \frac{W_0}{CV_m} \qquad (6.9)$$

where, h_{fg} [kJ kg^{-1}] is called the latent heat of vaporization. It can be determined by subtracting gas phase enthalpy and liquid phase enthalpy at a certain adsorption temperature E, n and k are the D–A equation fitting parameters. α is the thermal expansion coefficient (0.0025 K^{-1}) and R is the universal gas constant (8.314 J mol^{-1} K^{-1}).

6.4 Results and discussion

The experimental adsorption isotherm data of M–AC/R32 and WPT–AC/R32 pairs are shown in Table 6.3 and Table 6.4, respectively. A certain amount of vapor refrigerant is charged and adsorbed in the adsorbent. At a particular adsorption temperature – the initially charged refrigerant pressure ($P_{initial}$), final pressure after adsorption equilibrium is reached ($P_{equilibrium}$), and saturated adsorbed amount (C) is presented in the data tables.

Table 6.3. Experimental adsorption isotherm data of M–AC/R32 pair.

T_{ads} [°C]	$P_{initial}$ [kPa]	$P_{equilibrium}$ [kPa]	C [kg kg^{-1}]	T_{ads} [°C]	$P_{initial}$ [kPa]	$P_{equilibrium}$ [kPa]	C [kg kg^{-1}]
30.10	503.071	44.280	0.091	69.98	504.494	49.205	0.040
30.02	547.296	88.830	0.185	70.16	554.667	98.728	0.079
30.00	592.654	133.543	0.283	70.00	603.855	148.233	0.118
30.00	936.633	207.215	0.439	70.00	1250.595	264.105	0.207
30.00	1010.617	281.203	0.581	70.02	1367.750	381.230	0.296
30.00	1084.379	355.531	0.707	70.00	1484.047	499.448	0.380
30.00	1158.786	429.970	0.820	70.00	1602.318	619.094	0.462
30.00	1232.620	504.596	0.924	70.01	1722.677	740.124	0.538
30.00	1307.404	579.339	1.022	70.00	2043.664	889.678	0.626
29.99	1381.880	654.092	1.115	70.00	2190.602	1042.294	0.709
30.00	1657.373	750.504	1.234	70.00	2343.192	1199.086	0.789
30.00	1752.101	847.444	1.352	70.00	2500.237	1359.873	0.865
30.00	1849.561	944.707	1.472	69.99	2655.906	1525.771	0.940
30.00	1947.187	1042.159	1.594	70.00	2323.725	1619.669	0.981
30.00	2045.443	1140.336	1.713	69.99	2415.780	1714.599	1.021
30.00	2143.367	1238.194	1.825	70.00	2611.478	1826.490	1.068
30.00	2239.972	1337.375	1.921	70.00	2621.769	1925.335	1.108
30.00	2338.766	1436.969	1.993	70.00	2722.176	2026.575	1.149
30.00	2439.069	1537.901	2.040	69.99	2832.001	2149.589	1.197
				70.01	2925.974	2859.056	1.453
50.04	505.739	46.848	0.063	89.98	703.653	73.238	0.040
50.13	551.448	93.647	0.124	90.02	777.475	147.094	0.078
50.00	597.072	140.407	0.185	90.00	1450.038	294.298	0.154
50.00	1145.045	239.030	0.312	90.00	1597.299	444.232	0.230
50.00	1241.111	338.027	0.433	90.00	1747.641	596.757	0.305
50.00	1341.468	437.531	0.544	90.01	1900.580	752.587	0.378
50.00	1441.851	537.845	0.647	90.00	2852.083	1118.905	0.535
49.99	1541.269	638.687	0.740	90.00	2411.384	1287.255	0.600
50.00	1641.878	740.258	0.828	90.00	2579.971	1462.087	0.664
50.01	1742.457	842.241	0.910	90.00	2758.878	1645.999	0.728
50.01	1844.503	945.276	0.989	90.00	2441.001	1749.574	0.762
50.00	1948.451	1048.848	1.065	90.02	2547.439	1855.880	0.796
50.01	2050.479	1153.142	1.139	90.00	2654.252	1964.756	0.830
50.00	2154.632	1258.513	1.212	90.01	2764.276	2078.075	0.864
50.01	2259.145	1364.765	1.285	90.00	2575.193	2144.486	0.885
49.99	2876.912	1652.810	1.478	90.00	2642.397	2212.183	0.904
50.00	1960.664	1960.245	1.578	90.00	2702.472	2280.081	0.924
50.01	2257.346	2256.773	1.725	90.00	2778.657	2350.679	0.944
50.00	2552.096	2551.473	1.824	90.00	2759.620	2407.285	0.960
50.00	3002.768	2848.961	1.981	90.00	2820.549	2489.568	0.983
				90.00	2878.716	2841.428	1.077

Table 6.4. Experimental adsorption isotherm data of WPT–AC/R32 pair.

T_{ads} [°C]	$P_{initial}$ [kPa]	$P_{equilibrium}$ [kPa]	C [kg kg^{-1}]	T_{ads} [°C]	$P_{initial}$ [kPa]	$P_{equilibrium}$ [kPa]	C [kg kg^{-1}]
30.02	603.293	53.089	0.113	70.13	602.879	59.548	0.042
30.04	658.106	106.439	0.224	70.25	662.742	119.346	0.084
30.00	1010.456	188.552	0.394	70.00	1122.642	223.487	0.157
30.00	1092.271	270.872	0.548	69.99	1226.886	328.380	0.231
30.00	1174.859	353.447	0.687	69.99	1332.446	434.475	0.304
30.00	1256.472	435.904	0.811	69.99	1436.774	541.304	0.376
30.00	1339.456	518.670	0.926	69.99	1543.828	649.208	0.445
30.00	1422.307	601.369	1.035	70.00	1651.599	758.131	0.511
29.99	1105.586	645.319	1.091	70.00	1760.574	868.235	0.575
30.00	1148.104	689.135	1.147	69.99	1871.406	979.649	0.637
30.00	1491.531	761.572	1.239	70.01	1999.312	1094.011	0.696
30.00	1564.117	833.774	1.332	70.00	1597.948	1146.963	0.724
30.01	1636.594	906.005	1.427	70.00	1649.381	1199.960	0.750
30.00	1708.926	977.831	1.525	70.01	2200.040	1315.996	0.807
30.00	1780.717	1049.941	1.628	70.00	2315.609	1434.298	0.863
30.00	1853.376	1121.687	1.732	70.00	2434.810	1555.058	0.919
30.00	1875.417	1188.376	1.832	70.00	2555.078	1678.701	0.974
30.00	1942.038	1254.674	1.931	69.99	2629.057	1797.815	1.026
30.00	1907.613	1311.243	2.012	70.00	2489.773	1881.087	1.063
30.00	1913.496	1362.894	2.081	70.00	2576.039	1966.588	1.099
30.00	1965.774	1414.600	2.141	69.99	2763.685	2069.796	1.144
30.00	1916.625	1456.865	2.183	70.00	2565.086	2130.026	1.169
30.00	1959.720	1498.868	2.217	70.00	2623.721	2190.390	1.195
30.00	1951.347	1536.525	2.241	70.00	2685.988	2252.339	1.221
30.00	1888.978	1565.579	2.257	70.00	2596.801	2294.028	1.239
30.00	1918.451	1593.870	2.271	70.00	2640.853	2336.059	1.257
30.00	1946.195	1622.568	2.282	70.00	2684.222	2378.957	1.274
30.00	1675.836	1626.195	2.283	70.01	2724.390	2421.598	1.292

T_{ads} [°C]	$P_{initial}$ [kPa]	$P_{equilibrium}$ [kPa]	C [kg kg^{-1}]	T_{ads} [°C]	$P_{initial}$ [kPa]	$P_{equilibrium}$ [kPa]	C [kg kg^{-1}]
30.00	1679.093	1630.109	2.285	70.00	2619.732	2444.560	1.302
30.01	1682.539	1633.537	2.286	70.00	2793.953	2488.342	1.320
30.00	1936.275	1657.356	2.295	70.00	2867.198	2833.738	1.461
30.00	1759.998	1665.261	2.298	70.00	3096.948	2869.391	1.470
30.00	1818.431	1676.701	2.302	70.00	3147.048	2876.492	1.481
30.00	1919.637	1695.815	2.308	89.95	603.762	62.510	0.028
30.00	1848.643	1707.294	2.312	90.29	667.118	125.485	0.057
30.00	1929.752	1724.570	2.318	90.00	1129.029	234.938	0.106
30.00	1927.599	1740.431	2.324	89.99	1237.442	345.465	0.156
30.00	1943.180	1755.777	2.328	90.00	1349.095	457.360	0.207
30.00	1958.489	1771.195	2.334	90.00	1460.050	570.347	0.257
30.00	1972.881	1786.528	2.338	89.98	1574.647	685.014	0.307
30.00	1988.961	1801.996	2.343	90.02	1686.869	800.668	0.356
30.00	2004.897	1815.937	2.348	90.00	1803.138	918.587	0.404
30.00	2019.437	1825.510	2.352	90.00	1919.826	1038.146	0.452
30.00	2028.537	1832.897	2.354	90.01	2040.316	1160.035	0.499
30.00	2085.839	1843.910	2.358	90.01	2161.741	1284.502	0.546
30.00	2096.314	1857.489	2.363	90.00	2286.448	1411.613	0.592
30.00	2111.074	1872.079	2.370	90.00	2413.927	1542.576	0.637
30.00	2125.261	1886.348	2.375	90.00	2850.854	1805.568	0.724
30.00	2139.378	1900.967	2.383	89.99	2501.595	1897.682	0.754
30.00	2154.240	1914.921	2.392	90.00	2592.138	1991.619	0.783
50.03	606.017	56.685	0.072	90.00	2686.732	2088.302	0.813
50.19	660.042	113.291	0.139	90.00	2634.879	2163.006	0.835
49.98	1117.903	211.838	0.260	90.01	2607.651	2223.057	0.853
50.00	1214.501	310.513	0.376	90.00	2668.905	2284.384	0.871
50.00	1314.141	409.991	0.486	90.00	2731.184	2346.817	0.891
50.00	1414.484	510.078	0.589	90.00	2547.822	2371.724	0.898
50.00	1513.289	610.685	0.684	89.99	2566.310	2397.575	0.905

T_{ads} [°C]	$P_{initial}$ [kPa]	$P_{equilibrium}$ [kPa]	C [kg kg^{-1}]	T_{ads} [°C]	$P_{initial}$ [kPa]	$P_{equilibrium}$ [kPa]	C [kg kg^{-1}]
50.00	1611.627	711.576	0.773	90.00	2594.622	2424.259	0.912
50.00	1715.119	813.384	0.858	89.99	2620.922	2450.292	0.921
50.01	1816.132	915.801	0.939	90.01	2644.597	2476.771	0.928
50.00	1917.259	1018.624	1.017	90.00	2724.367	2511.814	0.938
50.00	2015.580	1121.806	1.093	90.00	2660.350	2531.326	0.944
50.00	2123.233	1226.650	1.170	90.00	2677.779	2551.351	0.949
50.00	2227.926	1332.487	1.248	90.00	2700.602	2570.941	0.955
50.00	2327.369	1438.800	1.325	90.00	2718.227	2591.178	0.961
50.00	2432.060	1546.135	1.405	90.01	2739.172	2610.436	0.966
50.00	2540.077	1654.910	1.486	90.01	2758.224	2630.828	0.972
50.00	2647.296	1765.412	1.570	90.00	2780.362	2651.360	0.977
50.00	2761.651	1878.556	1.656	90.00	2802.247	2672.492	0.983
50.00	2870.666	2460.203	2.050	90.00	2817.008	2708.076	0.993
50.00	2921.545	2877.164	2.180	90.00	2849.484	2833.646	1.029
50.00	3658.428	2875.575	2.181	90.01	2914.041	2856.943	1.033
50.00	2941.994	2891.848	2.191	90.01	3082.952	2905.995	1.045
50.00	2961.009	2894.235	2.195	90.00	3273.872	2915.172	1.053
50.00	2971.577	2909.000	2.188	90.00	3357.038	2938.202	1.058
50.00	2985.549	2912.936	2.188				
49.99	2964.338	2918.589	2.190				
50.00	2979.908	2919.599	2.192				

Experimentally obtained data of M–AC/R32 pair is correlated with D–A and Tóth models. Empirical and fitted data is plotted in Fig. 6.2 and Fig. 6.3. The plots show good fitting with both the isotherm models. Correlation coefficients for this pair is shown in Table 6.5. The RMSD (root-mean-square deviation) fitting error for D–A and Tóth model is 3.60% and 6.09%, respectively.
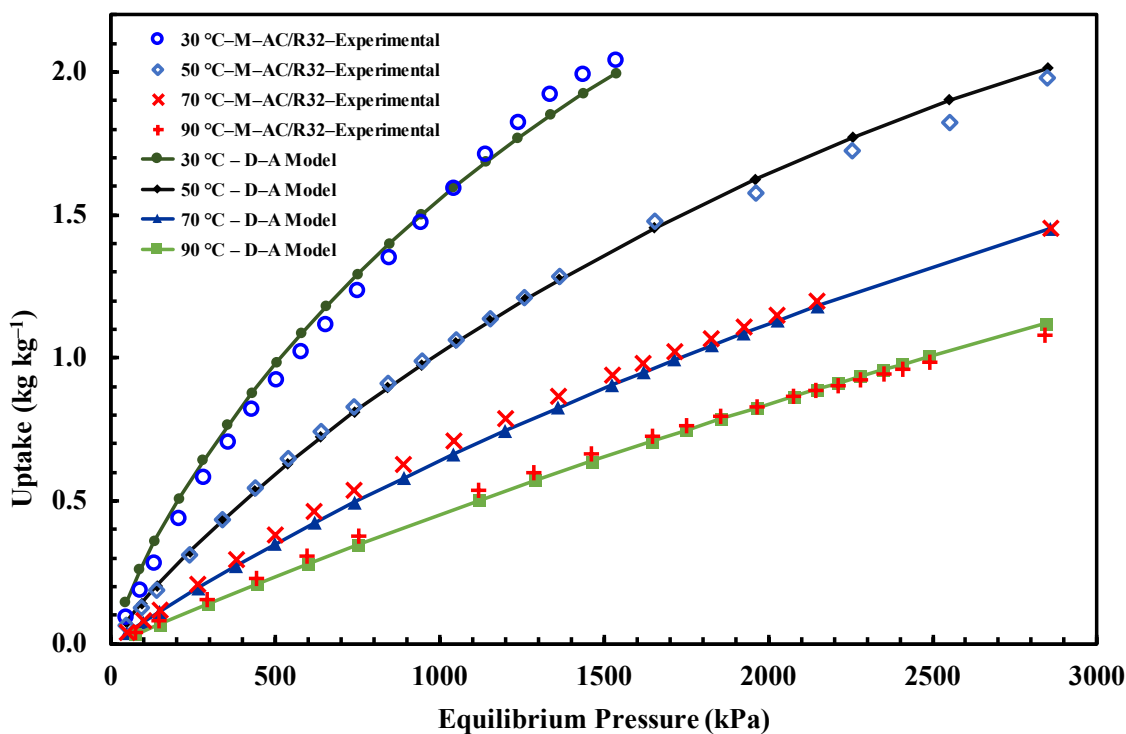
Fig. 6.2.   R32 adsorption onto M–AC: experimental and D–A model.
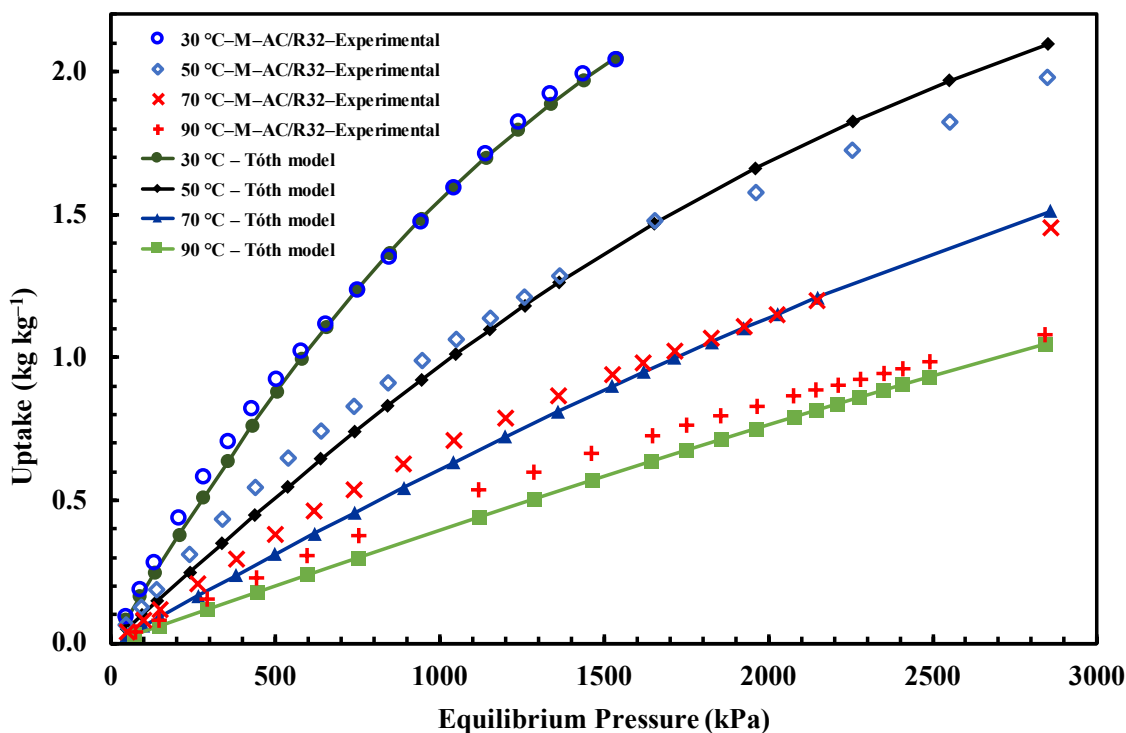
Fig. 6.3.   R32 adsorption onto M–AC: experimental and Tóth model.

Table 6.5. Correlation coefficients of the isotherm models for M–AC/R32 pair.

Isotherm parameters		D–A	Tóth
C_0	[kg kg^{-1}]	–	3.28
b_0	[kPa^{-1}]	–	5.23×10^{-8}
Q_{st}	[kJ mol^{-1}]	–	23.407
t	[–]	–	1.75
k	[–]	2.08	–
W_0	[cm^3 g^{-1}]	2.34	–
E	[kJ mol^{-1}]	4.055	–
n	[–]	1.18	–

The isosteric heat of adsorption (Q_{st}) trend for M–AC/R32 pair is shown in Fig. 6.4. The plot indicates that, for a particular temperature, Q_{st} tends to decrease with surface coverage. For higher adsorption temperature, the trend line shifts to lower values. When the adsorption temperature exceeds critical value, the trend line starts shifting upward with temperature increment. However, the change is very slight. In the plot of Fig. 6.4, Q_{st} of three temperatures are below critical and only one (T_{ads} = 90 °C) is above critical. Coincidentally, Q_{st} trend line of 70 °C and 90 °C almost overlaps.
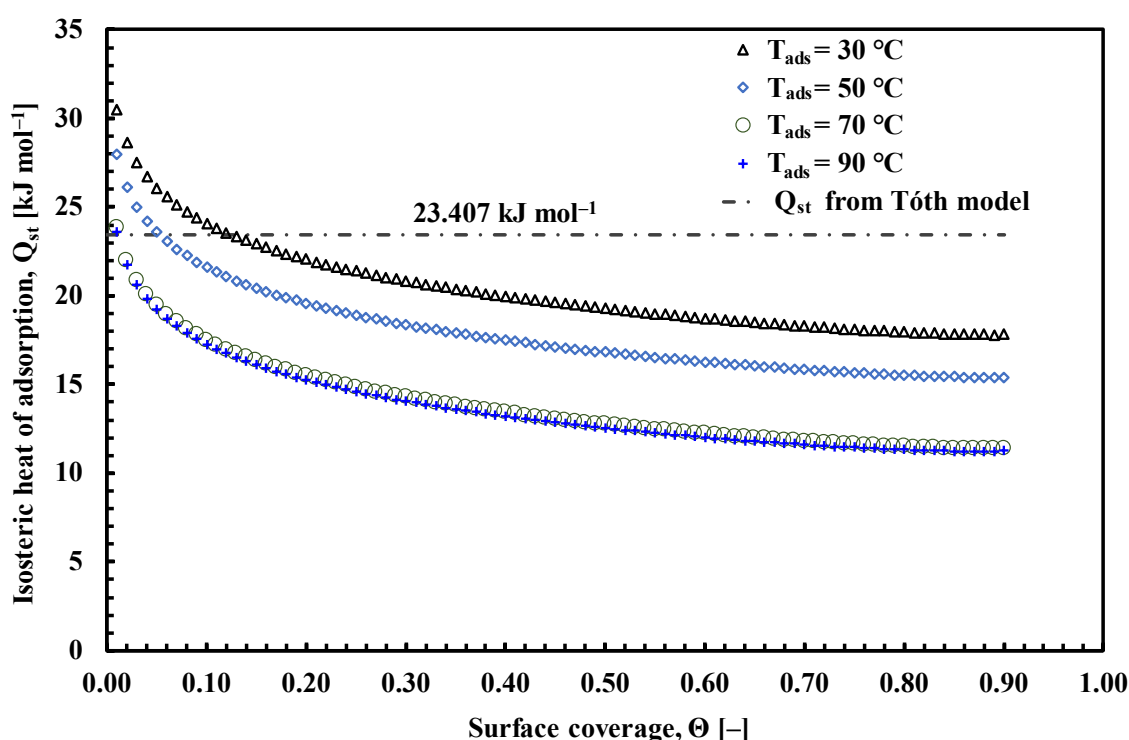
Fig. 6.4. Isosteric heat of adsorption for M–AC/R32 pair at various adsorption temperature below and above critical.

Experimentally obtained data of WPT–AC/R32 pair is correlated with D–A and Tóth models. Empirical and fitted data is plotted in Fig. 6.5 and Fig. 6.6. The figures show good fitting with both the isotherm models. Correlation coefficients for this pair is shown in Table 6.6. The RMSD (root-mean-square deviation) fitting error for D–A and Tóth model is 3.76% and 5.86%, respectively.
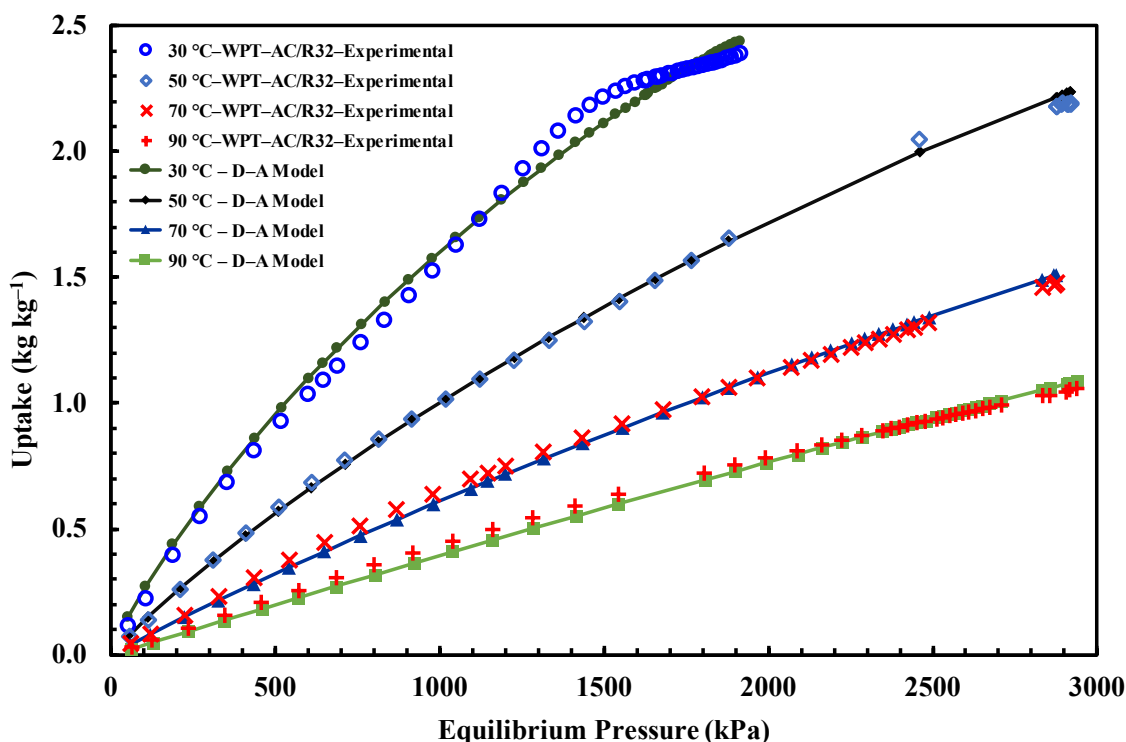
Fig. 6.5.   R32 adsorption onto WPT–AC: experimental and D–A model.
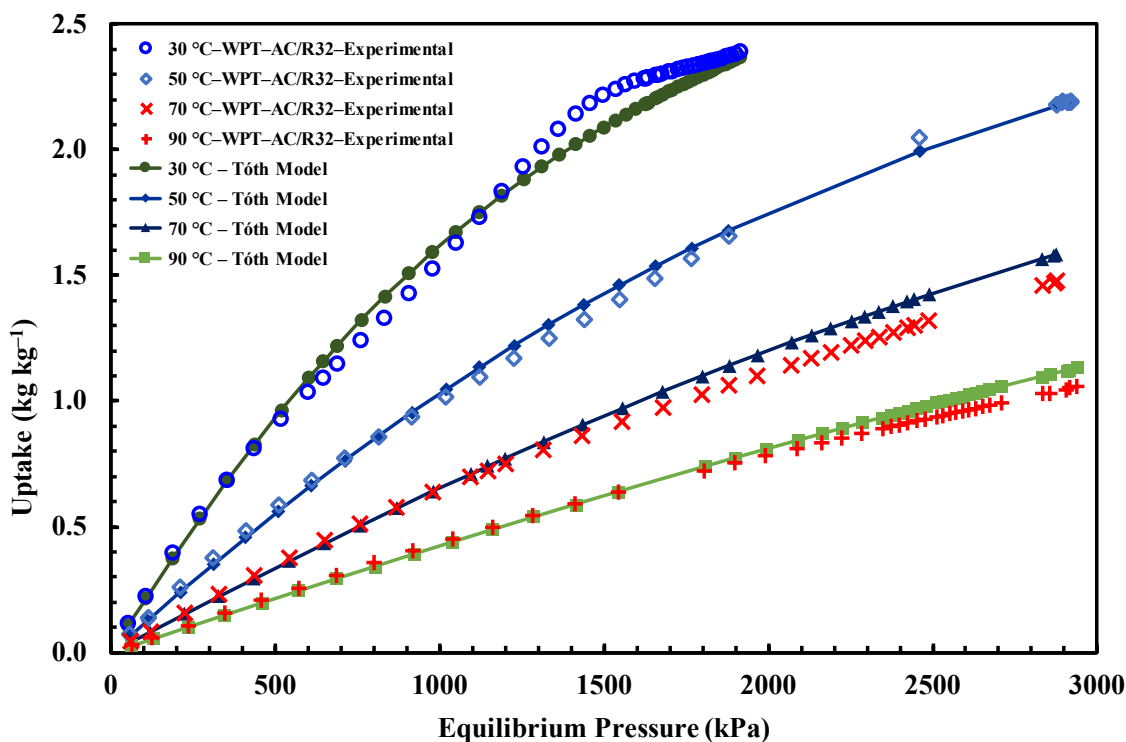
Fig. 6.6.   R32 adsorption onto WPT–AC: experimental and Tóth model.

Table 6.6. Correlation coefficients of the isotherm models for WPT–AC/R32 pair.

Isotherm parameters		D–A	Tóth
C_0	[kg kg^{-1}]	–	3.53
b_0	[kPa^{-1}]	–	5.12×10^{-8}
Q_{st}	[kJ mol^{-1}]	–	23.512
t	[–]	–	1.55
k	[–]	4.24	–
W_0	[cm^3 g^{-1}]	2.60	–
E	[kJ mol^{-1}]	3.591	–
n	[–]	1.11	–

The isoteric heat of adsorption (Q_{st}) trend for WPT–AC/R32 pair is plotted in Fig. 6.7. The plot has similar behavior like the previous pair. Q_{st} tends to decrease with surface coverage and trend line shifts to lower values for higher adsorption temperature. For $T > T_C$, the trend lines start shifting upward with temperature increment. However, the change is not that much. In the plot of Fig. 6.7, Q_{st} trend line of 30 °C and 90 °C nearly coincides on one another.
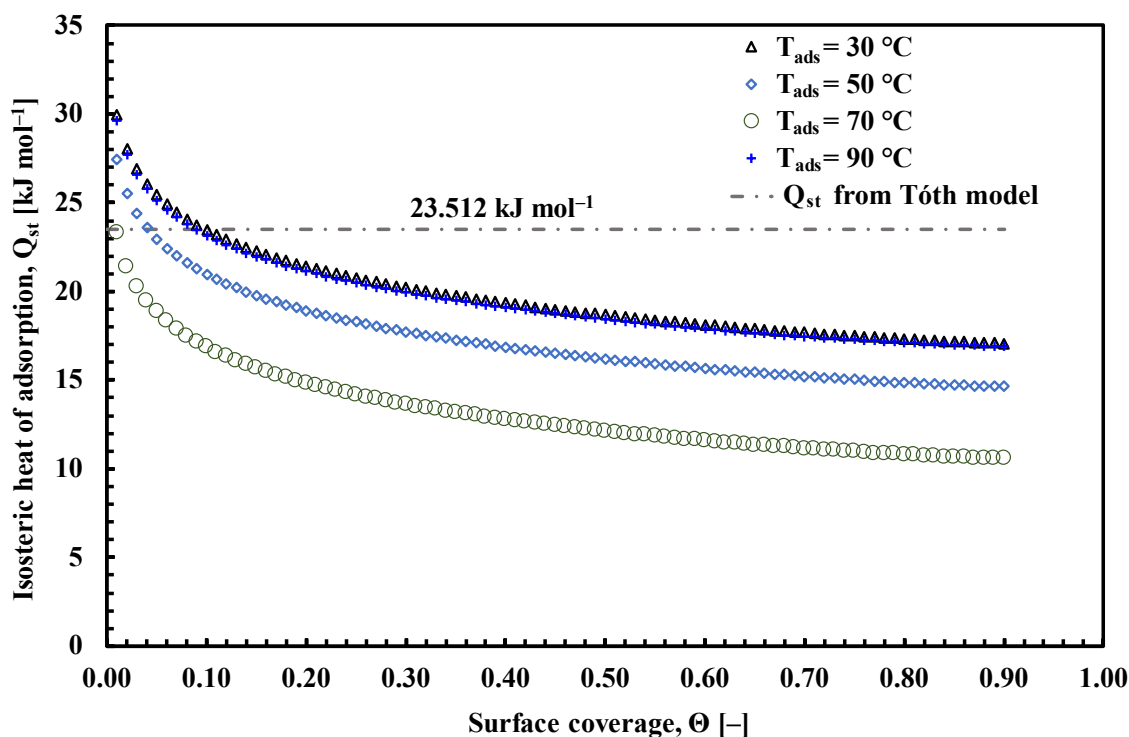

Fig. 6.7.   Isoteric heat of adsorption for WPT–AC/R32 pair at various adsorption temperature below and above critical.

6.5   Conclusions

In this study, adsorption isotherm of low GWP refrigerant R32 onto two biomass derived activated carbon is experimentally investigated. The samples are M–AC (from mangrove wood) and WPT–AC (from palm trunk). The experiment has been carried out for a wide range of adsorption temperatures 30, 50, 70 and 90 °C. Adsorption data is successfully correlated with two prominent isotherm models: D–A and Tóth. Isosteric heat of adsorption has been evaluated with modified Clausius-Clapeyron model for both the pairs.

M–AC/R32 pair has a very high adsorption uptake of 2.04 kg kg^{-1} at 30 °C and 1537.9 kPa. Whereas, WPT–AC/R32 pair has even higher uptake of 2.392 kg kg^{-1} at 30 °C and 1914.9 kPa. Both the uptake values are higher than commercially available activated carbon powder reported by Askalany et al. [183]. Uptake of WPT–AC/R32 is higher than the uptake of phenol resin based activated carbon (2.34 kg kg^{-1}) reported by Sultan et al. [59]. To the best of our knowledge, it is the highest R32 adsorption capacity onto any adsorbent available in the articles.

Correlation fitting of M–AC/R32 and WPT–AC/R32 agrees well with D–A and Tóth models with an acceptable error margin. Isosteric heat of adsorption (Q_{st}) values from Tóth fitting are 23.407 and 23.512 kJ mol^{-1} for M–AC/R32 and WPT–AC/R32, respectively. However, surface coverage (Θ) and adsorption temperature (T_{ads}) dependent Clausius-Clapeyron model shows that Q_{st} decreases from 30.48 (at Θ=0.01) to 17.81 kJ mol^{-1} (at Θ=0.90) at 30 °C adsorption temperature for M–AC/R32 pair. For similar conditions, Q_{st} changes from 29.96 to 17.07 kJ mol^{-1} for WPT–AC/R32.

The outcome of the study indicates that, the incredibly high adsorption uptake of low GWP HFC32 refrigerant onto biomass derived activated carbons might lead to develop an enhanced adsorption system for next generation cooling applications.

Chapter 7

Conclusions and recommendations

7.1   Overall conclusions

The main objective of this thesis is to establish some methods to enhance the performance of an adsorption cooling systems. The necessity to switch from conventional vapor compression system is illustrated by quantitative assessment of global warming impact for both conventional and adsorption cooling system. Since adsorption cooling concept is fairly new, there are a lot of scopes to improve the performance of this system. Material characterization, modification of adsorbent material, and exploring the possibility to use new adsorbent/adsorbent pairs have been investigated in this research work. The significant findings of this research is summarized in the following sections.

__Comparison of environmental impact: conventional vs. adsorption cooling system:__

(i)   Three types of cooling applications (room air-conditioning, medium and low temperature application) with same operating conditions have been considered for both conventional and adsorption cooling system. Evaporation temperature of these three applications is set to 12, –7 and –25 °C. Condensation temperature is considered as 40 °C and the cooling load is 10 kW. R32, R134a and R404A refrigerants are chosen for conventional cooling systems since these are currently used in the existing systems. Contrarily, silica gel/water, activated carbon/methanol, and activated carbon/ammonia pairs have been chosen for adsorption cooling system.

(ii)   Total equivalent warming impact (TEWI) have been assessed by aggregating indirect and direct global warming impact. Indirect warming impact is evaluated considering two factors – (a) electricity consumption by the system, (b) extraction process of the raw materials that is used to build the cooling system. Direct impact is due to the global warming potential of the leaked refrigerant from the system.

(iii)   The results indicate that, annual TEWI for conventional system for room air-conditioning application is about 4.816 t-CO_2 eq. Besides, an adsorption

cooling system can cause about 1.912 t-CO_2 eq. global warming for the considered operating conditions. Hence, global warming can be reduced about 60% for room air-conditioning system.

(iv)   Adsorption cooling system is even better for lower temperature cooling applications. TEWI of medium temperature (–7 °C) and low temperature (–25 °C) adsorption cooling system causes 70% and 85% less global warming than conventional vapor compression systems.

(v)   Thermodynamic properties have been determined and refrigeration cycles have been plotted on P-h and T-s diagram for these three applications.

(vi)   Co-efficient of performance (COP) of both the systems have computed based on the considerations and refrigeration cycle to compare the efficiency among the systems. COP values of conventional vapor compression systems are 5.989, 3.029 and 1.54 for room air-conditioning, medium and low temperature application, respectively. On the other hand, thermal COP of adsorption cooling systems are 0.6, 0.4 and 0.2 for the same applications. However, electrical COP values (12.5, 7.143, 5 respectively) are very high for the same adsorption cooling systems.

Hence, replacing conventional vapor compression cooling system by adsorption based systems can tremendously decrease the global warming impact. However, adsorption cooling systems have a lot of scope for improvement. Many properties of most commonly used adsorbents are still unavailable in the literature. These data are required to simulate and predict the performance of a system.

Characterization of adsorbents:

(i)   Porosimetry of six types of silica gels (RD, type A, type B, type A indicator, home, high purity Chromatorex) have been experimentally investigated. RD silica gel have five samples with different particle sizes. Each of the type A, type B and indicator type A silica gels have two different particle size samples. All these samples contain both micro and mesopores.

(ii)   RD silica gel with large particle diameter have higher surface area (about 775 m^2/g) than the smaller particle (about 625 m^2/g) one. Pore width of large

particle samples are in the range from 1 – 5.5 nm. Whereas, the smaller particles have additional micropores in the range from 0.6 – 0.86 nm.

(iii)   Type B and home silica gels have more mesopores and the size of mesopores are also larger for these samples. The micropore range is 1.20 – 1.80 nm and mesopore range is 2.40 – 14.0 for type B silica gel. For home silica gel, micropore rang is almost similar 1.20 – 1.80 and mesopore rang is 2.40 – 9.80 nm. These two samples have lowest BET surface area than other silica gel samples.

(iv)   Specific heat capacity of all these silica gels have been measured within 30 – 100 °C temperature. The temperature range is not increased beyond 100° because the chemical structure of silica gel could be destroyed at higher temperature. Specific heat capacity of all these samples tend to increase with temperature. A temperature depended specific heat capacity model (known as Green and Perry model) is successfully correlated with the experimental data.

(v)   RD silica gel of five different particle sizes show variations in specific heat capacity. In the measured temperature range, largest particle (D ≥ 3.3 mm) sample show lowest specific heat capacity (0.870 to 1.008 kJ kg^{-1} K^{-1}) and smallest (0.075 to 0.25 mm) particle sample have highest specific heat capacity (0.946 to 1.079 kJ kg^{-1} K^{-1}). This might occur due the more mobile atoms on the surface of large particle silica gel samples.

(vi)   Lowest specific heat capacity is found for type B silica gel (0.822 to 0.935 kJ kg^{-1} K^{-1}).

(vii)   Four types of activated carbon (Maxsorb III, H$_2$ treated Maxsorb III, KOH–H$_2$ treated Maxsorb III, KOH6 treated spherical phenol resin) samples and two thermal conductivity enhancer graphite (EC–1000 and EC–1500) samples have been reported within 30 – 150 °C. Spherical phenol resin based carbon shows lowest specific heat capacity (0.751 to 0.942 kJ kg^{-1} K^{-1}) and KOH-H$_2$ treated Maxsorb III have the highest value (1.060 to 1.324 kJ kg^{-1} K^{-1}). Commercially available parent Maxsorb III have moderate (0.844 to 1.068 kJ kg^{-1} K^{-1}) value.

(viii)   Between the two thermal conductivity enhancer EC–1500 have the lowest specific heat capacity (0.738 to 1.029 1.068 kJ kg^{-1} K^{-1}) in the measured temperature range.

(ix)   Higher surface area leads to higher adsorption amount. Lower specific heat capacity is preferred for faster desorption since the adsorbent material itself consumes low power. Hence, RD silica gel of higher particle diameter is best among the silica gel samples. Contrarily, activated carbon synthesized from spherical phenol resin is superior than the other three.

Pore structure modification of activated carbon:

(i)   Pore size distribution of activated carbon (Maxsorb III) shows the presence of a significant amount of ultramicropores (< 0.7 nm pore width) and mesopores. Since these pores do not contribute to the adsorption process, removal of these unusable pores could enhance some thermophysical properties of the adsorbent. Hence, chemical vapor deposition (CVD) of methane and benzene have been performed by varying temperature (800 to 1000 °C), flow rate (5 o 50 ml/min).and time (5 to 30 min). The objective is to find the optimum parameters which would remove most of the unusable pores without affecting the regular micropores.

(ii)   Pyrolization of activated carbon with methane has been carried out for 800, 850, 900 and 1000 °C. Flow rate of methane and carrier gas (Argon) is kept constant at 50 mL/min. Pyrolization time for all the cases is 30 min. Most of the unusable micro and mesopores are removed at 1000 °C pyrolization temperature. However, a significant amount of usable pores is also blocked. Additionally, the surface area reduces from 3140 m^2/g to 760 m^2/g after pyrolization.

(iii)   One molecule of benzene has more carbon atoms than methane. Hence, similar experimental conditions (T_{pyr} = 800 °C, $\dot{m}$ = 50 mL/min, t = 30 min) block all the existing pores and surface area becomes zero. Numerical experiments have been carried out to find out the optimum condition. At 800 °C, 25 mL/min flow rate for 10 min pyrolization duration blocks the unusable pores. At this condition, blocking of usable pores are less than methane.

Adsorption characteristics of novel adsorbent/adsorbate pairs:

(i)   Adsorption isotherm of R32 onto mangrove and waste palm trunk based activated carbon (M–AC/R32 and WPT–AC/R32) has been experimentally investigated for the first time ever. The experiment has been carried out for a wide range of adsorption temperatures 30, 50, 70 and 90 °C. The Dubinin Astakhov (D–A) and Tóth models are successfully employed to correlate the adsorption isotherms of the assorted pairs. A modified Clausius–Clapeyron model is adopted to evaluate the isosteric heat of adsorption (Q_{st}) data.

(ii)   Both the pairs have remarkably high uptake. For example, adsorption amount of M–AC/R32 pair is 2.04 kg kg^{-1} at 30 °C and 1537.9 kPa. Moreover, WPT–AC/R32 pair has even higher uptake (2.392 kg kg^{-1} at 30 °C and 1914.9 kPa) which exceeds the highest uptake value mentioned in the literatures.

(iii)   D–A and Tóth models are successfully employed to correlate the experimental data. The adjustable parameters of these two models are optimized with a marginal error.

(iv)   Isosteric heat of adsorption (Q_{st}) values found from Tóth model are 23.407 and 23.512 kJ mol^{-1} for M–AC/R32 and WPT–AC/R32, respectively. Furthermore, a temperature dependent modified Clausius-Clapeyron model is adopted to observe the variation of isosteric heat of adsorption with surface coverage. The isosteric heat of adsorption have a decreasing trend with surface coverage at any particular adsorption temperature. Isosteric heat of adsorption decreases from 30.48 kJ mol^{-1} (at one percent coverage) to 17.81 kJ mol^{-1} (at ninety percent coverage) at 30 °C adsorption temperature for M–AC/R32 pair. For similar conditions, isosteric heat of adsorption changes from 29.96 to 17.07 kJ mol^{-1} for WPT–AC/R32. The curve shifts downwards for higher adsorption temperature (when $T_{ads} < T_C$). The trend line starts moving upward for adsorption temperature higher than critical.

7.2   Recommendations

The following recommendations are made by the author for future researchers which are related to the topics higlighted in this thesis:

(i)   Temperature dependent specific heat capacity data of promising adsorbents (e. g. natural and synthetic zeolites, MOFs, consolidated composites) are still unavailable in the literatures. Measurement of specific heat capacity of these samples would be beneficial for the future researchers to accurately simulate an adsorption cooling system.

(ii)   Adsorbed phase (adsorbent + adsorbate) specific heat capacity could be measured to illustrate the actual thermal scenario that is occurring during the adsorption process.

(iii)   Different organic compounds (pyrene, methylpyrene, thiophene etc.) can be used for the pyrolization of carbon adsorbents to achieve better selectivity for the removal of unusable pores.

(iv)   Pore shaping concept can be extended for other prospective adsorbents to obtain faster kinetics, increase higher thermal conductivity, decrease isosteric heat of adsorption.

(v)   Computer simulation can be performed for the biomass derived activated carbons to understand the system behavior.

(vi)   Possibility to synthesize superior activated carbons can be explored from residential/industrial waste materials.

(vii)   Adsorption characteristics of biomass derived activated carbon with next generation working fluids (HFOs, natural refrigerants) can be studied.

References

[1]   B.O. Bolaji, Z. Huan, Ozone depletion and global warming: Case for the use of natural refrigerant - A review, Renew. Sustain. Energy Rev. 18 (2013) 49–54. doi:10.1016/j.rser.2012.10.008.

[2]   J.M. Calm, The next generation of refrigerants – Historical review, considerations, and outlook, Int. J. Refrig. 31 (2008) 1123–1133. doi:10.1016/j.ijrefrig.2008.01.013.

[3]   Technical Specification of 10 kW Bry-Chill Adsorption Chiller; Bry-Air (Asia) Pvt. Ltd., (2019). https://www.bryair.com/products-solutions/adsorption-chillers/brychilltm-adsorption-chiller/ (accessed April 23, 2019).

[4]   R.C. Arora, Refrigeration and Air Conditioning, PHI Learning Pvt. Ltd., 2012.

[5]   A. Kilicarslan, N. Müller, A comparative study of water as a refrigerant with some current refrigerants, Int. J. Energy Res. 29 (2005) 947–959. doi:10.1002/er.1084.

[6]   D.Q. T.F. Stocker, P.M. G.-K. Plattner, M. Tignor, S.K. Allen, J. Boschung, A. Nauels, Y. Xia, V. Bex, M. (Eds.), Contribution of Working Group I to the Fifth Assessment Report of the Intergovernmental Panel on Climate Change, Cambridge University Press, Cambridge, United Kingdom and New York, NY, USA, 2013, 2013. doi:http://www.climatechange2013.org/images/report/WG1AR5_ALL_FINAL.pdf.

[7]   F. Poggi, H. Macchi-Tejeda, D. Leducq, A. Bontemps, Refrigerant charge in refrigerating systems and strategies of charge reduction, Int. J. Refrig. 31 (2008) 353–370. doi:10.1016/j.ijrefrig.2007.05.014.

[8]   N. Abas, A.R. Kalair, N. Khan, A. Haider, Z. Saleem, M.S. Saleem, Natural and synthetic refrigerants, global warming: A review, Renew. Sustain. Energy Rev. 90 (2018) 557–569. doi:10.1016/j.rser.2018.03.099.

[9]   R.K. Shah, D.P. Sekulik, Fundamentals of Heat Exchanger Design, 1st ed., JOHN WILEY & SONS, INC., 2003. doi:10.1002/9781118403198.ch4.

[10]   S.-Y. Zhao, Q. Chen, Design criteria of different heat exchangers for the optimal thermodynamic performance of regenerative refrigeration systems, Appl. Therm. Eng. 93 (2016) 1164–1174. doi:10.1016/j.applthermaleng.2015.10.031.

[11]   Ernst U. Schlünder, Heat Exchanger Design Handbook, Taylor & Francis Inc, 1983.

[12]   A.A. Abbasian Arani, R. Moradi, Shell and tube heat exchanger optimization using new baffle and tube configuration, Appl. Therm. Eng. 157 (2019) 113736. doi:10.1016/j.applthermaleng.2019.113736.

[13]   T. Giampaolo, Compressor Handbook - Principles and Practice, Fairmont Press, Inc., 2010.

[14]   Compressors, Bitzer Inc., (n.d.). https://www.bitzer.de/gb/en/ (accessed May 26, 2019).

[15]   R. Wang, L. Wang, J. Wu, Adsorption Refrigeration Technology - Theory and Application, Wiley & Sons Singapore Pte. Ltd. Registered, 2014.

[16]   I.I. El-Sharkawy, A. Pal, T. Miyazaki, B.B. Saha, S. Koyama, A study on consolidated composite adsorbents for cooling application, Appl. Therm. Eng. 98 (2016) 1214–1220. doi:10.1016/j.applthermaleng.2015.12.105.

[17]   A. Pal, I.I. El-Sharkawy, B.B. Saha, S. Jribi, T. Miyazaki, S. Koyama, Experimental investigation of CO_2 adsorption onto a carbon based consolidated composite adsorbent for adsorption cooling application, Appl. Therm. Eng. 109 (2016) 304–311. doi:10.1016/j.applthermaleng.2016.08.031.

[18]   A. Pal, M.S.R. Shahrom, M. Moniruzzaman, C.D. Wilfred, S. Mitra, K. Thu, B.B. Saha, Ionic liquid as a new binder for activated carbon based consolidated composite adsorbents, Chem. Eng. J. 326 (2017) 980–986. doi:10.1016/j.cej.2017.06.031.

[19]   I.I.I. El-Sharkawy, K. Uddin, T. Miyazaki, B.B.B.B. Saha, S. Koyama, J. Miyawaki, S.-H.S.H. Yoon, Adsorption of ethanol onto parent and surface treated activated carbon powders, Int. J. Heat Mass Transf. 73 (2014) 445–455. doi:10.1016/j.ijheatmasstransfer.2014.02.046.

[20]   A. Pal, K. Thu, S. Mitra, I.I. El-Sharkawy, B.B. Saha, H.S. Kil, S.H. Yoon, J. Miyawaki, Study on biomass derived activated carbons for adsorptive heat pump application, Int. J. Heat Mass Transf. 110 (2017) 7–19. doi:10.1016/j.ijheatmasstransfer.2017.02.081.

[21]   I.I.I. El-Sharkawy, K. Kuwahara, B.B.B. Saha, S. Koyama, K.C.C. Ng, Experimental investigation of activated carbon fibers/ethanol pairs for adsorption cooling system application, Appl. Therm. Eng. 26 (2006) 859–865. doi:10.1016/j.applthermaleng.2005.10.010.

[22]   K.C. Ng, H.T. Chua, C.Y. Chung, C.H. Loke, T. Kashiwagi, A. Akisawa, B.B. Saha,

Experimental investigation of the silica gel-water adsorption isotherm characteristics, Appl. Therm. Eng. 21 (2001) 1631–1642. doi:10.1016/S1359-4311(01)00039-4.

[23]   S. Kayal, S. Baichuan, B.B. Saha, Adsorption characteristics of AQSOA zeolites and water for adsorption chillers, Int. J. Heat Mass Transf. 92 (2016) 1120–1127. doi:10.1016/j.ijheatmasstransfer.2015.09.060.

[24]   I. Solmuş, C. Yamali, B. Kaftanoğlu, D. Baker, A. Çağlar, Adsorption properties of a natural zeolite-water pair for use in adsorption cooling cycles, Appl. Energy. 87 (2010) 2062–2067. doi:10.1016/j.apenergy.2009.11.027.

[25]   B.B. Saha, I.I. El-Sharkawy, T. Miyazaki, S. Koyama, S.K. Henninger, A. Herbst, C. Janiak, Ethanol adsorption onto metal organic framework: Theory and experiments, Energy. 79 (2015) 363–370. doi:10.1016/j.energy.2014.11.022.

[26]   D.M. (Douglas M. Ruthven, Principles of adsorption and adsorption processes, Wiley, 1984.

[27]   A.L. Myers, Thermodynamics of adsorption in porous materials, AIChE J. 48 (2002) 145–160. doi:10.1002/aic.690480115.

[28]   S.M. Sami, C. Tribes, An improved model for predicting the dynamic behaviour of adsorption systems, Appl. Therm. Eng. 16 (1996) 149–161. doi:10.1016/1359-4311(95)00054-H.

[29]   H.T. Chua, K.C. Ng, A. Malek, T. Kashiwagi, A. Akisawa, B.B. Saha, Modeling the performance of two-bed, sillica gel-water adsorption chillers, Int. J. Refrig. 22 (1999) 194–204. doi:10.1016/S0140-7007(98)00063-2.

[30]   E.C. Boelman, B.B. Saha, T. Kashiwagi, Experimental investigation of a silica gel-water adsorption refrigeration cycle -- The influence of operating conditions on cooling output and COP, ASHRAE Trans. 101 (1995) 358–366.

[31]   K. Chihara, M. Suzukl, Air drying by pressure swing adsorption., J. Chem. Eng. Japan. 16 (1983) 293–299. doi:10.1252/jcej.16.293.

[32]   B.B. Saha, A. Chakraborty, S. Koyama, Y.I. Aristov, A new generation cooling device employing CaCl2-in-silica gel-water system, Int. J. Heat Mass Transf. 52 (2009) 516–524. doi:10.1016/j.ijheatmasstransfer.2008.06.018.

[33]   A. Myat, K. Thu, Y.D. Kim, B.B. Saha, K. Choon Ng, Entropy generation minimization: A practical approach for performance evaluation of temperature cascaded co-generation plants,

Energy. 46 (2012) 493–521. doi:10.1016/j.energy.2012.07.062.

[34] K. Thu, Y.D. Kim, M.W. Shahzad, J. Saththasivam, K.C. Ng, Performance investigation of an advanced multi-effect adsorption desalination (MEAD) cycle, Appl. Energy. 159 (2015) 469–477. doi:10.1016/j.apenergy.2015.09.035.

[35] S. Mitra, N. Aswin, P. Dutta, Scaling analysis and numerical studies on water vapour adsorption in a columnar porous silica gel bed, Int. J. Heat Mass Transf. 95 (2016) 853–864. doi:10.1016/j.ijheatmasstransfer.2015.12.011.

[36] S.M. Ali, A. Chakraborty, Adsorption assisted double stage cooling and desalination employing silica gel + water and AQSOA-Z02 + water systems, Energy Convers. Manag. 117 (2016) 193–205. doi:10.1016/j.enconman.2016.03.007.

[37] S. Jribi, B.B. Saha, S. Koyama, H. Bentaher, Modeling and simulation of an activated carbon-CO2 four bed based adsorption cooling system, Energy Convers. Manag. 78 (2014) 985–991. doi:10.1016/j.enconman.2013.06.061.

[38] A.A. Askalany, B.B. Saha, M.S. Ahmed, I.M. Ismail, Adsorption cooling system employing granular activated carbon-R134a pair for renewable energy applications, Int. J. Refrig. 36 (2013) 1037–1044. doi:10.1016/j.ijrefrig.2012.11.009.

[39] K.C. Chan, C.Y.H. Chao, G.N. Sze-To, K.S. Hui, Performance predictions for a new zeolite 13X/CaCl2 composite adsorbent for adsorption cooling systems, Int. J. Heat Mass Transf. 55 (2012) 3214–3224. doi:10.1016/j.ijheatmasstransfer.2012.02.054.

[40] Y.I. Aristov, Adsorptive transformation of heat: Principles of construction of adsorbents database, Appl. Therm. Eng. 42 (2012) 18–24. doi:10.1016/j.applthermaleng.2011.02.024.

[41] C.H. Jiang, L.F. Song, C.L. Jiao, J. Zhang, L.X. Sun, F. Xu, H.Z. Zhang, Q.Y. Xu, Z. Gabelica, Determination of heat capacities and thermodynamic properties of two structurally unrelated but isotypic calcium and manganese(II) 2,6-naphthalene dicarboxylate-based MOFs, J. Therm. Anal. Calorim. 103 (2011) 1095–1103. doi:10.1007/s10973-010-1197-7.

[42] F.A. Kloutse, R. Zacharia, D. Cossement, R. Chahine, Specific heat capacities of MOF-5, Cu-BTC, Fe-BTC, MOF-177 and MIL-53 (Al) over wide temperature ranges: Measurements and application of empirical group contribution method, Microporous Mesoporous Mater. 217 (2015) 1–5. doi:10.1016/j.micromeso.2015.05.047.

[43]   K. Uddin, M. Amirul Islam, S. Mitra, J. Lee, K. Thu, B.B. Saha, S. Koyama, Specific heat capacities of carbon-based adsorbents for adsorption heat pump application, Appl. Therm. Eng. 129 (2018) 117–126. doi:10.1016/j.applthermaleng.2017.09.057.

[44]   Y. Kawabuchi, M. Kishino, S. Kawano, D.D. Whitehurst, I. Mochida, Carbon Deposition from Benzene and Cyclohexane onto Active Carbon Fiber To Control Its Pore Size, Langmuir. 12 (1996) 4281–4285. doi:10.1021/la960292a.

[45]   S.K. Verma, P.L. Walker, Alteration of molecular sieving properties of microporous carbons by heat treatment and carbon gasification, Carbon N. Y. 28 (1990) 175–184. doi:10.1016/0008-6223(90)90111-B.

[46]   S.K. Verma, Development of molecular sieving properties in microporous carbons, Carbon N. Y. 29 (1991) 793–803. doi:10.1016/0008-6223(91)90018-E.

[47]   M.H. Kim, E.K. Lee, J.H. Jun, S.J. Kong, G.Y. Han, B.K. Lee, T.J. Lee, K.J. Yoon, Hydrogen production by catalytic decomposition of methane over activated carbons: Kinetic study, Int. J. Hydrogen Energy. 29 (2004) 187–193. doi:10.1016/S0360-3199(03)00111-3.

[48]   Y. Kawabuchi, C. Sotowa, M. Kishino, S. Kawano, D.D. Whitehurst, I. Mochida, Chemical Vapor Deposition of Some Heterocyclic Compounds over Active Carbon Fiber to Control Its Porosity, Chem. Lett. 25 (1996) 941–942. doi:10.1246/cl.1996.941.

[49]   V.A. Astakhov, M. M. Dubinin, P.G. Romankov:, Adsorption equilibrium of vapors on microporous adsorbents, Osn. Khim. Techn. Theor. 3 (1969) 292.

[50]   V.A. Astakhov, M.M. Dubinin, Development of the concept of volume filling of micropores in the adsorption of gases and vapors by microporous adsorbents, Bull. Acad. Sci. USSR Div. Chem. Sci. 20 (1971) 13–16. doi:10.1007/BF00849309.

[51]   T. J., State Equation of the Solid-Gas Interface Layers, Acta Chim. Hung. 69 (1971) 311–328. http://ci.nii.ac.jp/naid/10017154947/en/ (accessed May 26, 2019).

[52]   H. Freundlich, Über die adsorption in lösungen, J. Phys. Chem. 57 (1906) 385–470.

[53]   D.D. Do, Adsorption Analysis: Equilibria and Kinetics, 1998. doi:10.1142/p111.

[54]   I. Langmuir, The constitution and fundamental properties of solids and liquids. Part I. Solids., J. Am. Chem. Soc. 38 (1916) 2221–2295.

[55]   I. Langmuir, The constitutional and fundamental properties of solids and liquids. Part II. Liquids,

116

J. Am. Chem. Soc. 39 (1917) 1848–1906.

[56]   H.T. Chua, K.C. Ng, A. Chakraborty, N.M. Oo, M.A. Othman, Adsorption Characteristics of Silica Gel + Water Systems, J. Chem. Eng. Data. 47 (2002) 1177–1181. doi:10.1021/je0255067.

[57]   I.I. El-Sharkawy, K. Uddin, T. Miyazaki, B.B. Saha, S. Koyama, J. Miyawaki, S.H. Yoon, Adsorption of ethanol onto parent and surface treated activated carbon powders, Int. J. Heat Mass Transf. 73 (2014) 445–455. doi:10.1016/j.ijheatmasstransfer.2014.02.046.

[58]   S. Jribi, T. Miyazaki, B.B. Saha, A. Pal, M.M. Younes, S. Koyama, A. Maalej, Equilibrium and kinetics of CO 2 adsorption onto activated carbon, Int. J. Heat Mass Transf. 108 (2017) 1941–1946. doi:10.1016/j.ijheatmasstransfer.2016.12.114.

[59]   M. Sultan, T. Miyazaki, B.B. Saha, S. Koyama, H.S. Kil, K. Nakabayashi, J. Miyawaki, S.H. Yoon, Adsorption of Difluoromethane (HFC-32) onto phenol resin based adsorbent: Theory and experiments, Int. J. Heat Mass Transf. 127 (2018) 348–356. doi:10.1016/j.ijheatmasstransfer.2018.07.097.

[60]   A. Chakraborty, B.B. Saha, S. Koyama, K.C. Ng, On the thermodynamic modeling of the isosteric heat of adsorption and comparison with experiments, Appl. Phys. Lett. 89 (2006). doi:10.1063/1.2360925.

[61]   K.A. Rahman, A. Chakraborty, B.B. Saha, K.C. Ng, On thermodynamics of methane+carbonaceous materials adsorption, Int. J. Heat Mass Transf. 55 (2012) 565–573. doi:10.1016/j.ijheatmasstransfer.2011.10.056.

[62]   K. Uddin, I.I. El-Sharkawy, T. Miyazaki, B.B. Saha, S. Koyama, H.S. Kil, J. Miyawaki, S.H. Yoon, Adsorption characteristics of ethanol onto functional activated carbons with controlled oxygen content, Appl. Therm. Eng. 72 (2014) 211–218. doi:10.1016/j.applthermaleng.2014.03.062.

[63]   I.I.I. El-Sharkawy, K. Uddin, T. Miyazaki, B. Baran Saha, S. Koyama, H.-S.H.-S. Kil, S.-H.S.-H. Yoon, J. Miyawaki, Adsorption of ethanol onto phenol resin based adsorbents for developing next generation cooling systems, Int. J. Heat Mass Transf. 81 (2015) 171–178. doi:10.1016/j.ijheatmasstransfer.2014.10.012.

[64]   M.A. Islam, K. Srinivasan, K. Thu, B.B. Saha, Assessment of total equivalent warming impact (TEWI) of supermarket refrigeration systems, Int. J. Hydrogen Energy. 42 (2017) 26973–

26983. doi:10.1016/j.ijhydene.2017.07.035.

[65]   S.K. Wang, Handbook of air conditioning and refrigeration, 2nd ed., McGraw-Hill, 2000.

[66]   S. Rahman, A. de Castro, Environmental impacts of electricity generation: a global perspective, IEEE Trans. Energy Convers. 10 (1995) 307–314. doi:10.1109/60.391897.

[67]   B. Bose, Global Warming: Energy, Environmental Pollution, and the Impact of Power Electronics, IEEE Ind. Electron. Mag. 4 (2010) 6–17. doi:10.1109/MIE.2010.935860.

[68]   A. Cherp, V. Vinichenko, J. Jewell, M. Suzuki, M. Antal, Comparing electricity transitions: A historical analysis of nuclear, wind and solar power in Germany and Japan, Energy Policy. 101 (2017) 612–628. doi:10.1016/j.enpol.2016.10.044.

[69]   S.A. Tassou, I.N. Grace, Fault diagnosis and refrigerant leak detection in vapour compression refrigeration systems, Int. J. Refrig. 28 (2005) 680–688. doi:10.1016/j.ijrefrig.2004.12.007.

[70]   C. Francis, G. Maidment, G. Davies, An investigation of refrigerant leakage in commercial refrigeration, Int. J. Refrig. 74 (2016) 12–21. doi:10.1016/j.ijrefrig.2016.10.009.

[71]   J.M. Calm, Emissions and environmental impacts from air-conditioning and refrigeration systems, Int. J. Refrig. 25 (2002) 293–305. doi:10.1016/S0140-7007(01)00067-6.

[72]   P. Makhnatch, R. Khodabandeh, The Role of Environmental Metrics (GWP, TEWI, LCCP) in the Selection Of Low GWP Refrigerant, Energy Procedia. 61 (2014) 2460–2463. doi:10.1016/j.egypro.2014.12.023.

[73]   T.W. Davies, O. Caretta, A low carbon, low TEWI refrigeration system design, Appl. Therm. Eng. 24 (2004) 1119–1128. doi:10.1016/j.applthermaleng.2003.12.026.

[74]   H. Kruse, Refrigerant use in Europe, ASHRAE J. 42 (2000) 16-18+21.

[75]   B.B. Saha, I.I. El-Sharkawy, A. Chakraborty, S. Koyama, N.D. Banker, P. Dutta, M. Prasad, K. Srinivasan, Evaluation of minimum desorption temperatures of thermal compressors in adsorption refrigeration cycles, Int. J. Refrig. 29 (2006) 1175–1181. doi:10.1016/j.ijrefrig.2006.01.005.

[76]   K. Thu, A. Chakraborty, B.B. Saha, K.C. Ng, Thermo-physical properties of silica gel for adsorption desalination cycle, Appl. Therm. Eng. 50 (2013) 1596–1602. doi:10.1016/j.applthermaleng.2011.09.038.

[77] I.I. El-Sharkawy, B.B. Saha, S. Koyama, J. He, K.C. Ng, C. Yap, Experimental investigation on activated carbon–ethanol pair for solar powered adsorption cooling applications, Int. J. Refrig. 31 (2008) 1407–1413. doi:10.1016/j.ijrefrig.2008.03.012.

[78] K. Habib, B.B. Saha, S. Koyama, Study of various adsorbent-refrigerant pairs for the application of solar driven adsorption cooling in tropical climates, Appl. Therm. Eng. 72 (2014) 266–274. doi:10.1016/j.applthermaleng.2014.05.102.

[79] A. Kasaeian, S.M. Hosseini, M. Sheikhpour, O. Mahian, W.M. Yan, S. Wongwises, Applications of eco-friendly refrigerants and nanorefrigerants: A review, Renew. Sustain. Energy Rev. 96 (2018) 91–99. doi:10.1016/j.rser.2018.07.033.

[80] B.. Saha, A. Akisawa, T. Kashiwagi, Solar/waste heat driven two-stage adsorption chiller: the prototype, Renew. Energy. 23 (2001) 93–101. doi:10.1016/S0960-1481(00)00107-5.

[81] Mitsubishi Plastics launches a compact adsorption chiller with the highest cooling capacity per volume in the world, 14-03-2012. (n.d.). https://www.m-chemical.co.jp/en/news/mpi/201203140474.html (accessed March 24, 2019).

[82] Standard specification of adsorption chiller, Tokyo Boeki Machinery, Japan, (n.d.). http://www.tokyo-boeki-machinery.jp/adsorption_chiller/siyou.html (accessed April 23, 2019).

[83] Adsorption Chiller: Adref-Noa; Friendly to mankind and to the earth; Mayewaka-Mycom; Mayekawa Mfg. Ltd., (n.d.). http://www.mayekawa.co.id/pic/AdRef-Noa---English-828.pdf (accessed April 24, 2019).

[84] J. Rupp, SolarCombi+, SorTech package solution description., 06.10.2009. (n.d.). http://www.solarcombiplus.eu/docs/d44_sortech_v02_english.pdf (accessed April 23, 2019).

[85] A.A.M. Sayigh, J.C. McVeigh, Solar air conditioning and refrigeration, 1st ed., Pergamon Press, 1992.

[86] W.-S. Chang, C.-C. Wang, C.-C. Shieh, Experimental study of a solid adsorption cooling system using flat-tube heat exchangers as adsorption bed, Appl. Therm. Eng. 27 (2007) 2195–2199. doi:10.1016/j.applthermaleng.2005.07.022.

[87] S.-H. Cho, J.-N. Kim, Modeling of a silica gel/water adsorption-cooling system, Energy. 17 (1992) 829–839. doi:10.1016/0360-5442(92)90101-5.

[88]   J. Bassols-Rheinfelder, Solar cooling using an open-cycle adsorption system with adiabatical mass transfer and external heat exchange, Sol. Energy. 35 (1985) 93–104. doi:10.1016/0038-092X(85)90040-4.

[89]   A. Buonomano, F. Calise, A. Palombo, "Solar heating and cooling systems by absorption and adsorption chillers driven by stationary and concentrating photovoltaic/thermal solar collectors: Modelling and simulation," Renew. Sustain. Energy Rev. 81 (2018) 1112–1146. doi:10.1016/j.rser.2017.07.056.

[90]   V. Tangkengsirisin, A. Kanzawa, T. Watanabe, A solar-powered adsorption cooling system using a silica gel-water mixture, Energy. 23 (1998) 347–353. doi:10.1016/S0360-5442(98)00002-4.

[91]   A. Al Mers, A. Azzabakh, A. Mimet, H. El Kalkha, Optimal design study of cylindrical finned reactor for solar adsorption cooling machine working with activated carbon–ammonia pair, Appl. Therm. Eng. 26 (2006) 1866–1875. doi:10.1016/j.applthermaleng.2006.01.021.

[92]   W.-S. Chang, C.-C. Wang, C.-C. Shieh, Design and performance of a solar-powered heating and cooling system using silica gel/water adsorption chiller, Appl. Therm. Eng. 29 (2009) 2100–2105. doi:10.1016/j.applthermaleng.2008.10.021.

[93]   V.S. Reddy, N.L. Panwar, S.C. Kaushik, Exergetic analysis of a vapour compression refrigeration system with R134a, R143a, R152a, R404A, R407C, R410A, R502 and R507A, Clean Technol. Environ. Policy. 14 (2012) 47–53. doi:10.1007/s10098-011-0374-0.

[94]   Z. Du, P.A. Domanski, W.V. Payne, Effect of common faults on the performance of different types of vapor compression systems, Appl. Therm. Eng. 98 (2016) 61–72. doi:10.1016/j.applthermaleng.2015.11.108.

[95]   I.B.D. McIntosh, J.W. Mitchell, W.A. Beckman, Fault detection and diagnosis in chillers - Part I: model development and application, ASHRAE Trans. 106 (2000).

[96]   E.W. Lemmon, I.H. Bell, M.L. Huber, M.O. McLinden, NIST Standard Reference Database 23: Reference Fluid Thermodynamic and Transport Properties-REFPROP, Version 10.0, National Institute of Standards and Technology, (2018). doi:https://dx.doi.org/10.18434/T4JS3C.

[97]   A. López-Belchí, F. Illán-Gómez, Evaluation of a condenser based on mini-channels technology working with R410A and R32. Experimental data and performance estimate, Appl. Energy. 202 (2017) 112–124. doi:10.1016/j.apenergy.2017.05.122.

[98]   L. Vaitkus, V. Dagilis, Analysis of alternatives to high GWP refrigerants for eutectic refrigerating systems, Int. J. Refrig. 76 (2017) 160–169. doi:10.1016/j.ijrefrig.2017.01.024.

[99]   Electricity Review Japan (2018), The Federation of Electric Power Companies, (2018). http://www.fepc.or.jp/english/library/electricity_eview_japan/index.html (accessed February 14, 2019).

[100]   Hitachi Room Aircon Product Brochure, (n.d.). http://www2.tochi.hitachi.co.jp/ra.drowing/zumen/JT90J2E7.PDF (accessed April 8, 2019).

[101]   General - Product Catalogue 2018 - Air Conditioners Lineup, (2018). https://www.fujitsu-general.com/shared/g-eu/pdf-geur-support-ctlg-3eg019-1801e-01.pdf (accessed April 8, 2019).

[102]   D.-A. Chisalita, L. Petrescu, P. Cobden, H.A.. (Eric) van Dijk, A.-M. Cormos, C.-C. Cormos, Assessing the environmental impact of an integrated steel mill with post-combustion CO_2 capture and storage using the LCA methodology, J. Clean. Prod. 211 (2019) 1015–1025. doi:10.1016/j.jclepro.2018.11.256.

[103]   S. Kosai, E. Yamasue, Global warming potential and total material requirement in metal production: Identification of changes in environmental impact through metal substitution, Sci. Total Environ. 651 (2019) 1764–1775. doi:10.1016/j.scitotenv.2018.10.085.

[104]   M. Ebrahimi, A. Keshavarz, Combined Cooling, Heating and Power, Elsevier, 2014. doi:10.1016/C2013-0-18763-6.

[105]   G. Stryi-Hipp, Renewable heating and cooling : technologies and applications, 1st ed., Woodhead Publishing, Amsterdam, 2016.

[106]   M. Attalla, S. Sadek, M. Salem Ahmed, I.M. Shafie, M. Hassan, Experimental study of solar powered ice maker using adsorption pair of activated carbon and methanol, Appl. Therm. Eng. 141 (2018) 877–886. doi:10.1016/j.applthermaleng.2018.06.038.

[107]   L.W. Wang, R.Z. Wang, R.G. Oliveira, A review on adsorption working pairs for refrigeration, Renew. Sustain. Energy Rev. 13 (2009) 518–534. doi:10.1016/j.rser.2007.12.002.

[108]   A.A. Askalany, M. Salem, I.M. Ismael, A.H.H. Ali, M.G. Morsy, B.B. Saha, An overview on adsorption pairs for cooling, Renew. Sustain. Energy Rev. 19 (2013) 565–572. doi:10.1016/j.rser.2012.11.037.

[109] K. Rosset, V. Mounier, E. Guenat, J. Schiffmann, Multi-objective optimization of turbo-ORC systems for waste heat recovery on passenger car engines, Energy. 159 (2018) 751–765. doi:10.1016/j.energy.2018.06.193.

[110] B. Choudhury, B.B. Saha, P.K. Chatterjee, J.P. Sarkar, An overview of developments in adsorption refrigeration systems towards a sustainable way of cooling, Appl. Energy. 104 (2013) 554–567. doi:10.1016/j.apenergy.2012.11.042.

[111] A. Sakoda, M. Suzuki, Fundamental study on solar powered adsorption cooling system, J. Chem. Eng. JAPAN. 17 (1984) 52–57. doi:10.1252/jcej.17.52.

[112] A. Myat, K. Thu, N.K. Choon, The experimental investigation on the performance of a low temperature waste heat-driven multi-bed desiccant dehumidifier (MBDD) and minimization of entropy generation, Appl. Therm. Eng. 39 (2012) 70–77. doi:10.1016/j.applthermaleng.2012.01.041.

[113] K. Chihara, M. Suzukl, Air drying by pressure swing adsorption., J. Chem. Eng. Japan. 16 (1983) 293–299. doi:10.1252/jcej.16.293.

[114] P.C. Wankat, Adsorption engineering, Kodansha, 1991. doi:10.1016/0923-1137(91)90043-N.

[115] K. Thu, K.C. Ng, B.B. Saha, A. Chakraborty, S. Koyama, Adsorption desalination: Theory & Experiments, National University of Singapore, 2009. doi:10.1016/j.ijheatmasstransfer.2008.10.012.

[116] J.W. Wu, E.J. Hu, M.J. Biggs, Thermodynamic analysis of an adsorption-based desalination cycle (part II): Effect of evaporator temperature on performance, Chem. Eng. Res. Des. 89 (2011) 2168–2175. doi:10.1016/j.cherd.2010.12.012.

[117] S. Mitra, P. Kumar, K. Srinivasan, P. Dutta, Development and performance studies of an air cooled two-stage multi-bed silica-gel + water adsorption system, Int. J. Refrig. 67 (2016) 174–189. doi:10.1016/j.ijrefrig.2015.10.028.

[118] K.C. Ng, K. Thu, Y. Kim, A. Chakraborty, G. Amy, Adsorption desalination: An emerging low-cost thermal desalination method, Desalination. 308 (2013) 161–179. doi:10.1016/j.desal.2012.07.030.

[119] S. Mitra, K. Thu, B.B. Saha, P. Dutta, Modeling the Effect of Heat Source Temperature on the Performance of Two-stage Air Cooled Silica Gel + Water Adsorption System, Energy Procedia.

105 (2017) 2010–2015. doi:10.1016/j.egypro.2017.03.575.

[120] H.T. Chua, K.C. Ng, A. Malek, T. Kashiwagi, A. Akisawa, B.B. Saha, Modeling the performance of two-bed, silica gel-water adsorption chillers, Int. J. Refrig. 22 (1999) 194–204. doi:10.1016/S0140-7007(98)00063-2.

[121] B.B. Saha, A. Akisawa, T. Kashiwagi, Silica gel water advanced adsorption refrigeration cycle, in: Energy, 1997: pp. 437–447. doi:10.1016/S0360-5442(96)00102-8.

[122] A.R.M. Rezk, R.K. Al-Dadah, Physical and operating conditions effects on silica gel/water adsorption chiller performance, Appl. Energy. 89 (2012) 142–149. doi:10.1016/j.apenergy.2010.11.021.

[123] M.Z.I. Khan, K.C.A. Alam, B.B. Saha, A. Akisawa, T. Kashiwagi, Performance evaluation of multi-stage, multi-bed adsorption chiller employing re-heat scheme, Renew. Energy. 33 (2008) 88–98. doi:10.1016/j.renene.2007.01.012.

[124] K. Thu, A. Chakraborty, Y.D. Kim, A. Myat, B.B. Saha, K.C. Ng, Numerical simulation and performance investigation of an advanced adsorption desalination cycle, Desalination. 308 (2013) 209–218. doi:10.1016/j.desal.2012.04.021.

[125] A. Freni, A. Sapienza, I.S. Glaznev, Y.I. Aristov, G. Restuccia, Experimental testing of a lab-scale adsorption chiller using a novel selective water sorbent "silica modified by calcium nitrate," Int. J. Refrig. 35 (2012) 518–524. doi:10.1016/j.ijrefrig.2010.05.015.

[126] W.J. Parker, R.J. Jenkins, C.P. Butler, G.L. Abbott, Flash method of determining thermal diffusivity, heat capacity, and thermal conductivity, J. Appl. Phys. 32 (1961) 1679–1684. doi:10.1063/1.1728417.

[127] A. Göbel, F. Hemberger, S. Vidi, H.-P. Ebert, A new method for the determination of the specific heat capacity using laser-flash calorimetry down to 77K, Int. J. Thermophys. 34 (2013) 883–893. doi:10.1007/s10765-012-1255-4.

[128] Y. Takahashi, H. Yokokawa, H. Kadokura, Y. Sekine, T. Mukaibo, Laser-flash calorimetry I. Calibration and test on alumina heat capacity, J. Chem. Thermodyn. 11 (1979) 379–394. doi:10.1016/0021-9614(79)90058-2.

[129] K. Shinzato, T. Baba, A laser flash apparatus for thermal diffusivity and specific heat capacity measurements, J. Therm. Anal. Calorim. 64 (2001) 413–422. doi:10.1023/A:1011594609521.

[130] P. Huang, A. Zeidler, W. shao Chang, M.P. Ansell, Y.M.J. Chew, A. Shea, Specific heat capacity measurement of Phyllostachys edulis (Moso bamboo) by differential scanning calorimetry, Constr. Build. Mater. 125 (2016) 821–831. doi:10.1016/j.conbuildmat.2016.08.103.

[131] R.L. Danley, New heat flux DSC measurement technique, Thermochim. Acta. 395 (2002) 201–208. doi:10.1016/S0040-6031(02)00212-5.

[132] E.S. Watson, M.J. O'Neill, J. Justin, N. Brenner, A Differential Scanning Calorimeter for Quantitative Differential Thermal Analysis., Anal. Chem. 36 (1964) 1233–1238. doi:10.1021/ac60213a019.

[133] M.J. O 'neill, The Analysis of a Temperature-Controlled Scanning Calorimeter, Anal. Chem. 57 (1964) 1356–1242.

[134] K.L. Ramakumar, M.K. Saxena, S.B. Deb, Experimental evaluation of procedures for heat capacity measurement by differential scanning calorimetry, J. Therm. Anal. Calorim. 66 (2001) 387–397. doi:10.1023/A:1013126414406.

[135] M.K. Saxena, S.B. Deb, K.L. Ramakumar, V. Venugopal, Optimization of different experimental parameters for the determination of heat capacity of thoria using Differential Scanning Calorimetry (DSC), Indian J. Chem. Technol. 9 (2002) 324–329.

[136] T. Kousksou, A. Jamil, K. El Omari, Y. Zeraouli, Y. Le Guer, Effect of heating rate and sample geometry on the apparent specific heat capacity: DSC applications, Thermochim. Acta. 519 (2011) 59–64. doi:10.1016/j.tca.2011.02.033.

[137] R. Danley, P. Caulfield, DSC Baseline Improvements Obtained by a New Heat Flow Measurement Technique, in: Proc. 29th Conf. N. Amer. Therm. Anal. Soc, 2001: pp. 1–7.

[138] 3 FLEX - Surface Characterizaion Analyzer, (2016) 12. https://www.micromeritics.com/Repository/Files/3flex_brochure_2016_v8.pdf (accessed May 7, 2019).

[139] Technical Datasheet, Thermal Analysis Instruments 60 Series, Shimadzu Corporation, Japan., (n.d.).

[140] D.W. Green, R.H. Perry, J.O. Maloney, Perry's Chemical Engineers' Handbook, 7th ed., McGraw-Hill Publishing Company, New York, NY, 1997.

[141] I.I. El-Sharkawy, K. Uddin, T. Miyazaki, B.B. Saha, S. Koyama, J. Miyawaki, S.-H. Yoon, Adsorption of ethanol onto parent and surface treated activated carbon powders, Int. J. Heat Mass Transf. 73 (2014) 445–455. doi:10.1016/j.ijheatmasstransfer.2014.02.046.

[142] I.I. El-Sharkawy, K. Uddin, T. Miyazaki, B. Baran Saha, S. Koyama, H.S. Kil, S.H. Yoon, J. Miyawaki, Adsorption of ethanol onto phenol resin based adsorbents for developing next generation cooling systems, Int. J. Heat Mass Transf. 81 (2015) 171–178. doi:10.1016/j.ijheatmasstransfer.2014.10.012.

[143] D.G. Archer, Thermodynamic Properties of Synthetic Sapphire (α-Al2O3, Standard Reference Material 720 and the Effect of Temperature-Scale Differences on Thermodynamic Properties, J. Phys. Chem. Ref. Data. 22 (1993) 1441–1453. doi:10.1063/1.555931.

[144] D.G. Archer, S. Rudtsch, Enthalpy of Fusion of Indium: A Certified Reference Material for Differential Scanning Calorimetry, (n.d.). doi:10.1021/je030112g.

[145] H.-S. Kil, T. Kim, K. Hata, K. Ideta, T. Ohba, H. Kanoh, I. Mochida, S.-H. Yoon, J. Miyawaki, Influence of surface functionalities on ethanol adsorption characteristics in activated carbons for adsorption heat pumps, Appl. Therm. Eng. 72 (2014) 160–165. doi:10.1016/j.applthermaleng.2014.06.018.

[146] J. Xiao, M. Hu, D. Cossement, P. Bénard, R. Chahine, Finite element simulation for charge-discharge cycle of cryo-adsorptive hydrogen storage on activated carbon, Int. J. Heat Mass Transf. 55 (2012) 6864–6872. doi:10.1016/j.ijheatmasstransfer.2012.06.093.

[147] B.B. Saha, S. Koyama, T. Kashiwagi, A. Akisawa, K.C. Ng, H.T. Chua, Waste heat driven dual-mode, multi-stage, multi-bed regenerative adsorption system, Int. J. Refrig. 26 (2003) 749–757. doi:10.1016/S0140-7007(03)00074-4.

[148] B.B. Saha, A. Chakraborty, S. Koyama, S.-H.H. Yoon, I. Mochida, M. Kumja, C. Yap, K.C. Ng, Isotherms and thermodynamics for the adsorption of n-butane on pitch based activated carbon, Int. J. Heat Mass Transf. 51 (2008) 1582–1589. doi:10.1016/j.ijheatmasstransfer.2007.07.031.

[149] P.J.M. Carrott, P.A.M. Mourão, M.M.L.R. Carrott, Controlling the micropore size of activated carbons for the treatment of fuels and combustion gases, Appl. Surf. Sci. 252 (2006) 5953–5956. doi:10.1016/j.apsusc.2005.11.016.

[150] T. Zhang, W.P. Walawender, L.T. Fan, Preparation of carbon molecular sieves by carbon

deposition from methane, Bioresour. Technol. 96 (2005) 1929–1935. doi:10.1016/j.biortech.2005.01.026.

[151] J. Alcañiz-Monge, · M José Illán-Gómez, Modification of activated carbon porosity by pyrolysis under pressure of organic compounds, Adsorption. 14 (2008) 93–100. doi:10.1007/s10450-007-9056-y.

[152] M.M.. Freitas, J.. Figueiredo, Preparation of carbon molecular sieves for gas separations by modification of the pore sizes of activated carbons, Fuel. 80 (2001) 1–6. doi:10.1016/S0016-2361(00)00066-1.

[153] B. Cagnon, X. Py, A. Guillot, J.P. Joly, R. Berjoan, Pore structure modification of pitch-based activated carbon by NaOCl and air oxidation/pyrolysis cycles, Microporous Mesoporous Mater. 80 (2005) 183–193. doi:10.1016/j.micromeso.2004.12.009.

[154] M.M.A. Freitas, J.L. Figueiredo, Preparation of activated carbons with controlled pore size, in: Stud. Surf. Sci. Catal., Elsevier, 2002: pp. 261–265. doi:10.1016/S0167-2991(02)80143-4.

[155] PubChem; U.S. National Library of Medicine, National Center for Biotechnology Information., (n.d.). https://pubchem.ncbi.nlm.nih.gov/compound/297 (accessed May 15, 2019).

[156] One zone tubular furnace, Asahi Rika Corporation., (n.d.). http://www.asahi-rika.co.jp/ (accessed May 15, 2019).

[157] A. Yataganbaba, A. Kilicarslan, I. Kurtbaş, Exergy analysis of R1234yf and R1234ze as R134a replacements in a two evaporator vapour compression refrigeration system, Int. J. Refrig. 60 (2015) 26–37. doi:10.1016/j.ijrefrig.2015.08.010.

[158] C. Yıldırım, D.B. Özkan, C. Onan, Theoretical study of R32 to replace R410A in variable refrigerant flow systems, Int. J. Ambient Energy. 39 (2018) 87–92. doi:10.1080/01430750.2016.1269682.

[159] Y.A. Cengel, M.A. Boles, Thermodynamics: an engineering approach, 2002.

[160] C. Aprea, A. Greco, A. Maiorino, An experimental evaluation of the greenhouse effect in the substitution of R134a with CO 2, Energy. 45 (2012) 753–761. doi:10.1016/j.energy.2012.07.015.

[161] A.H.P. Antunes, E.P. Bandarra Filho, Experimental investigation on the performance and global

environmental impact of a refrigeration system retrofitted with alternative refrigerants, Int. J. Refrig. 70 (2016) 119–127. doi:10.1016/j.ijrefrig.2016.06.027.

[162] Y. Liu, K.C. Leong, The effect of operating conditions on the performance of zeolite/water adsorption cooling systems, Appl. Therm. Eng. 25 (2005) 1403–1418. doi:10.1016/J.APPLTHERMALENG.2004.09.013.

[163] S. Kayal, S. Baichuan, B.B. Saha, Adsorption characteristics of AQSOA zeolites and water for adsorption chillers, Int. J. Heat Mass Transf. 92 (2016) 1120–1127. doi:10.1016/j.ijheatmasstransfer.2015.09.060.

[164] I.I.I. El-Sharkawy, M. Hassan, B.B.B. Saha, S. Koyama, M.M.M. Nasr, Study on adsorption of methanol onto carbon based adsorbents, Int. J. Refrig. 32 (2009) 1579–1586. doi:10.1016/j.ijrefrig.2009.06.011.

[165] M. Louajari, A. Mimet, A. Ouammi, Study of the effect of finned tube adsorber on the performance of solar driven adsorption cooling machine using activated carbon–ammonia pair, Appl. Energy. 88 (2011) 690–698. doi:10.1016/j.apenergy.2010.08.032.

[166] Z. Tamainot-Telto, S.J. Metcalf, R.E. Critoph, Y. Zhong, R. Thorpe, Carbon–ammonia pairs for adsorption refrigeration applications: ice making, air conditioning and heat pumping, Int. J. Refrig. 32 (2009) 1212–1229. doi:10.1016/j.ijrefrig.2009.01.008.

[167] Z. Tamainot-Telto, R.. Critoph, Adsorption refrigerator using monolithic carbon-ammonia pair, Int. J. Refrig. 20 (1997) 146–155. doi:10.1016/S0140-7007(96)00053-9.

[168] A. Hines, S.-L. Kuo, N. Dural, A New Analytical Isotherm Equation for Adsorption on Heterogeneous Adsorbents, Sep. Sci. Technol. 25 (1990) 869–888. doi:10.1080/01496399008050371.

[169] C. Shen, C.A. Grande, P. Li, J. Yu, A.E. Rodrigues, Adsorption equilibria and kinetics of CO2 and N2 on activated carbon beads, Chem. Eng. J. 160 (2010) 398–407. doi:10.1016/j.cej.2009.12.005.

[170] A. Mota-Babiloni, J. Navarro-Esbrí, Á. Barragán-Cervera, F. Molés, B. Peris, Analysis based on EU Regulation No 517/2014 of new HFC/HFO mixtures as alternatives of high GWP refrigerants in refrigeration and HVAC systems, Int. J. Refrig. 52 (2015) 21–31. doi:10.1016/j.ijrefrig.2014.12.021.

[171] B.B. Saha, I.I. El-Sharkawy, R. Thorpe, R.E. Critoph, Accurate adsorption isotherms of R134a

onto activated carbons for cooling and freezing applications, Int. J. Refrig. 35 (2012) 499–505. doi:10.1016/j.ijrefrig.2011.05.002.

[172] A.A. Askalany, B.B. Saha, M. Ghazy, K. Harby, A.A. Askalany, B.B. Saha, Adsorption isotherms and kinetics of activated carbon/difluoroethane adsorption pair: theory and experiments, Int. J. Refrig. 49 (2016) 160–168. doi:10.1016/j.ijrefrig.2016.01.012.

[173] A.A. Askalany, B.B. Saha, K. Uddin, T. Miyzaki, S. Koyama, K. Srinivasan, I.M. Ismail, Adsorption isotherms and heat of adsorption of difluoromethane on activated carbons, J. Chem. Eng. Data. 58 (2013) 2828–2834. doi:10.1021/je4005678.

[174] NIST Chemistry WebBook, SRD 69, (n.d.). https://webbook.nist.gov/cgi/inchi/InChI%3D1S/CH2F2/c2-1-3/h1H2 (accessed May 20, 2019).

[175] J.A. Kohler, G.C. Briley, E.M. Clark, D.R. Dorman, S.W. Duda, D.M. Halel, D.R. Kuespert, J.T. Parker, D.T. Reindl, W. V Richards, K.M. Schoonover, E.F. Troy, J.I. Vucci, G.W. Westermeyer, J.F. Hogan, F.E. Jakob, ANSI/ASHRAE Standard 15-2016; Safety Standard for Refrigeration Systems, 2016.

[176] M.M. Rahman, A. Pal, K. Uddin, K. Thu, B.B. Saha, Statistical Analysis of Optimized Isotherm Model for Maxsorb III/Ethanol and Silica Gel/Water Pairs, Evergreen. 5 (2018) 1–12. doi:10.5109/2174852.

[177] K.C. Ng, K. Thu, B.B. Saha, A. Chakraborty, Study on a waste heat-driven adsorption cooling cum desalination cycle, Int. J. Refrig. 35 (2012) 685–693. doi:10.1016/j.ijrefrig.2011.01.008.

[178] S. Ozawa, S. Kusumi, Y. Ogino, Physical adsorption of gases at high pressure. IV. An improvement of the Dubinin—Astakhov adsorption equation, J. Colloid Interface Sci. 56 (1976) 83–91. doi:10.1016/0021-9797(76)90149-1.

[179] B.B. Saha, S. Koyama, I.I. El-Sharkawy, K. Habib, K. Srinivasan, P. Dutta, Evaluation of Adsorption Parameters and Heats of Adsorption through Desorption Measurements, J. Chem. Eng. Data. 52 (2007) 2419–2424. doi:10.1021/je700369j.

[180] K.A. Rahman, W.S. Loh, H. Yanagi, A. Chakraborty, B.B. Saha, W.G. Chun, K.C. Ng, Experimental Adsorption Isotherm of Methane onto Activated Carbon at Sub- and Supercritical Temperatures, J. Chem. Eng. Data. 55 (2010) 4961–4967. doi:10.1021/je1005328.

[181] H.Y.S. Julian Szekely, James W. Evans, Gas-Solid Reactions, Illustrate, Academic Press Inc., 1976.

[182] T. Miyazaki, A. Akisawa, B.B. Saha, I.I. El-Sharkawy, A. Chakraborty, A new cycle time allocation for enhancing the performance of two-bed adsorption chillers, Int. J. Refrig. 32 (2009) 846–853. doi:10.1016/j.ijrefrig.2008.12.002.

[183] A.A. Askalany, B.B. Saha, Experimental and theoretical study of adsorption kinetics of Difluoromethane onto activated carbons, Int. J. Refrig. 49 (2015) 160–168. doi:10.1016/j.ijrefrig.2014.10.009.